



Universidad  
Carlos III de Madrid

STABILIZER ARCHITECTURE  
FOR HUMANOID ROBOTS  
COLLABORATING WITH HUMANS

*Paolo Pierro*

Ph.D. Thesis

Department of Systems Engineering and Automation  
Leganés, May 2012



STABILIZER ARCHITECTURE  
FOR HUMANOID ROBOTS COLLABORATING WITH HUMANS

Candidate

*Paolo Pierro*

Advisers

*Carlos Balaguer Bernaldo de Quirós*

*Concepción Alicia Monje Micharet*

Review Committee

*Miguel Ángel Salichs* (Chair)

\_\_\_\_\_

*Giulio Sandini* (Member)

\_\_\_\_\_

*Eiichi Yoshida* (Member)

\_\_\_\_\_

*Philippe Souères* (Member)

\_\_\_\_\_

*María Dolores Blanco* (Secretary)

\_\_\_\_\_

Grade:

Leganés, June 20, 2012



# Abstract

Nowadays, the advances in information, communication technologies and robotics permit the use of robots as companions in activities with humans.

While most of the existing research is dedicated to the interaction between humans and robots, the framework of this research is the use of robots as collaborative agents.

In particular, this study is dedicated to humanoid robots which should assist people in several tasks in working environments. Humanoid robots are certainly the most adequate for such situations: they can use the same tools as humans and are most likely accepted by them.

After explaining the advantages of collaborative tasks among humans and robots and the differences with respect to interaction and teleoperation systems, this work focuses on the level of technologies which is necessary in order to achieve such a goal.

The most complex problem in humanoid control is the balance of the structure. This study focuses on novel techniques for the attitude estimation of the robot, to be used for the control. The control of the robot is based on a very well-known and simplified model: the double (inverted) pendulum. This model permits to have a real-time control of the structure while submitted to external forces/disturbances.

The control actions are strongly dependent on the three stability regions, which are determined by the position of the ZMP in the support polygon.

Smooth trajectories for the humanoid control have been proposed and tested on real platforms: these allow reducing the impacts of the robot with its environment.

Finally, the study extends these results to a contribution for a human-humanoid collaboration architecture. Two types of human-humanoid collaborations are analyzed: a physical collaboration, where robot and human share the same space and have a physical contact (or by means of an object), and a remote collaboration, in which the human is relatively far away from the robot and the two agents collaborate using an interface.

The basic paradigm for this robotic collaboration is: what is difficult (or dangerous) for the human is done by the robot, and what is difficult for the robot is better done by the human.

Importantly, the testing context is not only based on a single humanoid platform; on the contrary, three platforms have been object of the experiments: the Hoap-3,

HRP-2 and TEO robot have been used.

# Resumen

Hoy en día, los avances en las tecnologías de información, comunicación y robótica permiten el uso de robots como compañeros en las actividades con los seres humanos.

Mientras que la mayoría de las investigaciones existentes se dedica a la interacción entre humanos y robots, el marco de esta investigación está centrado en el uso de robots como agentes de colaboración.

En particular, este estudio está dedicado a los robots humanoides que puedan ayudar a la gente en varias tareas en entornos de trabajo. Los robots humanoides son sin duda los más adecuados para este tipo de situaciones: pueden usar las mismas herramientas que los seres humanos y probablemente son lo más aceptados por ellos.

Después de explicar las ventajas de las tareas de colaboración entre los humanos y los robots y las diferencias con respecto a los sistemas de interacción y de teleoperación, este trabajo se centra en el nivel de las tecnologías que es necesario para lograr ese objetivo.

El problema más complejo en el control de humanoides es el balance de la estructura. Este estudio se centra en técnicas novedosas para la estimación de la actitud del robot, que se utilizarán para el control. El control del robot se basa en un modelo muy conocido y simplificado: el double péndulo (invertido). Este modelo permite tener un control en tiempo real sobre la estructura mientras está sometida a fuerzas externas / perturbaciones.

Se han propuesto y probado trayectorias suaves para el control de humanoides en plataformas reales: éstas permiten reducir los impactos del robot con su entorno.

Finalmente, el estudio extiende estos resultados a una contribución respecto a la arquitectura de colaboración humano–humanoide. Se analizan dos tipos de colaboraciones humano–humanoide: la colaboración física, donde robots y humanos comparten el mismo espacio y tienen un contacto físico (o por medio de un objeto), y una colaboración a distancia, en la que el ser humano está relativamente lejos del robot y los dos agentes colaboran por medio de una interfaz.

El paradigma básico de esta colaboración robótica es: lo que es difícil (o peligroso) para el ser humano se hace por medio del robot, y lo que es difícil para el robot lo puede mejor hacer el humano.

Es importante destacar que el contexto de los experimentos no se basa en una

única plataforma humanoide; por el contrario, tres plataformas han sido objeto de los experimentos: se han empleado los robots HOAP-3, HRP-2 y TEO.

# Acknowledgments

When I had the chance to come to the Universidad Carlos III de Madrid, I felt really free to choose among the huge quantity of different projects I could enter.

And now, after completing my PhD I consider really lucky in having made the choice to work in the Humanoid group. My supervisor, Carlos, has been a special tutor, which always supported me and gave me all the opportunities to investigate. I owe everything I learnt to him.

I would like to acknowledge my tutor Concha which guided me in a exceptional way, giving me valuable advises and correcting my non-conventional way of doing research.

I consider these years in Madrid could not be the same without the special presence of many friends, which actually – at the beginning – entered my life as colleagues. Among them, Álvaro and Fer need a special mention. Their way to face the life taught me a lot.

All the other strict collaborators in the Humanoid team – Santiviri, Boyi, Davide, George, Dani and Miguel – and in the RoboticsLab group – in particular María, Alberto, Johnny, Javi, Fabio, Raul, Cla – have always been more than simple work-mates. My (university)-life could not be so easy without the presence of Angy, Giuseppe, Fernando, Sonia and Edu. With all of them I shared a lot of “free-time”, between one experiment and another and between one meeting and another.

I would also thank Miguel Ángel and Luis which have been always tutoring me in all the possible troubles I could encounter in my university-time.

Nice discussions rose with Dolores, Mohamed, Ramón and Santiago: I learnt a lot from them, while I was their teaching assistant.

I would like also to thank the groups which hosted me during my investigation development: in special way Drs. Yokoi, Kheddar and Stasse (from JRL@AIST group) which supplied me with a great background in humanoid walking pattern generation and Drs. Lamoune, Souères and Mansard (from LAAS group) which shared their deep knowledge in humanoid control.

An important part of this research has been based on the strong collaboration established with many partners in the Robot@CWE project, among whom I would like to mention Lorenzo, who took part in many experimental setups.

Most of my research time was accompanied with the music by Banco del Mutuo Soccorso and Premiata Forneria Marconi. All the nights I was writing code or reports would not be so fruitful without their music.

Finally, I express gratitude to prof. Siciliano who opened me the doors of the charming world of robotics and to prof. Marano which introduced me to the world of the critical learning. Agostino was really a special friend who gave me valuable advises for all my research.

And last but not the least I would like to say thank you to my family. Elisa and Anna with their smiles helped me in overcoming all the stressing moments. My parents with Ilia and Luca always gave me their irreplaceable support.

While I was writing this document I heard the sad news about Dr. Vukobratović: I would like to express my gratitude also to him, who gave me a lot of inputs for this work through his papers.

# Abbreviations

**2D** Two-dimensional Space

**3D** Three-dimensional Space

**CMD** Command

**CNT** Control

**CoM** Center of Mass

**DH** Denavit–Hartenberg

**DH↔DR** Difficult for the Human, Done by the Robot and *vice versa*

**DM** Direct-Mode

**DOF** Degree of Freedom

**EE** End-effector

**EKF** Extended Kalman Filter

**F-ZMP** Fictitious Zero Moment Point

**FRI** Foot-Rotation Indicator

**HAM** Hardware Abstraction Module

**HMI** Human Machine Interface

**HOAP** Humanoid for Open Architecture Platform

**HRP** Humanoid Robotics Project

**IMU** Inertial Measurement Unit

**OpenHRP** Open Architecture Humanoid Robotics Platform

**RCP** Robot Command Protocol

**RR** Rotational–Rotational

**TEO** Task Environment Operator

**UC3M** University Carlos III of Madrid

**ZMP** Zero Moment Point

# Contents

<b>Abstract</b>	<b>i</b>
<b>Resumen</b>	<b>iii</b>
<b>Acknowledgments</b>	<b>v</b>
<b>Abbreviations</b>	<b>vii</b>
<b>1 Introduction</b>	<b>1</b>
1.1 Motivation . . . . .	5
1.2 Situation of the research in human–robot collaboration . . . . .	8
1.3 Robots collaborating with humans . . . . .	9
1.4 Objectives and approach . . . . .	15
1.5 Document organization . . . . .	16
<b>2 Literature Review</b>	<b>17</b>
2.1 Humanoid equilibrium and balance . . . . .	19
2.2 Zero Moment Point (ZMP) concept . . . . .	21
2.3 Foot–Rotation Indicator (FRI) Point and Fictitious ZMP (F–ZMP) . . . . .	22
2.4 Extensions of the ZMP concept . . . . .	23
2.5 Control and stability . . . . .	24
2.6 A taxonomy on humanoid control . . . . .	25
2.6.1 A classification based on the control techniques . . . . .	25
2.6.2 A classification based on the dynamical model of the robot . . . . .	28
2.6.3 A classification based on the type of disturbance . . . . .	29
2.6.4 A classification based on the application . . . . .	30
2.7 Chapter summary . . . . .	31
<b>3 Basic Representations</b>	<b>33</b>
3.1 Pose of a rigid body . . . . .	35
3.2 Direct kinematics . . . . .	36

3.3	Differential kinematics . . . . .	37
3.3.1	Time derivative of a rotation matrix . . . . .	38
3.3.2	Trajectory generation . . . . .	38
3.4	Reversing a kinematic chain . . . . .	39
3.5	Statics and dynamics . . . . .	41
3.6	A simple case study: the Rotational–Rotational (RR) manipulator . . . . .	42
3.6.1	A joint trajectory generation . . . . .	44
3.6.2	The double pendulum . . . . .	46
3.6.3	The reversed case . . . . .	48
3.6.4	The double inverted pendulum . . . . .	49
3.7	Full humanoid body trajectory generation . . . . .	50
3.8	The double pendulum as a model for the floating leg . . . . .	51
3.9	Floating leg trajectory generation . . . . .	58
3.10	Chapter summary . . . . .	61
<b>4</b>	<b>Humanoid Attitude Estimation</b>	<b>65</b>
4.1	Fusion of sensors estimations . . . . .	68
4.2	Extended Kalman Filter . . . . .	70
4.3	Estimation without considering real acceleration . . . . .	71
4.4	Estimation using real acceleration and mechanical flexibility . . . . .	71
4.5	Chapter summary . . . . .	78
<b>5</b>	<b>Stabilizer Architecture for a Humanoid Robot</b>	<b>81</b>
5.1	Task definition . . . . .	83
5.2	ZMP regions . . . . .	83
5.3	The full humanoid body as a composition of inverted pendulums . . . . .	84
5.4	Attitude control . . . . .	85
5.5	Static balance control . . . . .	87
5.6	Dynamic balance control . . . . .	87
5.7	Walking pattern generation . . . . .	90
5.7.1	Walking generation with velocity continuity . . . . .	94
5.8	Attitude and balance control . . . . .	97
5.9	Chapter summary . . . . .	102
<b>6</b>	<b>Human–robot Collaboration</b>	<b>105</b>
6.1	Architecture for human–robot collaboration . . . . .	109
6.2	Close collaboration . . . . .	111
6.2.1	Simulation Results . . . . .	115
6.3	Remote collaboration . . . . .	117
6.3.1	System architecture . . . . .	117
6.3.2	Shared decision–making module . . . . .	119

6.3.3	Experimental results . . . . .	121
6.4	System assessment . . . . .	122
6.5	Chapter summary . . . . .	127
<b>7</b>	<b>Conclusions and Future Works</b>	<b>129</b>
7.1	Conclusions . . . . .	131
7.2	Main contributions . . . . .	134
7.3	Future works . . . . .	134
<b>A</b>	<b>TEO Robot</b>	<b>137</b>
<b>B</b>	<b>HOAP-3 Robot</b>	<b>141</b>
<b>C</b>	<b>HRP-2 Robot</b>	<b>145</b>
<b>D</b>	<b>Humanoid Models</b>	<b>149</b>
<b>E</b>	<b>The Robot Command Protocol (RCP)</b>	<b>157</b>
	<b>Bibliography</b>	<b>165</b>



# List of Tables

3.1	DH parameters for the RR manipulator in forward chain . . . . .	43
3.2	DH parameters for the RR manipulator in reversed chain . . . . .	48
5.1	Elapsed times for the attitude and balance controllers on a dual-core 1.86GHz processor . . . . .	103
6.1	Comparison between the different interaction modalities possible in a collaborative working environment . . . . .	110
D.1	DH parameters for a humanoid floating leg (Figure D.1) . . . . .	151
D.2	DH parameters for a humanoid standing leg (Figure D.2) . . . . .	151
D.3	Dimensions for humanoid legs . . . . .	152
D.4	DH parameters for a humanoid flexible ankle (Figure D.3) . . . . .	152
D.5	DH parameters for a humanoid torso (Figure D.4) . . . . .	153
D.6	Dimensions for humanoid torso . . . . .	154
D.7	DH parameters for a humanoid arm (Figure D.5) . . . . .	155
D.8	Dimensions for humanoid arms . . . . .	156
E.1	RCP Sub-protocols . . . . .	163
E.2	RCP commands . . . . .	164



# List of Figures

1.1	ASIMO opening a bottle of water . . . . .	10
1.2	Kobian . . . . .	11
1.3	Robonaut 2 . . . . .	12
1.4	HRP-2 in a collaborative task . . . . .	13
1.5	PETMAN . . . . .	13
1.6	Requirements for different robotic systems . . . . .	14
1.7	General control scheme . . . . .	15
1.8	Thesis organization . . . . .	16
2.1	Humanoid on single-support and forces acting on the contact . . . . .	20
2.2	A taxonomy on humanoid control . . . . .	26
3.1	World and body frames . . . . .	36
3.2	Scheme of the second-order inverse kinematics algorithm [1] . . . . .	39
3.3	A simple RR manipulator . . . . .	42
3.4	A reference trajectory for the RR manipulator . . . . .	45
3.5	Joints trajectories for the RR manipulator . . . . .	45
3.6	The norm of the acceleration for the RR manipulator . . . . .	46
3.7	Jacobian and Hessian contributions . . . . .	47
3.8	Double pendulum . . . . .	47
3.9	The reversed RR manipulator . . . . .	48
3.10	Double inverted pendulum . . . . .	49
3.11	CoM reference trajectory . . . . .	51
3.12	Left foot position reference trajectory . . . . .	52
3.13	Initial to final configuration of the simulated experiment . . . . .	52
3.14	Right leg joints angles with respective angle limits . . . . .	53
3.15	Left leg joints angles with respective angle limits . . . . .	53
3.16	Waist pitch joint angles with respective torque limits . . . . .	54
3.17	Right arm joints angles with respective angle limits . . . . .	54
3.18	Left arm joints angles with respective angle limits . . . . .	55
3.19	SimMechanics <sup>TM</sup> model of the HOAP-3 robot . . . . .	55

3.20	Right leg joints torques with respective torque limits . . . . .	56
3.21	Left leg joints torques with respective torque limits . . . . .	56
3.22	Waist pitch joint torques with respective torque limits . . . . .	57
3.23	Right arm joints torques with respective torque limits . . . . .	57
3.24	Left arm joints torques with respective torque limits . . . . .	58
3.25	Full model compared with the double pendulum simplification . . . . .	59
3.26	The mean and the standard deviation of the torque of the first double pendulum joint . . . . .	60
3.27	Force measurement at the right foot . . . . .	61
3.28	Torque measurement at the left foot . . . . .	62
3.29	Force/torque sensor measurements in case of a standard trajectory . . . . .	62
3.30	Force/torque sensor measurements in case of the trajectory with via point . . . . .	63
4.1	Attitude estimation scheme . . . . .	68
4.2	Reference frames . . . . .	69
4.3	Estimation of roll angle with $\sigma(a_n) = 0.1\mathbf{I}[m/s^2]$ . . . . .	72
4.4	Estimation of pitch angle with $\sigma(a_n) = 0.1\mathbf{I}[m/s^2]$ . . . . .	72
4.5	Estimation of roll angle with $\sigma(a_n) = \mathbf{I}[m/s^2]$ . . . . .	73
4.6	Estimation of pitch angle with $\sigma(a_n) = \mathbf{I}[m/s^2]$ . . . . .	73
4.7	Estimation of roll angle with $\sigma(a_n) = 10\mathbf{I}[m/s^2]$ . . . . .	74
4.8	Estimation of pitch angle with $\sigma(a_n) = 10\mathbf{I}[m/s^2]$ . . . . .	74
4.9	Estimation of roll angle with $\sigma(a_n) = \mathbf{I}[m/s^2]$ . Robot on the crane and subjected to external pushing forces . . . . .	75
4.10	Estimation of pitch angle with $\sigma(a_n) = \mathbf{I}[m/s^2]$ . Robot on the crane and subjected to external pushing forces . . . . .	75
4.11	Roll angle estimation . . . . .	78
4.12	Pitch angle estimation . . . . .	79
4.13	Yaw angle estimation . . . . .	79
4.14	Estimation of the flexibility in the ankle . . . . .	80
5.1	Graphical example for stability regions: humanoid standing on right foot	84
5.2	Attitude control error . . . . .	86
5.3	Right leg joints angles for the attitude control . . . . .	86
5.4	Waist angles for the attitude control . . . . .	87
5.5	ZMP position for the static balance control . . . . .	88
5.6	Right leg joints angles for the static balance control . . . . .	88
5.7	Waist angles for the static balance control . . . . .	89
5.8	Right leg joints torques for the static balance control . . . . .	89
5.9	Waist torques for the static balance control . . . . .	90
5.10	ZMP position for the dynamic balance control by right standing leg . . . . .	91

5.11	Right leg joints torques for the dynamic balance control by right standing leg . . . . .	92
5.12	Waist torques for the dynamic balance control by right standing leg . . . . .	92
5.13	Position and velocity of the CoM in the lateral plane . . . . .	93
5.14	Position and velocity of the CoM in the step direction . . . . .	93
5.15	Relationship between lateral displacements and CoM height . . . . .	94
5.16	Position and velocity of the CoM in the step direction using third polynomial interpolation . . . . .	95
5.17	Position and velocity of the CoM in the lateral plane using third polynomial interpolation . . . . .	96
5.18	Attitude and balance control scheme . . . . .	97
5.19	ZMP position for the attitude and balance control . . . . .	98
5.20	Detail of the ZMP position for the attitude and balance control . . . . .	98
5.21	Attitude error for the attitude and balance control . . . . .	99
5.22	Right leg joints angles for the attitude and balance control . . . . .	99
5.23	Waist angles for the attitude and balance control . . . . .	100
5.24	Right leg joints torques for the attitude and balance control . . . . .	100
5.25	Waist torques for the attitude and balance control . . . . .	101
5.26	Right arm joints torques for the attitude and balance control . . . . .	101
5.27	Left arm joints torques for the attitude and balance control . . . . .	102
6.1	The general architecture for collaboration . . . . .	111
6.2	Modalities of the human–robot collaboration . . . . .	112
6.3	An example of a human and a robot jointly transporting a table . . . . .	112
6.4	Kinematic model of the arms . . . . .	113
6.5	Desired COM position in the horizontal plane . . . . .	116
6.6	Joint angles of the arms . . . . .	116
6.7	Position and orientation errors between left and right arm . . . . .	117
6.8	DH↔DR collaborative architecture . . . . .	118
6.9	State machine for the Shared decision–making server . . . . .	120
6.10	State machine for the Shared decision–making queue resolution . . . . .	120
6.11	Demonstration of the proposed teleoperated system on a ‘lunar scenario’ a) Robot HOAP–3 and a human operator work collaboratively on finding and moving the antenna. b) The operator teleoperates the robot with the HMI using a pocket PC. . . . .	122
6.12	Sequence of grasping operation using the techniques described in this chapter. . . . .	123
6.13	First development of the HMI . . . . .	123
6.14	New version of the HMI . . . . .	125
6.15	Real scenario at RoboticsLab . . . . .	126

6.16	The recreation of lunar scenario . . . . .	126
A.1	RH-1 and TEO platforms . . . . .	140
B.1	The HOAP-3 platform . . . . .	144
C.1	The HRP-2 platform . . . . .	148
D.1	Kinematic model for a humanoid floating leg . . . . .	152
D.2	Kinematic model for a humanoid standing leg . . . . .	153
D.3	Kinematic model for a humanoid flexible ankle . . . . .	153
D.4	Kinematic model for a humanoid torso . . . . .	154
D.5	Kinematic model for a humanoid arm . . . . .	155
D.6	HOAP-3 dynamical model . . . . .	156

# Chapter 1

## Introduction



Industrial robots started to enter the factories in the late 1970s, and even if technologies have made great strides since then, the industrial scenario has not changed a lot. Nowadays, with the help of increased computing power and improved navigation technologies, robots should move away from their simple and repetitive tasks they were at first assigned (the so-called “three D’s” — dull, dirty, or dangerous jobs).

Traditional and conventional industrial robots could only work in fixed environment and the only interaction with humans was by means of off-line task definition. All these limited characteristics entailed the image of the robots as stupid machines, limiting human acceptance towards them.

Significant ability to make independent decisions is required when a robot is asked to make varied and complex tasks, such as inspecting an underground pipeline with gaseous substances flowing in it, navigating rugged desert terrain without a driver, and even walking on muddy areas.

While consumers are warming to robots that vacuum floors and to those that play soccer, university researchers are developing robots that go beyond the same, predefined tasks performed repeatedly in exactly the same fashion. They are working in order to allow the robots to enter environments which are unpleasant or dangerous for humans to work in: it could be mentioned, for instance, space, underwater, underground or contaminated areas, and minefield.

The technology of robot distinctive elements has shown many improvements. In fact, while the first robots could rely only upon really simple sensors, which reduce the control possibility and then the complexity of the tasks, future industrial robots can exploit the Information and Communication Technology which leads to improved control and the chance of having a relatively autonomous robot (with decision making possibility). In order to improve the moving capabilities of the robot, the mechanical technology has decreased the weight of the robot, reducing also the risk of hurting a man who is interacting with it.

Traditional planning always produces plans the robotics agents are aware of and are asked to follow precisely to perform the task. But when a human agent participates as a partner in the task, his/her actions are not predictable: how the objective of a collaborative task can be realized when the robotic agents are not aware of human plans? This is an open problem that cannot be handled through a classical robotic approach.

In brief, modern robots offer a great potential, in terms of innovative opportunities and applications, to be used as agents within future collaborative working environment; however, there are still several new problems and challenges that need to be deeply considered to allow this technology to grow in a synergetic manner with our societies’ needs.

The context of this work is related to humanoid robots that could share the working environments with people and collaborate with them.

Humans are traditionally used to work in teams: starting from the “simple” case, when two humans jointly transport a table, up to more complex situations, such as in sports or associations. But which are the rules that govern the management of a team work and how is it possible that some people – each one with his/her own intentions – are able to reach a common goal?

Before thinking and defining what is intended as collaboration between a human and a robotic agent, a general definition of collaboration has to be given.

The term collaboration comes from the late Latin *collābōro* (*cum* + *laboro*, to labor together). A dictionary definition of collaboration<sup>1</sup> is:

- Collaboration: *the work and activity of a number of persons who individually contribute toward the efficiency of the whole.*

Consequently, the term collaboration implies only that two or more agents work on the same project or goal. But this definition should be contextualized and detailed in the framework of this research. In fact, this simple definition also refers to text editors people use to write: they work together in order to write a document. Whereas interaction involves only acting “on” someone else, collaboration requires acting “with”.

The collaborative task among different agents has several distinctive features that sociologists have outlined:

**Awareness:** a collaboration among different agents involves that all the agents share the same goal and they “know” they are sharing the same goal [2].

**Individuality:** when it is desired to use a collaborative-based system, it is fundamental to characterize the individual capabilities that are necessary to work together with the others [3].

**Work-division:** all the parts of the global task are covered by the agents: it means that all the agents work in conjunction in different subtasks [4].

**Responsibility:** each agent must make a significant contribution for archiving the goal. If one agent is not participating in the task, it will not actually collaborate.

**Communication:** there should be a possibility for the agents to communicate. This communication may also be implicit (without using human typical interfaces), but should be present (for instance, by means of one common object they share) [5].

**Synergy:** The synergy is one of the most important factor in the collaboration: the interaction of two or more agents should be so that their combined effect is greater than the sum of their individual effects. This also means that the common goal cannot be achieved without the presence of one of the agents.

---

<sup>1</sup><http://www.merriam-webster.com>, accessed on May 27, 2012

**Time–division:** All the agents should be working together on the task at the same time in a general sense. It does not make sense that an agent works on something to be continued by another later in time.

## 1.1 Motivation

The benefits of collaboration are well known in nature for the group survival. Several species, from social insects to vertebrates, commonly experience what the biologists define as inter–species collaboration.

The collaboration among humans has been the basis of organizations in academic research, business activities, art and so on. People tend to collaborate when there is too much work for a single agent or when they feel they can integrate different techniques in solving a problem.

Multi agent collaboration is not a new field of research, but this section tries to explain why a humanoid robot can be a convenient agent to be used in a human working environment.

From a technical point–of–view, designing robots with anthropomorphized structure can help to reuse typical tools and devices that humans are accustomed to work with [6][7]. For instance, in [8] a dynamically balancing robot with a dexterous arm designed to operate in built–for–human environments has been presented. An interesting example of remotely controlling a humanoid robot to drive an industrial vehicle has been presented in [9]. The HRP–1S was able to operate in a sitting posture a backhoe.

Additionally, humanoid robots can enter typical human environments in which simple mobile robots can hardly move [10].

From a social point–of–view, humanoid robots might be more acceptable than traditional robots. This is confirmed by a study of the impact of humanoid robots in human–life at Eindhoven University of Technology [11]. According to that study, computers and robots are treated as social actors and, consequently, they can be punished, just like human colleagues that do not actively participate for the benefit of the team’s performance. It has been shown that people behave differently towards a robot compared to interacting with a computer and, interestingly, anthropomorphic robots were praised more than other types.

As robotic systems are devoted to migrate to daily human environments (households, outdoors, etc.), it makes more sense to evoke human–robot teaming in various collaborative environment clusters, in which people and robots collaborate on tasks, sharing the same workspace and objects.

Robots can be used in order to cover human limitations or to assist them in numerous tasks. For instance, robots can go to places that are dangerous and, additionally, they can perform repetitive and mundane tasks. The oncoming future may

be characterized by humans and robot sharing the same areas, but already today we see applications for humanoid robots working in collaboration with people. Although a fully autonomous collaborative robot is far from being an imminent reality, different environments where it has been or can be introduced has to be analyzed. For instance, the introduction of a collaborative network of robots in the construction sites could lead to a substantial improvement of working conditions for humans and may potentially decrease the number of accidents and fatalities.

Rescue and security applications have always aroused great interest: the robots can replace the human in dangerous and contaminated environments and provide assistance in risky situations.

The idea behind the use of robots collaborating with humans in workplaces is that the human agent has different skills with respect to humanoid robot agents: every agent will contribute depending on their specific expertise. Robots may take part in the task through several modalities: a key-point of this research is offering different interfacing capabilities.

Humanoid robots that allow the users to perform tasks in the real world switching between continuous teleoperation and an autonomous operation have been proposed by Yokoi in [12].

There are several studies which have tried to robotize industrial vehicles to be used in dangerous work areas or adverse environments [13][14].

A humanoid robot is a potential tool to be used in areas affected by natural disasters and in construction sites. At the National Institute of Advanced Science and Technology in Japan, different applications of humanoid robots have been proposed [15], *i.e.* maintenance tasks of industrial plants, teleoperations of construction machines, and cooperative works in the open air.

Construction is certainly one of the most important European industries, but due to its harmful and difficult working conditions it is not considered as appealing for generations. The introduction of a collaborative network of robots in the construction sites could lead to a substantial improvement of working conditions for humans and may potentially decrease the number of accidents and fatalities. Moreover, since the sector is getting less attractive, the use of robots could be necessary to compensate a future lack of workforce. Various kinds of robots can operate in construction sites: flying drones for site overseeing, but also humanoid robots, as they are flexible enough to be used and reused for different tasks, and can reach zones that might be inaccessible to other robots. Finally, humanoid robots can replace humans for tedious and dangerous tasks, such as tasks in confined areas or in areas with risks of air pollution. Each robot can be connected to the same network and can be enabled to get various kinds of information (from the flying drones for example), and communicate it to human supervisors, workers or other robotic agents in order to adapt/adjust their on going plans consequently.

Anyway, the application field for humanoid robotics is not limited to civil engineering, and other industrial sectors can experience positively the presence of a humanoid robot.

Even if humanoids are designed likely to be service and/or personal robots, factories might benefit from them and they can be of use as complementary to industrial robotic systems. They will certainly have a different field of applications compared to traditional robotics, as the latter is specifically designed for one particular application. They will not for instance be as efficient as assembly robots in handling massive metal pieces in car assembly chains. On the other hand, their versatility might be of great interest for agile production lines such as cell-based factories. The main issue is to find an efficiency threshold that, if reached, might make robots more efficient than classical human-based low-cost production line. As it is very unlikely to have humanoid robots replacing completely humans in such environments, the key point is to have a very efficient collaboration between the three actors: information system-human-robots.

The main interest of robots in rescue applications is their ability to replace humans in dangerous and contaminated environments and their ability to provide assistance in risky situations. Indeed, the robot can be used as an exploratory unit to assess the degree of danger before sending humans, localize victims in needs, or to act in places where humans cannot access. The use of humanoid robots is interesting in well-structured environments even containing human beings, but they can be used in unstructured environments, too. Nevertheless, the related technology is not completed yet: mechanically, they are not robust enough to deal with difficult conditions, and from a control point of view, they are not able to cope with muddy, highly unstructured environments yet. Therefore, in unstructured environments, other types of robots, such as quadruped robots or small robots, are more suitable to explore places inaccessible to humans. However, a relevant application of humanoid robots in unstructured environments is their potential to perform physical collaboration with humans; for example, to remove and transport various objects in collaboration.

Humanoid robots are going to join also the field of space applications. Over the past five decades, space flight hardware has been designed for human servicing. But in order to achieve the increasing requirements of the space agencies, a robotic platform is needed to assist human operators during the extravehicular activities (EVAs, or spacewalks)<sup>2</sup>. The great quantity of human-oriented equipment acquired by space agencies during the past years requires only a humanoid shape. A great example for such an application is NASA JSC's Robonaut, where most of the work with Robonaut has been concerned on the teleoperation by the human agent [16]. The extra-vehicular activities are dangerous for the humans, and therefore, it becomes necessary to use a robot in substitution of an astronaut.

---

<sup>2</sup><http://er.jsc.nasa.gov>, accessed on May 27, 2012

Robots can be useful also in vigilance jobs: they can act as a guard, detecting intruders, and can easily send the gathered information using the network.

The domestic environment cannot only see robots interacting with us, but also robots working for us: they can do some domestic activities, such as transporting things from one place to another and cleaning the floor, etc.

The relevance of robotics to collaborative working environments could be envisaged through the integration of advanced robotic systems as collaborative working agents, in different working environments scenarios. This will open appealing research challenges and enormous extensions to what is traditionally understood by collaborative environments when only humans are involved.

Since robots have been expected to cooperate with humans in various fields, the humanoid robot is an excellent type of robot in order to work in human environments. To sum up, the advantages of using such a robot are:

- People accept more machines similar to them
- Humanoid robots have movements similar to humans
- Humanoids adapt better in human environments

Future robots will have raised interaction possibility and will work in dynamic environment. This means that collaborative tasks with humans are not only a dream.

## 1.2 Situation of the research in human–robot collaboration

In the robotics community little fundamental research is dedicated to the general robotic involvement in collaborative working environments. Research is rather targeted toward specific applications where collaborative working is a subsequent problematic.

In Japan, the New Energy and Industrial Technology Development Organization (NEDO) has started to push towards robotics to enter traditional human environments, such as offices and houses<sup>3</sup>.

In USA, robotics programs are also focused on many branches of robotic applications, generally traditional ones. Nevertheless there is a renewal for military robotics. In this last case, DARPA lunched several programs dealing with tactical robotics having subsequently a collaborative working context which is due to the presence of

---

<sup>3</sup>[http://www.nedo.go.jp/english/activities\\_nedoprojects.html](http://www.nedo.go.jp/english/activities_nedoprojects.html), accessed on May 27, 2012

different kind of unmanned robotic systems working in conjunction with soldiers and traditional defense systems<sup>4</sup>.

In Europe, most of the robotic programs are listed in the EURON network; research is more focused on traditional fundamental aspects of robotic systems with an emphasis toward cognition, intelligent planning and teleoperation.

Several eWorking calls and on-going projects related to collaborative environments with robots are financed under different European frameworks programmes.

The Acroboter (Autonomous collaborative robots to swing and work in everyday environment) project<sup>5</sup> aimed at developing a new technology that can effectively be used in home and/or in office environments for manipulating small objects autonomously or in close cooperation with humans.

The PHRIENDS (Physical human-robot interaction: dependability and safety) project<sup>6</sup> has mainly involved technologies of new robots which should share the environment and physically interact with people.

The objectives of the SMERobot (The European Robot Initiative for Strengthening the Competitiveness of SMEs in Manufacturing) project<sup>7</sup> were creating robots capable of understanding human-like instructions and of sharing human space.

Anyway, the research matter of this work is established in the framework of the Robot@CWE (Advanced robotic systems in future collaborative working environments)<sup>8</sup>, where the partners studied potential working agents collaborating with humans in different collaborative environment clusters. Human-centered robotics poses several challenges, such as: acceptability in the society, autonomy, interactivity, flexibility, and versatility.

## 1.3 Robots collaborating with humans

The advances in artificial intelligence and in mechanical and electronics engineering have increased the possibility of creating professional robots, *i.e.* robots that are able to work together with humans. Nowadays, robots can identify people and objects, understand human speech, and travel to a destination while avoiding obstacles. In the next few years, autonomous or semi-autonomous robots are expected to share the same working environments with humans.

Such robots are specifically designed to assist people in accomplishing specific working goals. These robots differ from industrial robots, since they are mobile, they

---

<sup>4</sup>[http://www.darpa.mil/our\\_work/DSO](http://www.darpa.mil/our_work/DSO), accessed on May 27, 2012

<sup>5</sup>[http://cordis.europa.eu/search/index.cfm?fuseaction=proj.document&PJ\\_RCN=11106167](http://cordis.europa.eu/search/index.cfm?fuseaction=proj.document&PJ_RCN=11106167), accessed on May 27, 2012

<sup>6</sup><http://www.phriends.eu>, accessed on May 27, 2012

<sup>7</sup><http://www.smerobot.org>, accessed on May 27, 2012

<sup>8</sup><http://robot-at-cwe.eu>, accessed on May 27, 2012



Figure 1.1: ASIMO opening a bottle of water

can interact with people and they are semi or completely autonomous.

Nowadays, we are still far from having a fully autonomous collaborative robot, but there is a trend of collaborative control for dynamic–autonomous robots [5][17]. Anyway, the existing work is concentrated still on the robot as an intelligent tool, but commanded by the human operator. For instance, a teleoperated robot does not rely on the notion of partnership, as elucidated in [3]. In fact, the simple case in which the robot asks for assistance in case of necessity or asks some advise to the human [18] is not a collaboration: the human operator is not collaborating but only supervising the robot.

NASA has put a lot of effort in such an area for space exploration [19]. The research for robotic systems thought to reduce human workload and danger, together with costs and risk, are nowadays matter of discussion within robotic communities.

Other companies, such as Honda<sup>9</sup>, Toyota<sup>10</sup> and Kawada<sup>11</sup> are working in order to develop robots that are supposed to share human environments.

On November 8, 2011, Honda unveiled the new ASIMO humanoid robot (Figure 1.1) equipped with autonomous behavior control technology<sup>12</sup>. The all–new ASIMO can now continue moving without being controlled by an operator. With significantly improved intelligence and the physical ability to adapt to situations, ASIMO took another step closer to practical use in an office or a public space where many people come and go.

---

<sup>9</sup><http://world.honda.com/ASIMO>, accessed on May 27, 2012

<sup>10</sup><http://www.toyota.co.jp/en/special/robot>, accessed on May 27, 2012

<sup>11</sup><http://global.kawada.jp/mechatronics>, accessed on May 27, 2012

<sup>12</sup><http://world.honda.com/news/2011/c111108A11-new-ASIMO/index.html>, accessed on May 27, 2012



Figure 1.2: Kobian

The combination of strengthened legs, an expanded range of leg movement and a newly developed control technology that enables ASIMO to change landing positions in the middle of a motion has enabled ASIMO to walk, run, run backward, hop on one leg or on two legs continuously.

WABIAN-2R (WAseda BIpedal humANoid No.2) has been designed at Takanishi Laboratory in Waseda University. Its dimensions are 1.5m in height and 64.5kg in weight, with 41 degrees of freedom (DOFs) and it has been designed in order to replicate human workspace [20]. The research related to WABIAN is focused on tasks in conditions where humans are present and collaborate with it. Recently, Takanishh Lab. has designed a new bipedal platform, named KOBIAN (Figure 1.2), which is also capable to express human-like emotions and is supposed to improve the interaction with humans [21].

Human-robot collaboration has been studied using autonomous vision-based robotic arms [22] and teleoperated humanoids, such as NASA JSC's Robonaut [23]. Robonaut<sup>13</sup> has been designed by the Robot Systems Technology Branch at NASA's Johnson Space Center together with DARPA, paying special attention for the manipulation and robotic human-like hands, which are needed to fit into all the required places and operate EVA (Extra Vehicular Activity) tools. The Robonaut control system combines operator commands, force data and kinematic algorithms with safety rules to provide real-time joint control for Robonaut. Robonaut uses several novel techniques for establishing remote control of its subsystems and enabling the human operator to maintain situation awareness. Recently, NASA and General Motors designed a new faster and more dexterous version of this robot: Robonaut 2 (Figure 1.3). Robonaut

---

<sup>13</sup><http://www.nasa.gov/audience/foreducators/robotics/home/index.html>, accessed on May 27, 2012

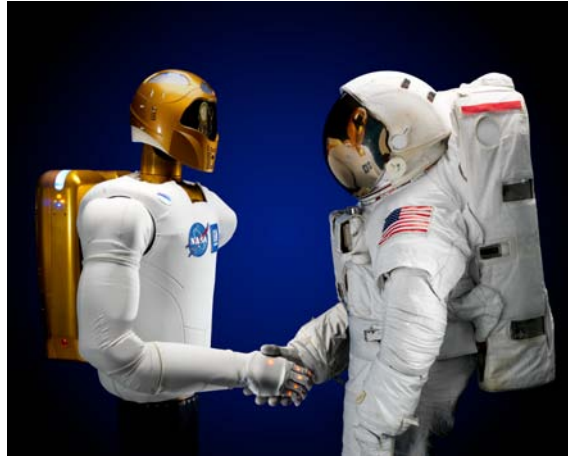


Figure 1.3: Robonaut 2

2 was moving aboard the International Space Station on October 13, 2011.

Another important platform in the field of the human–robot collaboration is, without any doubt, the HRP robot from Kawada industries [24]. A significant example of such an application is the HRP–2 driven by a controller of OpenHRP in cooperative tasks with a human, while assembling a panel onto a cottage (Figure 1.4). This is a unique example for human–humanoid collaboration.

Boston Dynamics<sup>14</sup> has recently designed an anthropomorphic robot for testing chemical protection clothing: PETMAN (Figure 1.5). PETMAN has been shown to balance itself and walking even with external disturbances.

As already described, in the framework of human–robot collaboration a key–point to take into account is the way the two agents interact. To communicate effectively with humans a robot should be able to perceive and interpret a wide range of communicative modalities and cues. Researchers are studying different types of interactive human–robot interfaces that are most meaningful and expressive for collaborative scenarios:

- gestures–based interfaces [25];
- non–verbal interfaces [26];
- sound–based interfaces [27];
- computer–based interfaces [28].

---

<sup>14</sup><http://www.bostondynamics.com/>, accessed on May 27, 2012



Figure 1.4: HRP-2 in a collaborative task



Figure 1.5: PETMAN

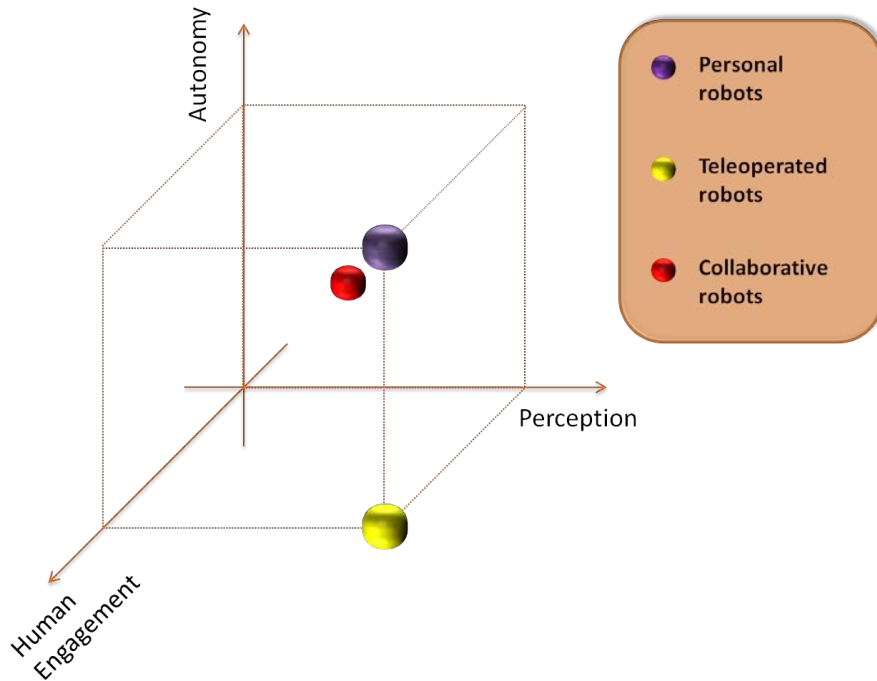


Figure 1.6: Requirements for different robotic systems

Figure 1.6 graphically explains the requirements for different robotic systems, based on the human engagement in the task, the perception capabilities and the robot autonomy.

The main characteristic of the telepresence is that a human operator needs to control the actions of a remotely operated robot.

Personal robots, even though being fully autonomous, need high perception capabilities in order to interact with a human partner, which is fully engaged for the fulfillment of the task.

Finally, collaborative robots are different from industrial robots and computers or other technology typically found in the work environment, because they are mobile, semi-autonomous and interactive. This new family of robots which now are used as service and personal robots have the potential to be used in collaborative environments with humans. In fact, nowadays, robots are not considered only mechanical devices having minimal sensorial supply: they have peculiar technology, with a complex sensor system (including vision and sound interfaces), together with possibilities of communication with other IT components, such as PDA and GPS.

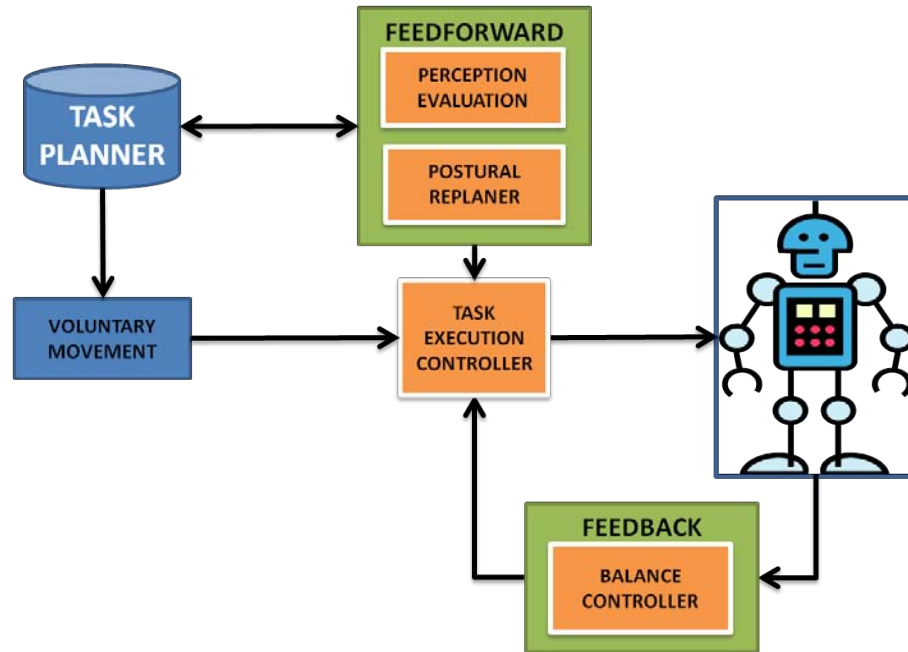


Figure 1.7: General control scheme

## 1.4 Objectives and approach

The framework of this Thesis is inserted in a general scheme depicted in Figure 1.7.

The task planner will plan a high level task to be executed by the robot based on a database (which could rely on learning algorithms) or on a quasi-off-line generator. A postural re-planner will be in charge on re-planning the input posture based on external input (a reactive action).

The task execution controller will switch between a voluntary or involuntary movement.

Finally this Thesis will be based on a postural controller which will try to balance the humanoid in specific tasks.

This study tries to be as much platform-independent as possible.

The different algorithms have been tried in different humanoid platforms:

**TEO:** a full-size humanoid robot being designed at RoboticsLab (described in Appendix A);

**HOAP-3:** a small-size commercial humanoid robot (in Appendix B);

**HRP-2:** a full-size commercial humanoid robot (described in Appendix C).

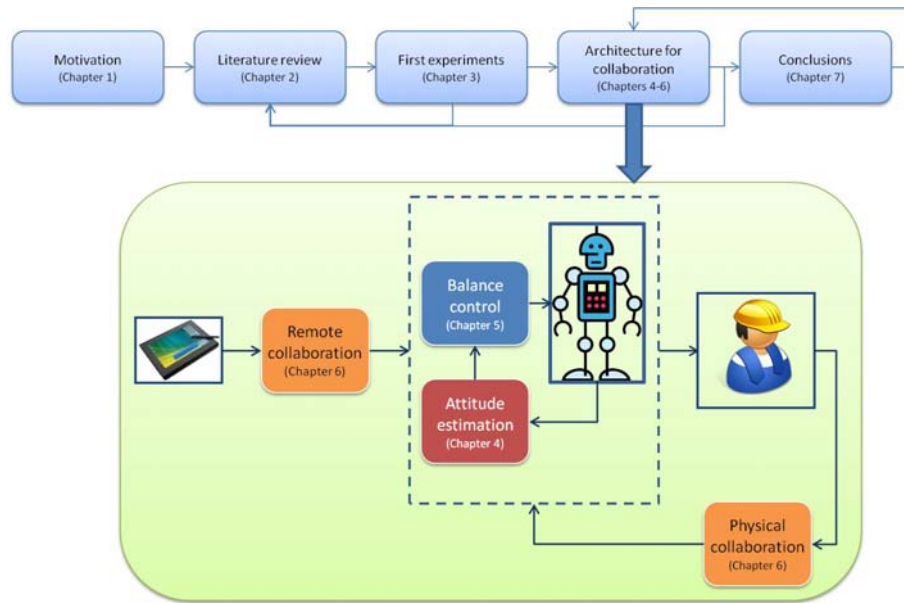


Figure 1.8: Thesis organization

## 1.5 Document organization

Figure 1.8 presents a schematic organization of this research.

Chapter 1 has given an introduction to humanoid robotics, with special emphasis to collaborative systems. The motivation and the objectives of the Thesis have also been presented.

A literature review for the balance control of humanoid platforms in response to external disturbances is presented in Chapter 2.

Chapter 3 provides with some basic representations that have been used in the research, together with some first experimental setups.

A novel attitude estimation, based on the Extended Kalman Filter, is resumed in Chapter 4.

The balance control algorithm for a humanoid robot is presented in Chapter 5. Two controllers are studied: a static and a dynamic one. The switching between one and another is also explained.

Chapter 6 describes two types of collaboration: the close collaboration and the remote one.

The concluding remarks and the possible future works are given in Chapter 7.

## Chapter 2

# Literature Review



The control of humanoid platforms which are supposed to interact with the surrounding environments including human presence is a complex task which has to be divided.

This section will initially provide an introduction of basic humanoid balance control: the definition of essential concepts such as the Zero Moment Point (ZMP) and its extensions are introduced.

The balance control of a humanoid platform is not a new field of study among robotics researchers. This chapter will try to give a taxonomy on the humanoid control based on the different control techniques which can be found in literature. The classification will be focused on the model of the robot, on the type of the disturbance affecting the robot and finally, on the final application.

## 2.1 Humanoid equilibrium and balance

One of the most important and complex tasks for a humanoid robot is to avoid overturning during a bipedal gait. To prevent the humanoid from falling during a walk, a necessary and sufficient condition is to ensure that the foot-ground contact in each instant is a surface and not a line or a point [29].

One basic concept when talking about the balance of a human/humanoid is the support area. In the particular case of rectangular-shaped foot, it has been defined also as support polygon. When only one foot is touching the ground (single-support phase), the support area is represented by the area of the foot which is actually in contact with the ground. On the contrary, when both feet are simultaneously on the ground (double-support phase), the support area is a convex area determined by the areas of the feet and the ground and common tangents, so that the encompassed area is maximized.

In this work the term “balance” is used in the sense of “maintaining an upright position of the overall humanoid” and a humanoid gait is dynamically balanced if there is no rotation of the supporting foot (or feet) about its (or their common) edge during walking. Dr. Miomir Vukobratović [29] distinguishes between balance and equilibrium (considering the D’Alembert’s principle). The D’Alembert’s principle states that the resultant of the external forces and the kinetic reaction acting on a body equals zero (condition of kinetic equilibrium).

When the humanoid is falling since it is rotating about one foot edge, the D’Alembert’s principle still holds for a point on the foot edge where the pressure force acts. Anyway, this case cannot be contemplated as balanced in the sense of the definition previously provided.

In order to get the equations for the equilibrium in a humanoid, let us consider the case on single-support (Figure 2.1). The field of pressure forces (normal to the sole) is equivalent to a single resultant force, exerted at the point where the resultant

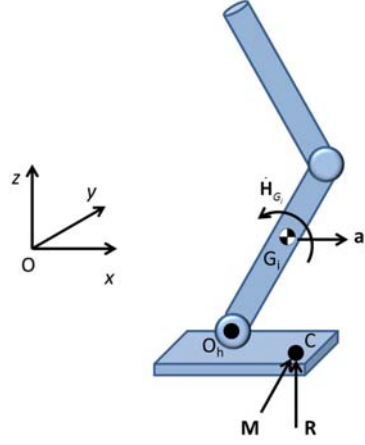


Figure 2.1: Humanoid on single-support and forces acting on the contact

moment is zero. This point is called Center of Pressure (CoP) [30] and is denoted by the symbol  $C$  in the Figure 2.1. If the entire biped robot is viewed as a system subjected to external forces/torques, such forces are acting at the CoP.

In order to get the conditions for the equilibrium, D'Alembert's principle may be applied. The equation for rotational dynamic equilibrium is obtained by noting that the sum of the external moments on the robot, computed either at any stationary reference point, is equal to the sum of the rates of change of angular momentum of the individual segments about the same point. Taking moments at the origin  $O$ , it is [31]:

$$\mathbf{M} + {}^O\mathbf{p}_C \times \mathbf{R} + \sum {}^O\mathbf{p}_{G_i} \times m_i \mathbf{g} = \sum \dot{\mathbf{H}}_{G_i} + \sum {}^O\mathbf{p}_{G_i} \times m_i \mathbf{a}_i \quad (2.1)$$

where  $m_i$  is the mass of the generic  $i$ -th link,  ${}^O\mathbf{p}_{G_i}$  is its CoM location,  $\mathbf{a}_i$  is its CoM linear acceleration, and  $\mathbf{H}_{G_i}$  is the angular momentum about such CoM. The vector  ${}^O\mathbf{p}_C$  connects the inertial reference system and the CoP.

If the effects of the entire humanoid robot on its standing foot are resumed as a couple force  $\mathbf{F}_H$  and torque  $\mathbf{M}_H$  acting on the point  $O_h$ , the dynamic equilibrium equation of the foot is

$$\mathbf{M} + {}^O\mathbf{p}_C \times \mathbf{R} + {}^O\mathbf{p}_{G_f} \times m_f \mathbf{g} + \mathbf{M}_H + {}^O\mathbf{p}_{O_h} \times \mathbf{F}_H = \dot{\mathbf{H}}_{G_f} + \sum {}^O\mathbf{p}_{G_f} \times m_f \mathbf{a}_f \quad (2.2)$$

where  $m_f$  is the mass of the foot,  ${}^O\mathbf{p}_{G_f}$  is the foot CoM location,  $\mathbf{a}_f$  is its CoM linear acceleration, and  $\mathbf{H}_{G_f}$  is the angular momentum about such CoM. The vector connecting the origin  $O$  and the point  $O_h$  is  ${}^O\mathbf{p}_{O_h}$ .

In static conditions (dynamic terms are zero), Equation (2.2) becomes:

$$\mathbf{M} + {}^O\mathbf{p}_C \times \mathbf{R} + {}^O\mathbf{p}_{G_f} \times m_f \mathbf{g} + \mathbf{M}_H + {}^O\mathbf{p}_{O_h} \times \mathbf{F}_H = 0 \quad (2.3)$$

If Equation (2.3) is applied at the stationary point  $C$ , it reduces to:

$$\mathbf{M} + {}^O\mathbf{p}_{G_f} \times m_f \mathbf{g} + \mathbf{M}_H + {}^O\mathbf{p}_{O_h} \times \mathbf{F}_H = 0 \quad (2.4)$$

## 2.2 Zero Moment Point (ZMP) concept

The standing foot/feet of a humanoid robot cannot be controlled directly but in an indirect way, by ensuring the appropriate dynamics of the mechanism above. Actually, the contact between the foot and the ground can be considered as an additional passive DOF [32].

This contact is responsible for a possible loss of the balance, but it is essential for the walk realization because the mechanism's position with respect to the environment depends on the relative position of the foot/feet with respect to the ground.

One way of tackling the problem of the balance is to find a unique indicator, which can be chosen as the point where the influence of all forces acting on the mechanism can be replaced by one single force. At the third All-Union Congress of theoretical and applied mechanics in Moscow in January 1968, and at the first international IFAC Symposium on technical and biological control problems in Yerevan in September of the same year [33][34], two papers entitled "Contribution to the Synthesis of the Biped Gait" were presented. In such papers the problem of finding a special point at which the dynamic reaction force influences the mechanical system was introduced, even if a formal definition of the ZMP was given only in the subsequent papers by Vukobratović and co-authors [35][36].

During the human gait, there is a point on the foot-ground contact-region in which – at all the times – the resulting dynamic reaction of the biped system is acting: such point is named ZPM.

In order to give a formal definition of the ZMP, the situation of a single-support on one foot is considered. Let us introduce a Cartesian frame with the origin at the mentioned point where the resultant pressure force is acting, the two axes ( $x$  and  $y$ ) being tangential to the ground and the third ( $z$ ) being normal. Now, Equation (2.4) can be written as [32]:

$$\begin{cases} \mathbf{M}_x = 0 \\ \mathbf{M}_y = 0 \end{cases} \quad (2.5)$$

The moments include gravity, inertial forces and other external forces acting on the humanoid body (such as wind, strike, etc.). Such conditions define the balance of the humanoid, but a third condition ( $\sum M_z = 0$ ) can be important for keeping the direction of the walking task in the case of insufficient friction between the foot and the ground [32].

The ZMP is the point on the support area (excluding the edge) for which the conditions (2.5) are satisfied. Since both relevant components to the realization of dynamic balance are equal to zero, a natural choice to name this point was ZMP.

Vukobratović [29] explains the difference between the CoP and ZMP: the CoP and ZMP coincide only when they are inside the support area. In fact, when the ZMP comes to the edge of the support area, the humanoid comes into a non-balanced motion and falls down. In such a case, the concept of ZMP does not make sense, but the CoP still exists. It is important to point out that, in the theoretical case of infinitely rigid links, it could be possible to keep the balance in a point infinitely close (from the inner side) to the edge.

### 2.3 Foot–Rotation Indicator (FRI) Point and Fictitious ZMP (F–ZMP)

From a mathematical point of view, the position of the point calculated by Equation (2.4) could reside outside the support surface. In fact, the idea proposed by Goswami [37] is that one can still find a point outside the support surface which satisfies the equilibrium conditions. Such a point was called the FRI (Foot–Rotation Indicator) point, and is defined as the point on the foot/ground contact surface, inside or outside the convex hull of the foot–support area, at which the resultant moment of the force/torque impressed on the foot is normal to the surface. By “impressed force/torque”, the author means the force and torque at the ankle joint, other external forces, plus the weight of the foot, and not the ground–reaction forces.

The FRI point can be used as a sign of the occurrence of foot rotation. Once the FRI is outside the support area, it indicates the magnitude of the unbalanced moment on the foot.

According to Goswami, the FRI point indicates the stability margin of the robot. The stability margin of a robot against foot rotation may be quantified by the minimum distance of the support polygon boundary from the current location of the FRI point within the footprint.

On the other hand, Vukobratović [29] claims that even if the mathematical solution to Equation (2.4) can result in a point which could be either inside or outside the support area, the solutions have different meanings and should have different names. In fact, due to its definition, ZMP can exist only within the support polygon.

In the situation when the mechanism dynamics changes so that the ZMP approaches the support polygon edge (in either single–support or double–support phases), the corresponding point will remain the ZMP only if no additional moments are acting at this point.

But if an additional moment appeared, the locomotion mechanism would start to

rotate about the foot edge and the mechanism would collapse. In such a situation, the acting point of ground reaction force would be on the foot edge, but this point would not be ZMP any more, since both conditions (2.5) would not be fulfilled simultaneously. Consequently, he suggests to denote the point as Fictitious ZMP [32], when the solution to Equation (2.4) is outside the support area.

## 2.4 Extensions of the ZMP concept

One of the major problems of the ZMP/FRI criteria is that these concepts are very focused on the specific case in which legged robots walk on a flat plane with a sufficient friction.

Many authors have tried to adopt other concepts that can be used when the robot is on a rough terrain or on an inclined plane.

For instance, Yoneda and Hirose [38] discussed the stability of manipulation and locomotion robots on general topography including irregular terrain. They introduced the concept of “tumble stability”, which focuses on passing through a two point support state which always happens when a manipulation and locomotion robot tumbles, and ask whether it will recover to the stable side or tumble from that state.

The problem of the balance when the robot is interacting with the environment is still an open issue. Kagami *et al* [39] proposed an algorithm based on the concept of enhanced ZMP, which enables calculating the robot stability even if several limbs are attached to the environment. In fact, considering that a humanoid robot has four limbs, the body may be supported by many points. Therefore, they consider the case in which the supporting points are placed both in only one inclined plane with respect to the ground plane and in several planes. The balance is achieved if at least one of them satisfies the ZMP constraints. A similar approach is used in [40]. The authors define a local ZMP at each contacting hand or foot.

In the paper by Harada *et al* [41], the balance of a humanoid robot during manipulation tasks is studied. They introduced the concept of Generalized Zero Moment Point (GZMP): when the robot hand does not contact the environment, the GZMP is equivalent to the CoP of the foot-ground contact. However, when the hand contacts the environment, the GZMP is different from the CoP of the foot-ground contact, and may exist outside of the foot-supporting area. After obtaining the region of the GZMP for keeping balance by considering both the infinitesimal displacement and the moment about the edges of the 3-D convex hull of the supporting points, the authors demonstrate the effectiveness of the proposed approach by simulation.

In 2003 Saida *et al* [42] proposed a new criterion for multi-legged robots. The FSW (Feasible Solution of Wrench) gives the feasible condition even on the mushy terrain from the viewpoint of “wrench” – a special representation of force screw. Three years later, Hirukawa *et al* [43] showed the validity of such a model. The

proposed method checks if the sum of the gravity and the inertia wrench applied to the CoM of the robot, which is proposed to be the stability criterion, is inside the polyhedral convex cone of the contact wrench between the feet of a robot and its environment.

## 2.5 Control and stability

In reality, while realizing the motion of the humanoid (like any other dynamical system), some disturbances will affect the fulfillment of the task. This will produce a deviation from the reference motion of the robot. Such a deviation may move the ZMP from the desired position. As explained before, if the ZMP comes close to the edge of the support area, the balance of the humanoid is undermined. The objective of the control in the humanoid framework is to guarantee the tracking of the reference for the powered joint while at the same time preserving dynamic balance.

Clearly, depending on the intensity of the disturbance, the control action could change. In effect, a small disturbance can be simply overcome by a correct choice of the reference, which could set the desired position of the ZMP far away from the limits of the support area.

But, when the disturbances come stronger, such strategy may not be sufficient. In that case, in a walking task, the ZMP position may be recovered first by the upper part of the robot (which is not directly involved in the task). If this is still not enough, one should stop the execution of the main task (for instance, the locomotion) and actuate on the whole robot in order to recover the dynamic balance. The paper by Vukobratović [29] explains some basic issues about that.

Let us consider some important features of a biped locomotion which make a point on the control:

- There is a presence of unpowered DOFs.

This has to be taken into account since the contact of the foot with the ground should be controlled through the active joints of the standing foot/feet.

- The dynamic balance may be achieved without realizing the planning motion.

When talking about balance, it is important to stress out that this does not mean stability. The robot can achieve a balance even if disturbances affect the planned motion.

- An impact appears when the robot passes from the single-support to the double-support.

The impact appearing at such a transition cannot be modeled exactly and a disturbance occurs.

- The motion is not continuous: there is a time limitation in the single-support phase.

This means that even if the ZMP is moving out of the support area, the robot would pass to a double-support in a limited time, recovering its balance. This time has to be considered.

One important definition of stability related to biped locomotion is the practical stability [29][44][45].

## 2.6 A taxonomy on humanoid control

The motion control for humanoid robots is a really multi-faceted subject. In this section a taxonomy for the humanoid control is given and several classifications are presented, as depicted in Figure 2.2.

A first classification is given on the basis of the control technique adopted by the author.

The humanoid robot is a complex dynamical system. Many authors have used different models to handle the control: a classification based on the model is also proposed.

Then, the different ways in which authors describe the disturbances are considered for classification.

Finally, a classification based on the final application of the robots is presented.

### 2.6.1 A classification based on the control techniques

The simplest approach to the control of a biped is the linear control. A PD controller is used to track joints trajectories, after linearizing the equation of the robot in in single-support phase [46][47].

Control algorithms based on the computed-torque control [48] and hybrid impedance/computed-torque control [49] have been proposed. An impedance control for supporting the feet or hands allowing the robot to adapt to low-friction ground without prior knowledge of the ground friction is considered in [50].

Jung-Hoon and Jun-Ho [51] presented three online controllers for maintaining dynamic balance of a humanoid robot using a force-torque sensor placed in the ankle: damping controller, landing orientation controller and landing position controller.

Okumura *et al* [52] presented a real-time ZMP compensation method using adaptive inertia force compensation. The proposed controller was implemented on the humanoid robot Morph3.

A hybrid force/position control in task space together with an inner joint position control loop is proposed by Lohmier *et al* [53]. The contact force trajectories are

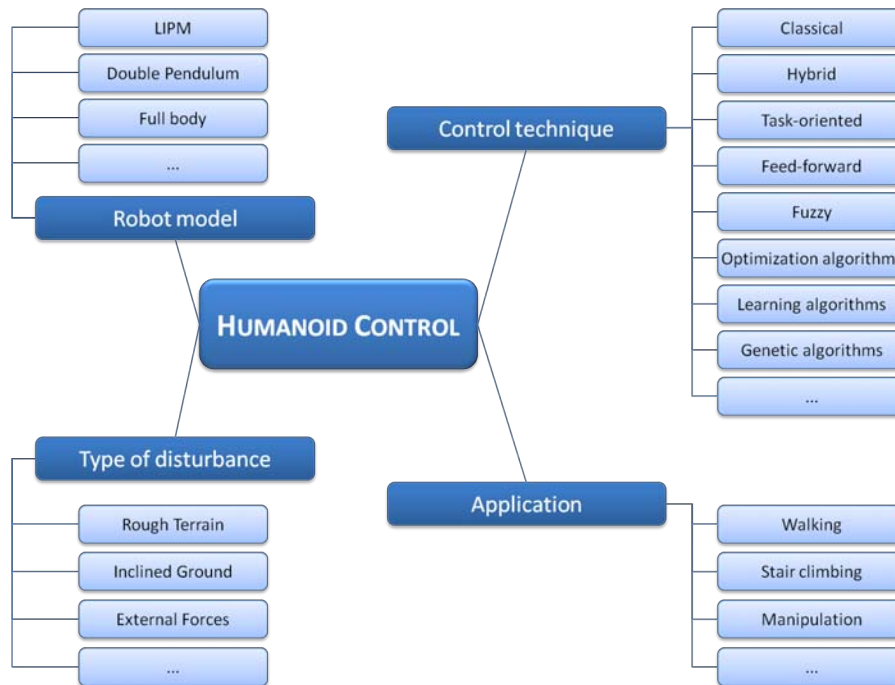


Figure 2.2: A taxonomy on humanoid control

modified in an outer control loop to provide inertial stabilization. The method uses a kinematic model of the robot describing the dependency of the workspace trajectories on the generalized coordinates. The workspace trajectories include relative positions of the feet with respect to the CoM, and the orientation of the feet with respect to the upper body.

A control method based on impedance control and impedance modulation has been proposed in [54].

An approach for the force control of legged locomotion close to grasping and manipulating an object in a multi-fingered hand has been faced in [55].

Inverse kinematics algorithms for floating base structures to achieve task space control on a real humanoid robot have been presented in [56]. The same authors in [57] show how to compute inverse dynamics torques for such a model.

Miura and Shimoyama [58] proposed a control focused on the function of foot placement feedforward control. They applied such control to their BIPER series robots approximating the robot motion during the single-leg support phase by an inverted pendulum.

Similarly, Hodgins and Raibert [59] studied the case of adjusting step length for rough terrain locomotion. The authors compare the performance of three different methods for controlling step length. Each method adjusts a parameter of the running

cycle, leaving the others set to nominal values. The parameters were forward running speed, running height, and duration of ground contact. According to the study, the forward speed method produced the widest range of step lengths.

Fuzzy control have also been used. For instance, Cocaud and Jnifene [60] showed the feasibility of using fuzzy logic to stabilize a biped during the dual-support phase. Taking the angular position and the angular velocity for each joint as inputs, the controller used a rule-base implemented with five membership functions to control the output torques. The proposed fuzzy control was used to allow the biped robot recover from a loss of balance defined by a pre-defined initial posture. The controller is composed of two parts. The first one corresponds to a high-level fuzzy controller that evaluates the current robot configuration in terms of the position of its CoM within the support area. The second part is a low level fuzzy controller that takes care of evaluating the output torques of the six joints based on the desired position and velocity of each joint.

Many authors proposed optimal control methods for the biped locomotion. A quadratic programming to control the posture, considering the physical constraints of the reactive force/torque on the foot has been proposed in [61]. Napoleon *et al* [62] proposed a controller design based on Linear Quadratic optimal control by considering output evaluation. Westervelt and Grizzle [63] proposed an optimization process which uses a sequential quadratic programming algorithm, able to satisfy kinematic and dynamic constraints while approximately minimizing energy consumption and ensuring stability.

The idea of dividing regular gaits in several phases was firstly considered by Sano and Furusho [64]. The authors considered a walking type of locomotion which consists of three phases containing a tiptoe-rotation phase. In their work, the motion of the robot was divided into the sagittal plane and the lateral plane. For the motion in the sagittal plane, a control method was proposed in which the angular momentum of the walking system is feedback-controlled. In single-support phase, the desired angular momentum function is designed based on the changes in the angular momentum of an inverted pendulum. The angular momentum is controlled by the ankle torque of the supporting leg. They used an Inertial Measurement Unit (IMU) and a torque sensor placed in the ankle.

A Virtual Model Control, which simulates virtual mechanical components to generate real actuator torques, has been used in [65] in order to control height, pitch angle and speed through the swing leg: the authors used a state machine in order to control Spring Flamingo during walking.

Choi *et al* [66] suggested a posture/walking control scheme divided as the kinematic resolution of CoM Jacobian with embedded motion and ZMP/CoM control. Experiments were presented in order to show the stability and robustness of humanoid motion control system to unknown disturbances. A kinematics-based approach was

presented by Wollher and Buss [67]: the Jacobi compensation to modify precalculated step trajectories for a humanoid robot. The authors propose to modify precalculated gait trajectories in order to compensate the errors or adapt the trajectories to make them applicable to situations other than those they have been computed for.

Sugihara [68][69] studied the balancing of humanoid robots by the combination of two kinds of absorption of disturbance. In the first phase, the referential CoM displacement is decided in accordance with both the short-term and the long-term absorption of disturbances. And in the second phase, the CoM is manipulated with the whole-body cooperation, using the CoM Jacobian.

Learning algorithms were used by Ogata *et al* [70]. A successful application of such techniques was presented in [71]: the authors proposed a two-stage learning approach to control a stairclimbing gait. Such gait is parameterized by the swing foot trajectory, hip joint trajectory, and torso angle trajectory; the selection of the gait parameters is formulated as a constrained nonlinear optimization problem with available optimization tools. The sensory controller consists of the torso attitude controller, ZMP compensator, and impact reducer. The parameters of these controllers are automatically regulated in each step by a two-stage policy gradient reinforcement learning method.

Genetic algorithms and recurrent neural networks were used to select the best postural configuration, using the ZMP as stabilization index [72].

Many authors [73][74][75][76] discussed methods to plan an off-line walking pattern, based on a complex humanoid model, and then, modify it in real-time based on sensor feedback.

A task-oriented control through prioritization [77] has been used to accomplish task proximities at the same time as physical constraints.

## 2.6.2 A classification based on the dynamical model of the robot

Many researchers have used simplified models to represent the complex dynamics of a humanoid. Some researchers focus on simple models that correspond to a lumped mass model at the CoM [78][79][80].

The most notable of these models is the Linear Inverted Pendulum Model (LIPM), which is a linear model due to the assumption that the height of the CoM is constant. Sometimes these lumped mass models are modified to include a rotational inertia term that models angular momentum, which can add significant capability to the system [81][82][83][84].

Miura and Shimoyama [58], Lohmier *et al* [53], and Fujimoto and Kawamura [61] approximated the robot motion during the single-leg support phase by an inverted pendulum. A simple inverted pendulum model with compliant joint is proposed in

[51]. Also Choi *et al* [66] simplify the walking related dynamics of bipedal robot as the equation of motion of a point mass concentrated on the position of the CoM.

Napoleon *et al* [62] proposed a two mass inverted pendulum model to be used to design a controller which allows tracking the desired position of the ZMP.

The study in [70] uses the three-dimensional Linear Inverted Pendulum Mode (3D-LIPM).

A full robot model is used in [85][86], where the authors used a full-body passivity-based force-level balancing control strategy incorporating gravity compensation.

Takubo *et al* [87] also use a full-body model, introducing the concept of Complement Zero Moment Point (CZMP) (the projection of the CoM). They use the CZMP for the modification control of the CoM with balancing control by assuming the statical balance.

Park [54] used the Gravity-Compensated Inverted Pendulum Mode (GCIPM) to generate the base-link trajectory not only for single-support phases but also for double-support ones.

One of the first studies on the control using a complete model was done by Chow and Jacobson [88]. The generation of gait patterns via optimal programming was studied in that paper.

### 2.6.3 A classification based on the type of disturbance

Like in any control system, controllers are required to guarantee satisfactory performance in the presence of disturbances and model uncertainty. As is well known, most controllers in use today employ some form of negative feedback. This is the reason why a sensor is needed to measure the controlled variable and compare its behavior to a reference signal.

The disturbance signal can be simply modeled as a constant variable or can be modeled as stochastic variables (mostly known as noise). In this case, the controller can make an estimation of the disturbance and use it in the control law in order to cancel the error with the reference.

The control in response to external forces (without being measured) is considered by Hyon *et al* [85][86]. The method identifies a desired applied force from the robot to the environment, such as antigravitational force, which is distributed optimally over the forces acting at arbitrary contact points, and which is then transformed directly into whole-body joint torques. The balancing experiments on a real hardware platform under unknown external forces demonstrated the effectiveness of the method.

Hwang *et al* [89] study whole body motions of a humanoid robot for heavy works. The drawback of such approach is that all the postures they evaluate are based only on the the static balance of the robot.

Hyon [50] demonstrated the applicability of contact force control framework presented in [86] to unknown external forces and rough terrain. Adaptation to uneven ground is achieved by optimally distributed antigravitational forces applied to preset contact points in a feedforward manner. Adaptation to unknown inclination is also possible by combining an active balancing controller based on the CoM measurements with respect to the inertial frame.

#### 2.6.4 A classification based on the application

Several control techniques have been proposed which try to control the robot while it is completing a task related to a particular application. The most common and most studied application for humanoid robots is, beyond a doubt, the standard gait.

Anyway, researchers have been designing controllers which try to balance the robot in different situations.

For instance, the validity of the method proposed in [71] was confirmed by stair-climbing experiments of an actual 32-DOF humanoid robot. Whole Body Cooperative Tasks are considered in [89]. Control on rough terrain is considered in [50]: the robot could adapt to uneven ground and inclination.

Nishihama *et al* [90] proposed a control method for humanoid robots of mobile manipulation. The robot controls its body pose and steps so that manipulability of both arms and robot stability can increase, coordinating with the motion of both hands for performing objective tasks. Because of the vibration caused by the impact of foot landing and the slip of the feet, the accuracy of the hand positions and robot stability decrease. For this problem, the robot measures real hand positions and body orientation with its camera and gyroscope. Then, the hand positions errors are transformed into correcting joint angles of the arms using arm Jacobian matrices. Adding the calculated joint angles to the desired joint angles of the arms, the arms can compensate the hand positions. New desired joint angles of the legs are calculated by inverse kinematics from real foot positions and desired shoulder position. Adding the correcting joint angles to the desired joint angles of the legs, the legs can compensate the shoulder position, thus increasing robot stability. The effectiveness of the proposed method is ascertained only by simulations.

Ogata *et al* [70] developed two falling detection methods, using the abnormality detection method. The authors have treated only periodic walking motion.

The controller by Takubo *et al* [87] responds to external forces acting on the end-effectors by the modification control of the CoM position.

The balance of a humanoid robot during manipulation tasks was extensively studied by Harada *et al* [41][91][92][93].

A real-time control method for a humanoid in mobile manipulation, doing tasks with its arms while moving, is proposed in [94].

## 2.7 Chapter summary

This chapter has introduced the definition of several meaningful concepts in the field of humanoid control. Even if there are many different further contributions, this work will be based on the ZMP concept. Finally, several classifications of the humanoid control have been presented. The related literature has been organized on the base of the adopted control technique, the further simplifications of the humanoid dynamical model, the analyzed type of disturbance, and the desired application. There is no general control technique which is able to react to any kind of disturbance or usable for different applications.



## Chapter 3

# Basic Representations



This chapter introduces basic tools for the solution of the problem analyzed in the Thesis.

After presenting the mathematical representation of the direct, inverse and differential kinematics and dynamics modeling for open-chain robotic systems, a trajectory reference for such manipulators is analyzed.

Thenceforth, several simplified models for a humanoid robot are shown. In particular, a double pendulum will be used to simplify a floating leg model in one plane. This simplified model will be used in order to generate a trajectory for the swinging leg which will reduce the dynamical effects upon the CoM.

### 3.1 Pose of a rigid body

The pose of an object is referred to as the combination of position and orientation. It completely describes a rigid body in the space with respect to a reference frame.

Let an inertial frame fixed to the world be  $\mathcal{W}$  and a body-fixed frame attached to the body be  $\mathcal{E}$ , as in Figure 3.1.

The position of the origin of  $\mathcal{E}$  with respect to  $\mathcal{W}$  can be represented by vector  $\mathbf{p} \in \mathbb{R}^3$ . On the other hand, in order to define the orientation of a body with respect to the base frame, there are several possibilities. One way is using the rotation matrix.

If  ${}^w\mathbf{R}_e$  denotes the rotation matrix of frame  $\mathcal{E}$  with respect to frame  $\mathcal{W}$ , then the relation  ${}^w\mathbf{p}_0 = {}^w\mathbf{R}_e {}^e\mathbf{p}_0$  holds between points in both frames, where vectors  ${}^w\mathbf{p}_0$  and  ${}^e\mathbf{p}_0$  denote the position of the point  $\mathbf{p}_0$  in frames  $\mathcal{W}$  and  $\mathcal{E}$ , respectively.

The above defined rotation matrix belongs to the special orthonormal group  $SO(3) \subset \mathbb{R}^{3 \times 3}$ , that is:

$$SO(3) = \{\mathbf{R} \in \mathbb{R}^{3 \times 3} : \mathbf{R}^T \mathbf{R} = \mathbf{I}, \det(\mathbf{R}) = 1\} \quad (3.1)$$

A minimal orientation representation  $\boldsymbol{\chi}$  of a frame with respect to another can be obtained by using a set of three angles (Euler angles). In this work the orientation is visually represented by the Roll-Pitch-Yaw (RPY) angles:

$$\boldsymbol{\chi} = [\phi, \theta, \psi]^T \quad (3.2)$$

In this case, the roll ( $\phi$ ), pitch ( $\theta$ ) and yaw ( $\psi$ ) angles, expressed in the fixed frame  $\mathcal{W}$ , represent the rotations around the axes  $x$ ,  $y$  and  $z$ .

If  $\mathbf{R}_Z(\psi)$  is the rotation along axis  $z_w$ ,  $\mathbf{R}_Y(\theta)$  is the rotation along axis  $y_w$  and  $\mathbf{R}_X(\phi)$  is the rotation along axis  $x_w$ , such orientation can be defined as [1]:

$$\begin{aligned} \mathbf{R}_{RPY} &= \mathbf{R}_Z(\psi) \mathbf{R}_Y(\theta) \mathbf{R}_X(\phi) = \\ &= \begin{bmatrix} c_\theta c_\psi & c_\psi s_\theta s_\phi - c_\phi s_\psi & s_\phi s_\psi + c_\phi c_\psi s_\theta \\ c_\theta s_\psi & c_\phi c_\psi + s_\theta s_\phi s_\psi & c_\phi s_\theta s_\psi - c_\psi s_\phi \\ -s_\theta & c_\theta s_\phi & c_\theta c_\phi \end{bmatrix} \end{aligned} \quad (3.3)$$

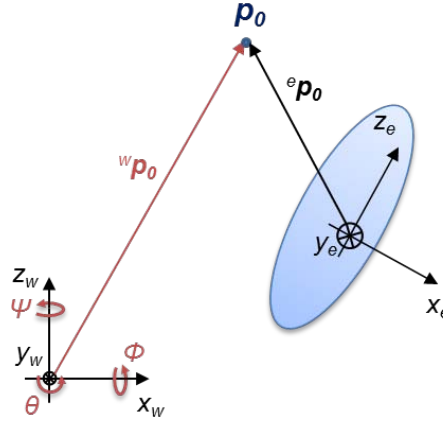


Figure 3.1: World and body frames

Anyway, in the algorithms used in this research, the well-known representation singularities of the Euler angles are overcome by the use of the quaternions. A quaternion  $\chi$  is a quadruple of real numbers and is defined by a scalar  $\eta$  and a 3D vector  $\epsilon$  [95]:

$$\chi = [\eta, \epsilon] \quad (3.4)$$

Normally, quaternions are associated to a rotation of an angle around an axis.

## 3.2 Direct kinematics

The direct kinematics relates joint space variables to operational space variables. For an  $n$ -DOF manipulator, the direct kinematics  $\mathbf{f}(\mathbf{q})$  relates a vector of joint variables  $\mathbf{q} \in \mathbb{R}^n$  to coordinate frames of interest, which in most cases is the frame of the so-called end-effector (EE):

$$\mathbf{x} = \mathbf{f}(\mathbf{q}) \quad (3.5)$$

In general  $\mathbf{x} \in \mathbb{R}^m$ , and its minimal representation for a full pose specification is  $\mathbf{x} \in \mathbb{R}^6$ .

The direct kinematics from the world frame  $\mathcal{W}$  to the frame  $\mathcal{E}$  can be represented through the homogeneous transformation matrix:

$$\mathbf{f}(\mathbf{q}) = {}^w\mathbf{T}_e(\mathbf{q}) = \begin{bmatrix} {}^w\mathbf{R}_e(\mathbf{q}) & {}^w\mathbf{p}_e(\mathbf{q}) \\ \mathbf{0}^T & 1 \end{bmatrix} \quad (3.6)$$

Such matrix belongs to the special Euclidean group  $SE(3) = \mathbb{R}^3 \times SO(3)$ .

The Denavit and Hartenberg (DH) convention permits to calculate this matrix in a consistent way.

A minimal representation of the orientation through, for instance, RPY angles would be defined as  $\mathbf{x}(\mathbf{q}) = [ {}^w\mathbf{p}_e(\mathbf{q}) \quad {}^w\boldsymbol{\chi}_e(\mathbf{q}) ]^T$ .

### 3.3 Differential kinematics

The nonlinear mapping  $\mathbf{f}(\mathbf{q})$  can be linearized using its first partial derivative, the analytical Jacobian matrix:

$$\dot{\mathbf{f}}(\mathbf{q}) = \mathbf{J}_A(\mathbf{q}) \dot{\mathbf{q}} \quad (3.7)$$

The analytical Jacobian is computed via differentiation of the direct kinematics function with respect to the joint variables, when the EE pose is expressed with reference to a minimal representation in the operational space:

$$\mathbf{J}_A(\mathbf{q}) = \frac{\partial \mathbf{f}(\mathbf{q})}{\partial \mathbf{q}} \quad (3.8)$$

It is important to note that computing the analytical Jacobian  $\frac{\partial \boldsymbol{\chi}(\mathbf{q})}{\partial \mathbf{q}}$  of the orientation is not straightforward, since the function  $\boldsymbol{\chi}(\mathbf{q})$  is not usually available in direct form, but requires computation of the elements of the relative rotation matrix [1].

For this reason, the differential kinematics, referred to as the relationship between the joint velocities and the corresponding EE linear and angular velocity, may be described by the geometric Jacobian matrix  $\mathbf{J}$ , which depends on the manipulator configuration. The geometric Jacobian can be calculated in closed form in a systematic way on the basis of direct kinematics relations as explained in [1]. The geometric Jacobian in general differs from the analytical one. The relationship between these two Jacobians is  $\mathbf{J} = \mathbf{T}_A(\boldsymbol{\chi}) \mathbf{J}_A(\mathbf{q})$ , where

$$\mathbf{T}_A(\boldsymbol{\chi}) = \begin{bmatrix} \mathbf{I} & \mathbf{O} \\ \mathbf{O} & \mathbf{T}(\boldsymbol{\chi}) \end{bmatrix} \quad (3.9)$$

and

$$\mathbf{T}(\boldsymbol{\chi}) = \begin{bmatrix} \cos(\theta) \cos(\psi) & -\sin(\psi) & 0 \\ \cos(\theta) \sin(\psi) & \cos(\psi) & 0 \\ -\sin(\theta) & 0 & 1 \end{bmatrix} \quad (3.10)$$

in the case of a representation of the orientation through RPY angles (Equation (3.2)).

In addition to the differential kinematics of Equation (3.7), several control techniques applications require the use of the second partial derivative of  $\mathbf{f}(\mathbf{q})$ .

In resolved acceleration control, the objective is to calculate joint accelerations  $\ddot{\mathbf{q}}$  based on the desired motion profile of the EE pose. This relationship can be derived from the relation:

$$\ddot{\mathbf{f}}(\mathbf{q}) = \mathbf{J}_A(\mathbf{q}) \ddot{\mathbf{q}} + \dot{\mathbf{J}}_A \dot{\mathbf{q}} = \mathbf{J}_A(\mathbf{q}) \ddot{\mathbf{q}} + \dot{\mathbf{q}}^T \mathbf{H}_A \dot{\mathbf{q}} \quad (3.11)$$

where the  $m \times n \times n$  3rd order tensor  $\mathbf{H}_A$  is the analytical Hessian.

As in the case of the geometric Jacobian, there is a consistent method to calculate the geometric Hessian, as explained in [96].

### 3.3.1 Time derivative of a rotation matrix

In order to get the time derivative of a rotation matrix  $\mathbf{R}$ , the skew-symmetric matrix  $\mathbf{S}$  can be introduced:

$$\mathbf{S}(\boldsymbol{\omega}(t)) = \begin{bmatrix} 0 & -\omega_z(t) & \omega_y(t) \\ \omega_z(t) & 0 & -\omega_x(t) \\ -\omega_y(t) & \omega_x(t) & 0 \end{bmatrix} \quad (3.12)$$

where the vector  $\boldsymbol{\omega}(t) = [\omega_x(t) \ \omega_y(t) \ \omega_z(t)]^T$  denotes the angular velocity of frame  $\mathbf{R}(t)$  with respect to the reference frame at time  $t$ .

Noting that the vector product of two vectors  $\boldsymbol{\omega}$  and  $\mathbf{p}$  can be expressed as

$$\boldsymbol{\omega} \times \mathbf{p} = \mathbf{S}(\boldsymbol{\omega})\mathbf{p} = -\mathbf{S}(\mathbf{p})\boldsymbol{\omega} \quad (3.13)$$

it is possible to show that the following relationships hold [1]:

$$\dot{\mathbf{R}}(t) = \mathbf{S}(\boldsymbol{\omega}(t))\mathbf{R}(t), \quad (3.14)$$

$$\mathbf{S}(\mathbf{R}_0\boldsymbol{\omega}) = \mathbf{R}_0\mathbf{S}(\boldsymbol{\omega})\mathbf{R}_0^T \quad (3.15)$$

### 3.3.2 Trajectory generation

When the desired motion is defined in the operational space, the motion generation is achieved through inverse kinematics algorithms [1].

In this work, trajectories are defined interpolating initial and final conditions of position, velocity and acceleration.

Several techniques are used to achieve such a goal [97], but in this work the motion through a sequence of two operational points (at times  $t = t_1$  and  $t = t_2$ ) is used:

$$\mathbf{x}_d(t) = \begin{cases} \mathbf{x}_{d,1}(t), & \text{if } t \leq t_1; \\ \mathbf{x}_{d,2}(t), & \text{if } t_1 < t \leq t_2; \\ \mathbf{x}_{d,3}(t), & \text{otherwise.} \end{cases} \quad (3.16)$$

where

$$\mathbf{x}_{d,i}(t) = (t - t_i)^3 \mathbf{a}_i + (t - t_i)^2 \mathbf{b}_i + (t - t_i) \mathbf{c}_i + \mathbf{d}_i \quad (3.17)$$

The parameters of such polynomials are calculated to set the desired initial and final conditions, while having continuity of position, velocity and acceleration.

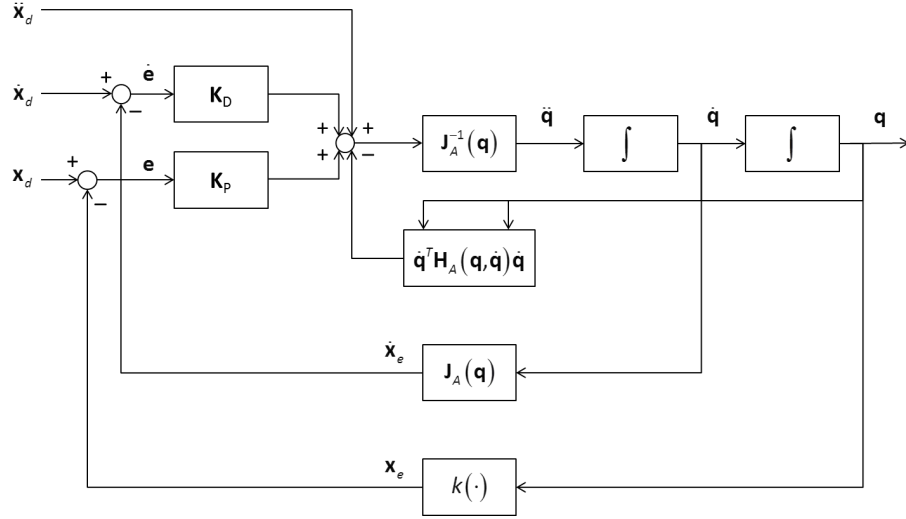


Figure 3.2: Scheme of the second-order inverse kinematics algorithm [1]

Two possible inverse differential kinematics algorithms can be used [1]. The inverse kinematics algorithm providing joint velocities is:

$$\dot{\mathbf{q}} = \mathbf{J}_A^{-1} (\dot{\mathbf{x}}_d + \mathbf{K}_P \mathbf{e}) \quad (3.18)$$

and the inverse kinematics algorithm providing joint accelerations is:

$$\ddot{\mathbf{q}} = \mathbf{J}_A^{-1} (\mathbf{q}) (\ddot{\mathbf{x}}_d + \mathbf{K}_D \dot{\mathbf{e}} + \mathbf{K}_P \mathbf{e} - \dot{\mathbf{q}}^T \mathbf{H}_A(\mathbf{q}, \dot{\mathbf{q}}) \dot{\mathbf{q}}) \quad (3.19)$$

The correct choice of constants  $\mathbf{K}_D$  and  $\mathbf{K}_P$  permits to achieve an asymptotically stable system. Such algorithm is depicted in Figure 3.2.

## 3.4 Reversing a kinematic chain

In this section, a useful property for a kinematic open chain is obtained.

If  $\mathcal{A}$  and  $\mathcal{B}$  represent the frames of the extremities of a kinematic manipulator, and  $\mathcal{W}$  an inertial frame fixed to the world, two cases are compared: when  $\mathcal{A}$  is fixed with respect to  $\mathcal{W}$  and when  $\mathcal{B}$  is fixed with respect to  $\mathcal{W}$ .

In brief, the direct kinematics when  $\mathcal{A}$  is fixed and  $\mathcal{B}$  moves relatively is:

$${}^A \mathbf{T}_B(\mathbf{q}) = \begin{bmatrix} {}^A \mathbf{R}_B(\mathbf{q}) & {}^A \mathbf{p}_B(\mathbf{q}) \\ \mathbf{0}^T & 1 \end{bmatrix} \quad (3.20)$$

where  $\mathbf{q}$  is the vector of joint variables, and the underlining denotes the fixed frame.

The differential kinematics can be summarized as:

$${}^A\dot{\mathbf{x}}_B(\mathbf{q}) = \begin{bmatrix} {}^A\mathbf{J}^{\mathbf{p}}_B(\mathbf{q}) \\ {}^A\mathbf{J}^{\mathbf{o}}_B(\mathbf{q}) \end{bmatrix} \dot{\mathbf{q}} \quad (3.21)$$

where  $\mathbf{J}^{\mathbf{p}}$  and  $\mathbf{J}^{\mathbf{o}}$  define the position and orientation Jacobians, respectively.

Using simple geometric considerations and considering that the transformation (3.20) is a block partitioned matrix, it is possible to calculate the direct kinematics of the reversed chain, *i.e.* when  $\mathcal{A}$  moves with respect to  $\mathcal{B}$ , fixed to  $\mathcal{W}$ :

$${}^B\mathbf{T}_A(\mathbf{q}) = {}^A\mathbf{T}_B^{-1}(-\mathbf{q}) = \begin{bmatrix} {}^A\mathbf{R}_B^T(-\mathbf{q}) & -{}^A\mathbf{R}_B^T(-\mathbf{q}) {}^A\mathbf{p}_B(-\mathbf{q}) \\ \mathbf{0}^T & 1 \end{bmatrix} \quad (3.22)$$

In order to get an analogous relationship for the differential kinematics – taking into account the upper right element of the matrix (3.22) – it can be considered that

$${}^B\dot{\mathbf{p}}_A(-\mathbf{q}) = \frac{\partial}{\partial t} ({}^A\mathbf{R}_B^T(\mathbf{q}) {}^A\mathbf{p}_B(\mathbf{q})) = {}^A\dot{\mathbf{R}}_B^T(\mathbf{q}) {}^A\mathbf{p}_B(\mathbf{q}) + {}^A\mathbf{R}_B^T(\mathbf{q}) {}^A\dot{\mathbf{p}}_B(\mathbf{q}) \quad (3.23)$$

Using Equation (3.14), the first member of the right-hand side of Equation (3.23) becomes

$${}^A\dot{\mathbf{R}}_B^T {}^A\mathbf{p}_B = -{}^A\boldsymbol{\omega}_B \times {}^A\mathbf{R}_B^T {}^A\mathbf{p}_B = {}^A\mathbf{R}_B^T {}^A\boldsymbol{\omega}_B \times {}^A\mathbf{p}_B = \mathbf{S} ({}^A\mathbf{R}_B^T {}^A\mathbf{p}_B) {}^A\boldsymbol{\omega}_B \quad (3.24)$$

Consequently, Equation (3.23) can be rewritten as:

$$\begin{aligned} {}^B\dot{\mathbf{p}}_A(-\mathbf{q}) &= \mathbf{S} ({}^A\mathbf{R}_B^T {}^A\mathbf{p}_B) {}^A\boldsymbol{\omega}_B + {}^A\mathbf{R}_B^T {}^A\dot{\mathbf{p}}_B \\ &= (\mathbf{S} ({}^A\mathbf{R}_B^T {}^A\mathbf{p}_B) {}^A\mathbf{J}^{\mathbf{o}}_B + {}^A\mathbf{R}_B^T {}^A\mathbf{J}^{\mathbf{p}}_B) \dot{\mathbf{q}} \end{aligned} \quad (3.25)$$

Considering that

$${}^B\dot{\mathbf{p}}_A(-\mathbf{q}) = \frac{\partial}{\partial t} {}^B\mathbf{p}_A(-\mathbf{q}) = -{}^B\mathbf{J}^{\mathbf{p}}_A(-\mathbf{q}) \dot{\mathbf{q}} \quad (3.26)$$

the velocity in the task space of the reverse chain can be calculated as:

$${}^B\dot{\mathbf{j}}_A(\mathbf{q}) \dot{\mathbf{q}} = \begin{bmatrix} \mathbf{S} ({}^A\mathbf{R}_B^T(-\mathbf{q}) {}^A\mathbf{p}_B(-\mathbf{q})) {}^A\mathbf{J}^{\mathbf{o}}_B(-\mathbf{q}) + {}^A\mathbf{R}_B^T(-\mathbf{q}) {}^A\mathbf{J}^{\mathbf{p}}_B(-\mathbf{q}) \\ {}^A\mathbf{J}^{\mathbf{o}}_B(-\mathbf{q}) \end{bmatrix} \dot{\mathbf{q}} \quad (3.27)$$

Equations (3.22) and (3.27) permit to calculate the direct and differential kinematics of a reverse of the chain, whose kinematics is expressed in Equations (3.20) and (3.21). They can be used, for instance, in order to calculate the equations of the pose and its time derivatives of the standing foot from the kinematics of the floating foot.

### 3.5 Statics and dynamics

The geometric Jacobian is fundamental for describing the mapping between forces applied to the EE  $\boldsymbol{\gamma}$  and the resulting torques at the joints  $\boldsymbol{\tau}$  (statics):

$$\boldsymbol{\tau} = \mathbf{J}^T \boldsymbol{\gamma} \quad (3.28)$$

The dynamic model of a manipulator provides a description of the relationship between the joint actuator torques and the motion of the structure.

Once the generalized coordinates are chosen, which describe the link positions of the manipulator, the Lagrangian of the mechanical system can be defined:

$$L \equiv T - U \quad (3.29)$$

where  $T$  and  $U$  denote the total kinetic energy and potential energy of the system, respectively.

The Euler–Lagrange differential equations are:

$$\frac{d}{dt} \left( \frac{\partial}{\partial \dot{\theta}_i} L \right) - \frac{\partial}{\partial \theta_i} L = \xi_i \quad (3.30)$$

where  $\xi_i$  is the generalized force associated with the generalized coordinate  $q_i$ .

In summary, the equations of motion for a manipulator can be rewritten in a compact matrix form which represents the joint space dynamic model [1]:

$$\mathbf{B}(\mathbf{q})\ddot{\mathbf{q}} + \mathbf{C}(\mathbf{q}, \dot{\mathbf{q}})\dot{\mathbf{q}} + \mathbf{F}_v(\dot{\mathbf{q}}) + \mathbf{F}_s \text{sgn}(\dot{\mathbf{q}}) + \mathbf{g}(\mathbf{q}) = \boldsymbol{\tau} - \mathbf{J}^T(\mathbf{q})\mathbf{h} \quad (3.31)$$

where  $\mathbf{B}$  represents the inertia matrix,  $\mathbf{C}$  represents the quadratic velocity terms,  $\mathbf{F}_v$  denotes the matrix of viscous friction coefficients,  $\mathbf{F}_s$  takes into account the Coulomb friction,  $\mathbf{g}$  includes the gravity terms,  $\boldsymbol{\tau}$  refers to the actuation torques and, finally,  $\mathbf{h}$  is the force and moment exerted by the EE on the environment.

Such equations can be simplified neglecting the friction terms:

$$\mathbf{B}(\mathbf{q})\ddot{\mathbf{q}} + \mathbf{C}(\mathbf{q}, \dot{\mathbf{q}})\dot{\mathbf{q}} + \mathbf{g}(\mathbf{q}) = \boldsymbol{\tau} - \mathbf{J}^T(\mathbf{q})\mathbf{h} \quad (3.32)$$

From these equations, it is possible to obtain the dynamical model in the task space.

First of all, the model for a trajectory in the task space is derived. From Equation (3.11), in the particular case of a square Jacobian  $\mathbf{J}_A$ , that is, for a non-redundant manipulator in a non-singular configuration, the following relation holds:

$$\ddot{\mathbf{q}} = \mathbf{J}_A^{-1} \ddot{\mathbf{x}} - \dot{\mathbf{J}}_A \mathbf{J}_A^{-1} \dot{\mathbf{x}} \quad (3.33)$$

Rearranging terms:

$$\mathbf{M}(\mathbf{q})\ddot{\mathbf{x}} + \mathbf{K}(\mathbf{q}, \dot{\mathbf{q}})\dot{\mathbf{x}} + \mathbf{g}(\mathbf{q}) = \boldsymbol{\tau} - \mathbf{J}^T(\mathbf{q})\mathbf{h} \quad (3.34)$$

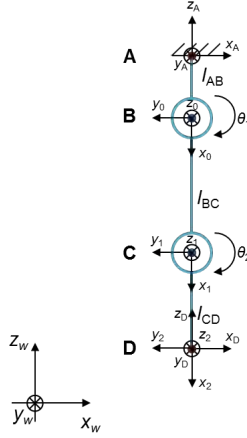


Figure 3.3: A simple RR manipulator

where

$$\begin{aligned} \mathbf{M} &= \mathbf{B}\mathbf{J}_A^{-1} \\ \mathbf{K} &= \left( \mathbf{C} - \mathbf{B}\mathbf{J}_A^{-1}\dot{\mathbf{J}}_A \right) \mathbf{J}_A^{-1} \end{aligned} \quad (3.35)$$

Using statics relationship of Equation (3.28) and rearranging terms, the Operational Space Dynamic Model is obtained [1]:

$$\mathbf{B}_A\ddot{\mathbf{x}} + \mathbf{C}_A\dot{\mathbf{x}} + \mathbf{g}_A = \boldsymbol{\gamma}_A - \mathbf{h}_A \quad (3.36)$$

where

$$\begin{aligned} \boldsymbol{\gamma}_A &= \mathbf{J}_A^{-T} \boldsymbol{\tau} \\ \mathbf{h}_A &= \mathbf{T}_A^T \mathbf{h} \\ \mathbf{B}_A &= \left( \mathbf{J}_A \mathbf{B}^{-1} \mathbf{J}_A^T \right)^{-1} \\ \mathbf{C}_A \dot{\mathbf{x}} &= \mathbf{B}_A \mathbf{J}_A \mathbf{B}^{-1} \mathbf{C} \dot{\mathbf{q}} - \mathbf{B}_A \dot{\mathbf{J}}_A \dot{\mathbf{q}} \\ \mathbf{g}_A &= \mathbf{B}_A \mathbf{J}_A \mathbf{B}^{-1} \mathbf{g} \end{aligned} \quad (3.37)$$

### 3.6 A simple case study: the Rotational–Rotational (RR) manipulator

A simple 2 DOF manipulator (also known as RR, since it is constituted by two rotational joints) is depicted in Figure 3.3. In the figure, frame  $\mathcal{A}$  is fixed with respect to the world frame  $\mathcal{W}$ , while frame  $\mathcal{D}$  is moving.

Link	$a_i$	$\alpha_i$	$d_i$	$\theta_i$
<b>B-C</b>	$l_{BC}$	0	0	$\theta_1$
<b>C-D</b>	$l_{CD}$	0	0	$\theta_2$

Table 3.1: DH parameters for the RR manipulator in forward chain

According to the DH parameters in Table 3.1, it is possible to calculate the transformation matrix  ${}^0\mathbf{T}_2$ :

$${}^0\mathbf{T}_2 = \begin{bmatrix} \cos(\theta_1 + \theta_2) & -\sin(\theta_1 + \theta_2) & 0 & l_{CD} \cos(\theta_1 + \theta_2) + l_{BC} \cos(\theta_1) \\ \sin(\theta_1 + \theta_2) & \cos(\theta_1 + \theta_2) & 0 & l_{CD} \sin(\theta_1 + \theta_2) + l_{BC} \sin(\theta_1) \\ 0 & 0 & 1 & 0 \\ 0 & 0 & 0 & 1 \end{bmatrix} \quad (3.38)$$

The geometric Jacobian associated to such chain is:

$${}^0\mathbf{J}_2 = \begin{bmatrix} -l_{CD} \sin(\theta_1 + \theta_2) - l_{BC} \sin(\theta_1) & -l_{CD} \sin(\theta_1 + \theta_2) \\ l_{CD} \cos(\theta_1 + \theta_2) + l_{BC} \cos(\theta_1) & l_{CD} \cos(\theta_1 + \theta_2) \\ 0 & 0 \\ 0 & 0 \\ 0 & 0 \\ 1 & 1 \end{bmatrix} \quad (3.39)$$

Considering the following transformations:

$${}^A\mathbf{T}_0 = \begin{bmatrix} 0 & -1 & 0 & 0 \\ 0 & 0 & 1 & 0 \\ -1 & 0 & 0 & -l_{AB} \\ 0 & 0 & 0 & 1 \end{bmatrix} \quad {}^2\mathbf{T}_D = \begin{bmatrix} 0 & 0 & -1 & 0 \\ -1 & 0 & 0 & 0 \\ 0 & 1 & 0 & 0 \\ 0 & 0 & 0 & 1 \end{bmatrix} \quad (3.40)$$

the homogeneous transformation matrix from frame **A** to **D** is:

$$\begin{aligned} {}^A\mathbf{T}_D &= {}^A\mathbf{T}_0 {}^0\mathbf{T}_2 {}^2\mathbf{T}_D = \\ &= \begin{bmatrix} \cos(\theta_1 + \theta_2) & 0 & \sin(\theta_1 + \theta_2) & -l_{CD} \sin(\theta_1 + \theta_2) - l_{BC} \sin(\theta_1) \\ 0 & 1 & 0 & 0 \\ -\sin(\theta_1 + \theta_2) & 0 & \cos(\theta_1 + \theta_2) & -l_{AB} - l_{CD} \cos(\theta_1 + \theta_2) - l_{BC} \cos(\theta_1) \\ 0 & 0 & 0 & 1 \end{bmatrix} \end{aligned} \quad (3.41)$$

The pose of frame  $\mathcal{D}$  with respect to frame  $\mathcal{A}$ , expressed in terms of RPY angles, is:

$${}^A\mathbf{x}_D = \begin{bmatrix} -l_{CD} \sin(\theta_1 + \theta_2) - l_{BC} \sin(\theta_1) \\ 0 \\ -l_{AB} - l_{CD} \cos(\theta_1 + \theta_2) - l_{BC} \cos(\theta_1) \\ 0 \\ \theta_1 + \theta_2 \\ 0 \end{bmatrix} \quad (3.42)$$

Since the Jacobian depends on the frame it is expressed, the following relationship holds:

$${}^A\mathbf{J}_D = \begin{bmatrix} {}^A\mathbf{R}_0 & \mathbf{O} \\ \mathbf{O} & {}^A\mathbf{R}_0 \end{bmatrix} {}^0\mathbf{J}_2 = \begin{bmatrix} -l_{CD} \cos(\theta_1 + \theta_2) - l_{BC} \cos(\theta_1) & -l_{CD} \cos(\theta_1 + \theta_2) \\ 0 & 0 \\ l_{CD} \sin(\theta_1 + \theta_2) + l_{BC} \sin(\theta_1) & l_{CD} \sin(\theta_1 + \theta_2) \\ 0 & 0 \\ 1 & 1 \\ 0 & 0 \end{bmatrix} \quad (3.43)$$

The analytical Jacobian,  ${}^A\mathbf{J}\mathbf{a}_D = \frac{\partial {}^A\mathbf{x}_D}{\partial \mathbf{q}}$  with  $\mathbf{q} = [\theta_1, \theta_2]$ , is easily shown to be identical, for this particular case, to the geometric one.

The Hessian  $\mathbf{H}$  for this manipulator is:

$$\mathbf{H}_1 = \begin{bmatrix} l_{CD} \sin(\theta_1 + \theta_2) + l_{BC} \sin(\theta_1) & l_{CD} \sin(\theta_1 + \theta_2) \\ l_{CD} \sin(\theta_1 + \theta_2) & l_{CD} \sin(\theta_1 + \theta_2) \end{bmatrix} \quad (3.44)$$

$$\mathbf{H}_3 = \begin{bmatrix} l_{CD} \cos(\theta_1 + \theta_2) + l_{BC} \cos(\theta_1) & l_{CD} \cos(\theta_1 + \theta_2) \\ l_{CD} \cos(\theta_1 + \theta_2) & l_{CD} \cos(\theta_1 + \theta_2) \end{bmatrix} \quad (3.45)$$

$$\mathbf{H}_i = \mathbf{0}_{3 \times 3}, \text{ with } i = \{2, 4, 5, 6\}. \quad (3.46)$$

$\mathbf{H}_i$  being the  $3 \times 3$  slices corresponding to the derivatives of the rows of  $\mathbf{J}$ .

### 3.6.1 A joint trajectory generation

For the presented manipulator a reference trajectory is provided like in Equation (3.16). The reference trajectory is depicted in Figure 3.4. The initial and final velocity and acceleration have been set to zero.

The algorithm for the inverse kinematics follows Equation (3.19), and explained in Figure 3.2. The results of the inverse kinematics are in Figure 3.5 and show the smoothness of the joints accelerations. As explained in Equation (3.11), the acceleration in the task space can be calculated as the sum of two contributions: one is the joint velocities contribution and the other one is related to joint accelerations.

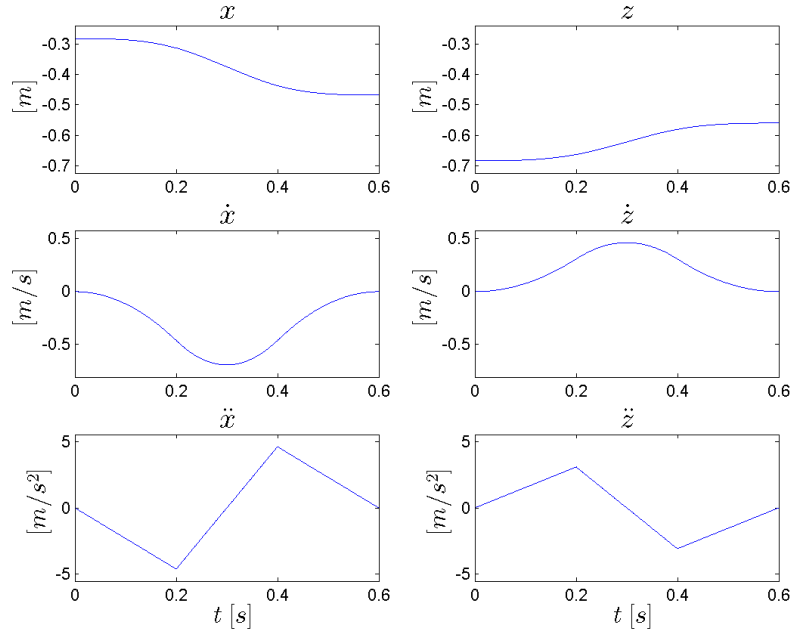


Figure 3.4: A reference trajectory for the RR manipulator

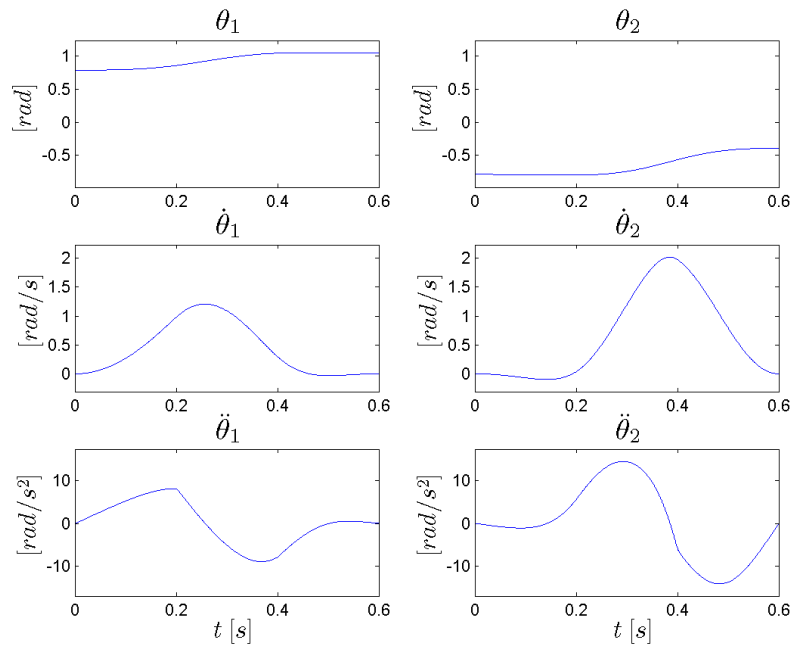


Figure 3.5: Joints trajectories for the RR manipulator

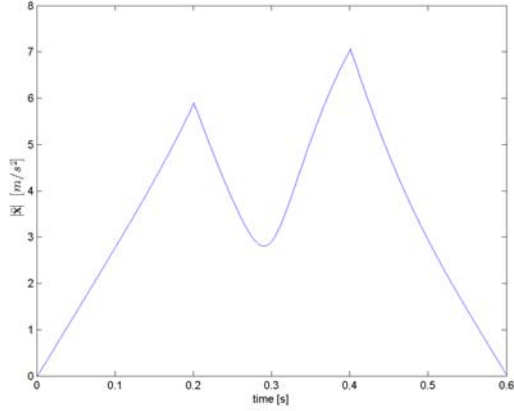


Figure 3.6: The norm of the acceleration for the RR manipulator

The norm of acceleration in the task space for the same example is in Figure 3.6. The two contributions are in Figure 3.7. This result shows that the main contribution for most of the time is the joint acceleration one.

### 3.6.2 The double pendulum

A special case of the RR manipulator is the double pendulum. The double bob pendulum has masses  $m_1$  and  $m_2$  attached by rigid massless wires of lengths  $l_1$  and  $l_2$ , as shown in Figure 3.8.

In summary, the equations of motion can be rewritten in the compact matrix form like in Equation (3.32):

$$\mathbf{B}(\mathbf{q})\ddot{\mathbf{q}} + \mathbf{C}(\mathbf{q}, \dot{\mathbf{q}})\dot{\mathbf{q}} + \mathbf{g}(\mathbf{q}) = \boldsymbol{\tau} \quad (3.47)$$

where

$$\mathbf{B}(\mathbf{q}) = \begin{bmatrix} m_1 l_1^2 + m_2 (l_1^2 + l_2^2 + 2l_1 l_2 \cos \theta_2) & m_2 l_2 (l_1 \cos \theta_2 + l_2) \\ (l_1 \cos \theta_2 + l_2) & m_2 l_2^2 \end{bmatrix} \quad (3.48)$$

$\mathbf{C}(\mathbf{q}, \dot{\mathbf{q}})$  is:

$$\mathbf{C}(\mathbf{q}, \dot{\mathbf{q}}) = \begin{bmatrix} -m_2 l_1 l_2 \sin \theta_2 \dot{\theta}_2 & -m_2 l_1 l_2 \sin \theta_2 (\dot{\theta}_1 + \dot{\theta}_2) \\ m_2 l_1 l_2 \sin \theta_2 \dot{\theta}_1 & 0 \end{bmatrix} \quad (3.49)$$

And  $\mathbf{g}(\mathbf{q})$  is:

$$\mathbf{g}(\mathbf{q}) = \begin{bmatrix} m_2 (l_2 \sin (\theta_1 + \theta_2) + l_1 \sin \theta_1) + m_1 l_1 \sin \theta_1 \\ m_2 l_2 \sin (\theta_1 + \theta_2) \end{bmatrix} g \quad (3.50)$$

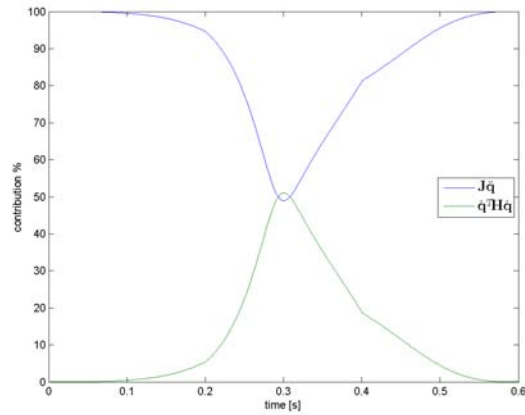


Figure 3.7: Jacobian and Hessian contributions

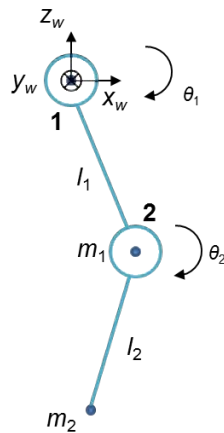


Figure 3.8: Double pendulum

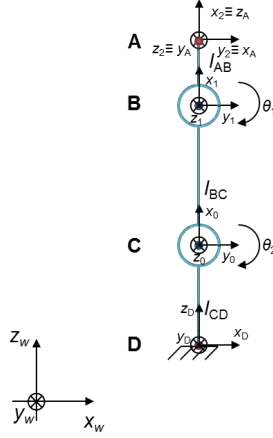


Figure 3.9: The reversed RR manipulator

Table 3.2: DH parameters for the RR manipulator in reversed chain

Link	$a_i$	$\alpha_i$	$d_i$	$\theta_i$
<b>B-C</b>	$l_{BC}$	0	0	$\theta_2$
<b>C-D</b>	$l_{AB}$	0	0	$\theta_1$

### 3.6.3 The reversed case

Now, to calculate the kinematics of the reversed chain, a different DH representation should be considered (Table 3.2), like the one in Figure 3.9.

The direct and differential kinematics are

$${}^D\mathbf{T}_A = \begin{bmatrix} \cos(\theta_1 + \theta_2) & 0 & \sin(\theta_1 + \theta_2) & l_{AB} \sin(\theta_1 + \theta_2) + l_{BC} \sin(\theta_2) \\ 0 & 1 & 0 & 0 \\ -\sin(\theta_1 + \theta_2) & 0 & \cos(\theta_1 + \theta_2) & l_{CD} + l_{AB} \cos(\theta_1 + \theta_2) + l_{BC} \cos(\theta_2) \\ 0 & 0 & 0 & 1 \end{bmatrix} \quad (3.51)$$

$${}^D\mathbf{J}_A = \begin{bmatrix} l_{AB} \cos(\theta_1 + \theta_2) + l_{BC} \cos(\theta_2) & l_{AB} \cos(\theta_1 + \theta_2) \\ 0 & 0 \\ -l_{AB} \sin(\theta_1 + \theta_2) - l_{BC} \sin(\theta_2) & -l_{AB} \sin(\theta_1 + \theta_2) \\ 0 & 0 \\ 1 & 1 \\ 0 & 0 \end{bmatrix} \quad (3.52)$$

$$(3.53)$$

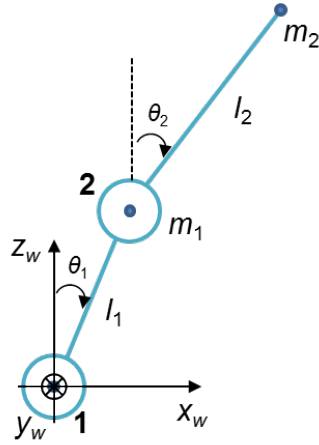


Figure 3.10: Double inverted pendulum

In a different way, it is possible to reverse the manipulator in Figure 3.3 using the relationships (3.22) and (3.27), and starting from (3.41) and (3.43):

$${}^D\mathbf{T}_A = \begin{bmatrix} \cos(\theta_1 + \theta_2) & 0 & \sin(\theta_1 + \theta_2) & l_{AB} \sin(\theta_1 + \theta_2) + l_{BC} \sin(\theta_2) \\ 0 & 1 & 0 & 0 \\ -\sin(\theta_1 + \theta_2) & 0 & \cos(\theta_1 + \theta_2) & l_{CD} + l_{AB} \cos(-\theta_1 - \theta_2) + l_{BC} \cos(\theta_2) \\ 0 & 0 & 0 & 1 \end{bmatrix} \quad (3.54)$$

$${}^D\mathbf{J}_A \dot{\mathbf{q}} = \begin{bmatrix} l_{AB} \cos(\theta_1 + \theta_2) & l_{AB} \cos(-\theta_1 - \theta_2) + l_{BC} \cos(\theta_2) \\ 0 & 0 \\ -l_{AB} \sin(\theta_1 + \theta_2) & -l_{AB} \sin(\theta_1 + \theta_2) - l_{BC} \sin(\theta_2) \\ 0 & 0 \\ 1 & 1 \\ 0 & 0 \end{bmatrix} \dot{\mathbf{q}} \quad (3.55)$$

which are, in essence, the same as (3.51) and (3.52).

### 3.6.4 The double inverted pendulum

A special case of the reversed RR manipulator is the double pendulum. As done for the double pendulum, a double bob pendulum with two masses  $m_i$  and massless wires of lengths  $l_i$  is considered, as depicted in Figure 3.10.

The pose is easily shown to be

$${}^w\mathbf{x}_2 = \begin{bmatrix} l_1 \sin \theta_1 + l_2 \sin \theta_2 \\ 0 \\ l_1 \cos \theta_1 + l_2 \cos \theta_2 \\ 0 \\ -\theta_2 \\ 0 \end{bmatrix} \quad (3.56)$$

The analytical Jacobian is

$${}^w\mathbf{J}_2 = \begin{bmatrix} l_1 \cos \theta_1 & l_2 \cos \theta_2 \\ 0 & 0 \\ -l_1 \sin \theta_1 & -l_2 \sin \theta_2 \\ 0 & 0 \\ 0 & -1 \\ 0 & 0 \end{bmatrix} \quad (3.57)$$

In summary, the equations of motion can be rewritten in the compact matrix form like in Equation (3.32):

$$\mathbf{B}(\mathbf{q})\ddot{\mathbf{q}} + \mathbf{C}(\mathbf{q}, \dot{\mathbf{q}})\dot{\mathbf{q}} + \mathbf{g}(\mathbf{q}) = \boldsymbol{\tau} \quad (3.58)$$

where  $\mathbf{B}(\mathbf{q})$ :

$$\mathbf{B} = \begin{bmatrix} (m_1 + m_2) l_1^2 & m_2 l_1 l_2 \cos(\theta_1 - \theta_2) \\ m_2 l_1 l_2 \cos(\theta_1 - \theta_2) & m_2 l_2^2 \end{bmatrix} \quad (3.59)$$

$\mathbf{C}(\mathbf{q}, \dot{\mathbf{q}})$  is:

$$\mathbf{C} = \begin{bmatrix} 0 & m_2 l_1 l_2 \sin(\theta_1 - \theta_2) \dot{\theta}_2 \\ -m_2 l_1 l_2 \sin(\theta_1 - \theta_2) \dot{\theta}_1 & 0 \end{bmatrix} \quad (3.60)$$

And  $\mathbf{g}(\mathbf{q})$  is:

$$\mathbf{g} = \begin{bmatrix} -(m_1 + m_2) l_1 \sin(\theta_1) \\ -m_2 l_2 \sin(\theta_2) \end{bmatrix} g \quad (3.61)$$

### 3.7 Full humanoid body trajectory generation

In this section, a trajectory for the humanoid robot HOAP-3 is generated. This trajectory is first analyzed by means of the full model of the robot and then such results are compared with simplified models. The kinematic model of the robot is presented in Appendix D.

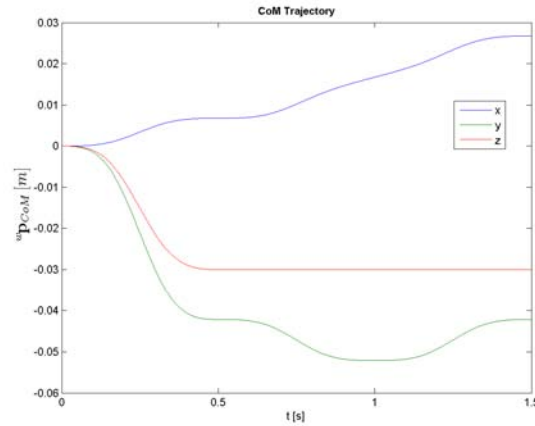


Figure 3.11: CoM reference trajectory

The trajectory represents a step forward of the robot standing on the right leg. The robot moves 10 cm forward and raises the left foot 5 cm from the ground. The reference trajectory for the CoM is in Figure 3.11, and for the left foot in Figure 3.12.

Such trajectories have been calculated using the ZMP criterion and generated through Equation (3.16). The arms are moved in order to compensate the effects on the ZMP. A general idea of the motion is given in Figure 3.13.

The algorithm for the inverse kinematics follows Equation (3.19), as previously explained. The results of the inverse kinematics are in Figures 3.14–3.18, where the joints limits are detailed.

The inverse dynamics algorithm has been developed in SimMechanics<sup>TM</sup>, whose HOAP-3 model is depicted in Figure 3.19. Here the robot is represented by its joints and its links. Every link is visually represented as a convex hull, function of its mass and inertia.

The results of the SimMechanics<sup>TM</sup> simulation are in Figures 3.20–3.24, where the admissible motor torques are also shown. Such results refer to the robot attached to the world through its CoM.

### 3.8 The double pendulum as a model for the floating leg

The floating leg may be modeled in a simplified way as a two link kinematic chain (double pendulum) during the single-support phase.

In this section, a comparison of the inverse dynamics of the floating leg and its simplification in the sagittal plane through the double pendulum is presented.

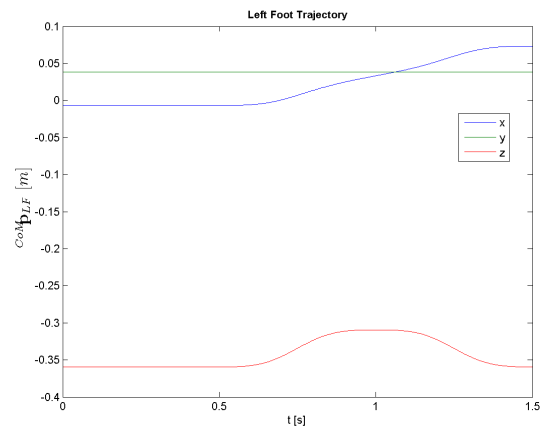


Figure 3.12: Left foot position reference trajectory

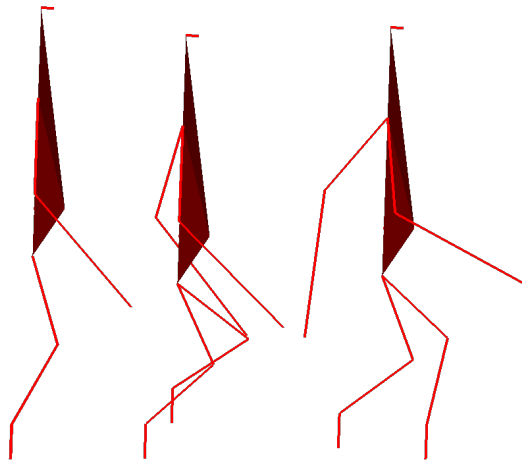


Figure 3.13: Initial to final configuration of the simulated experiment

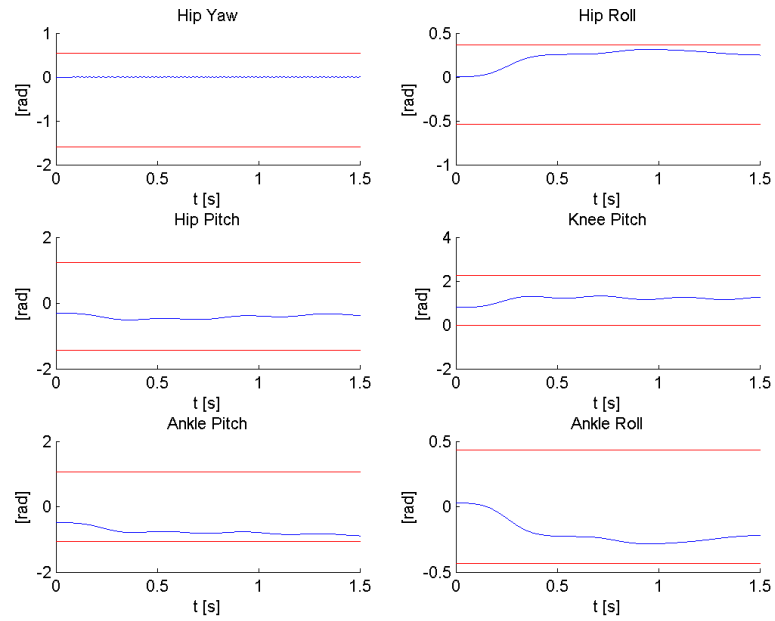


Figure 3.14: Right leg joints angles with respective angle limits

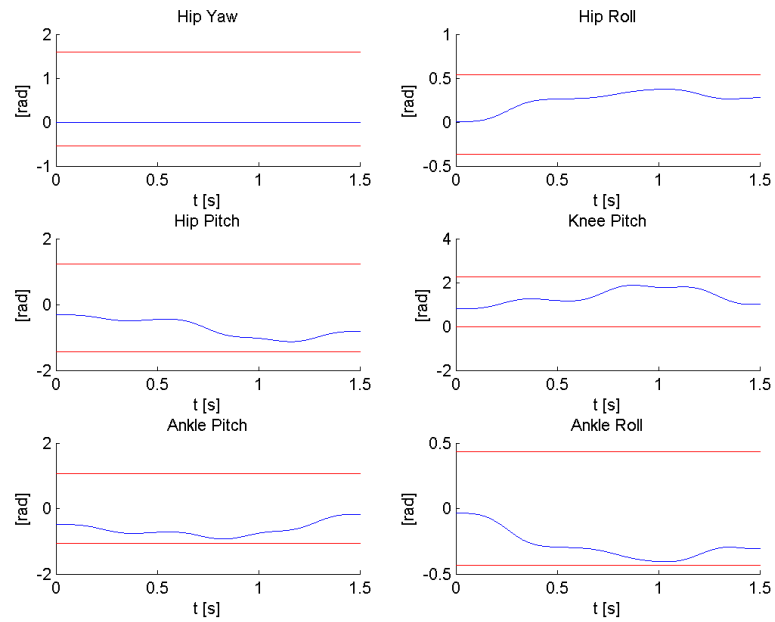


Figure 3.15: Left leg joints angles with respective angle limits

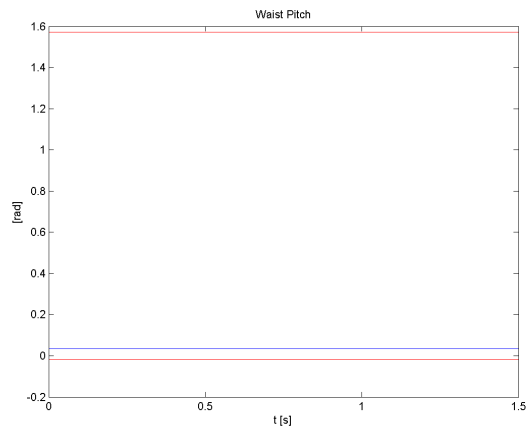


Figure 3.16: Waist pitch joint angles with respective torque limits

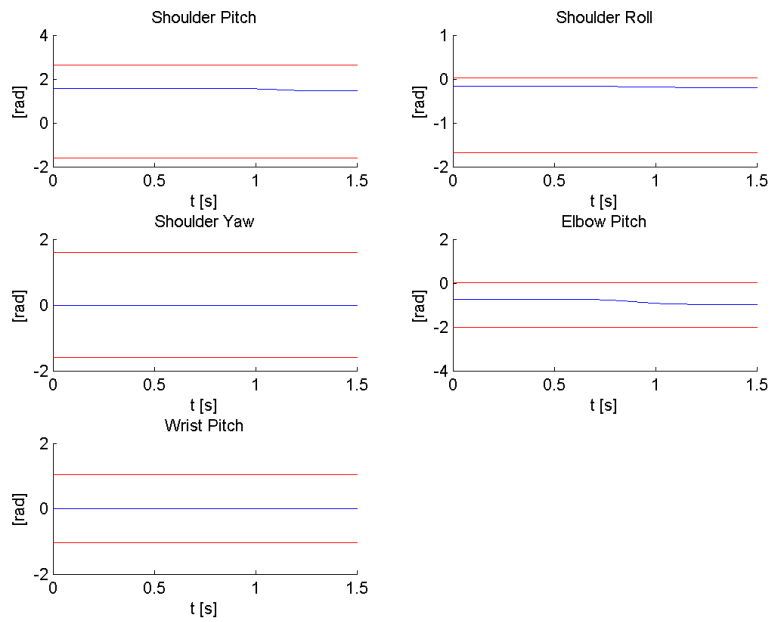


Figure 3.17: Right arm joints angles with respective angle limits

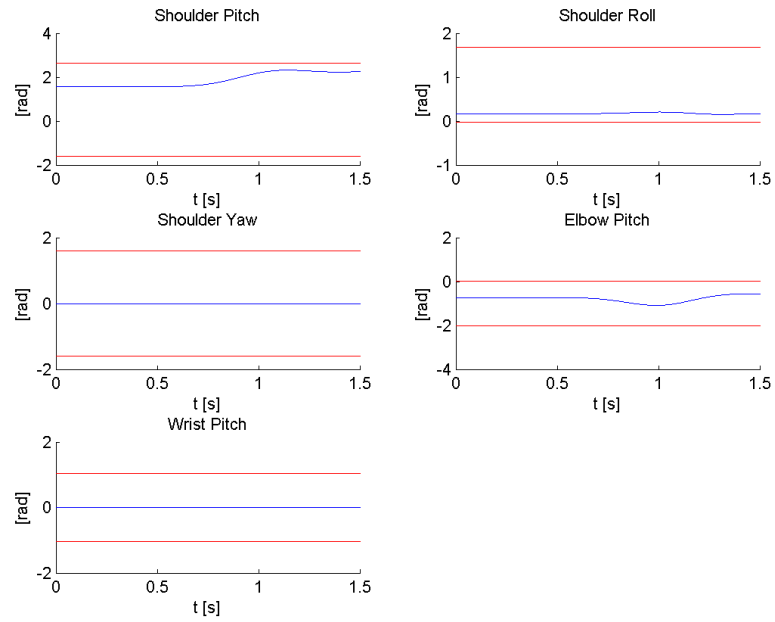
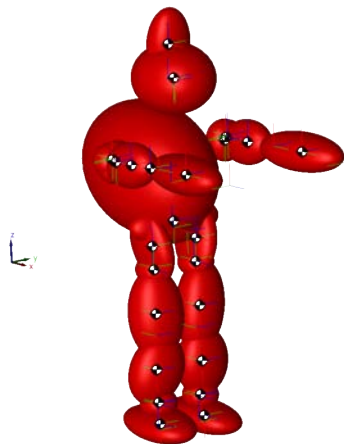


Figure 3.18: Left arm joints angles with respective angle limits

Figure 3.19: SimMechanics<sup>TM</sup> model of the HOAP-3 robot

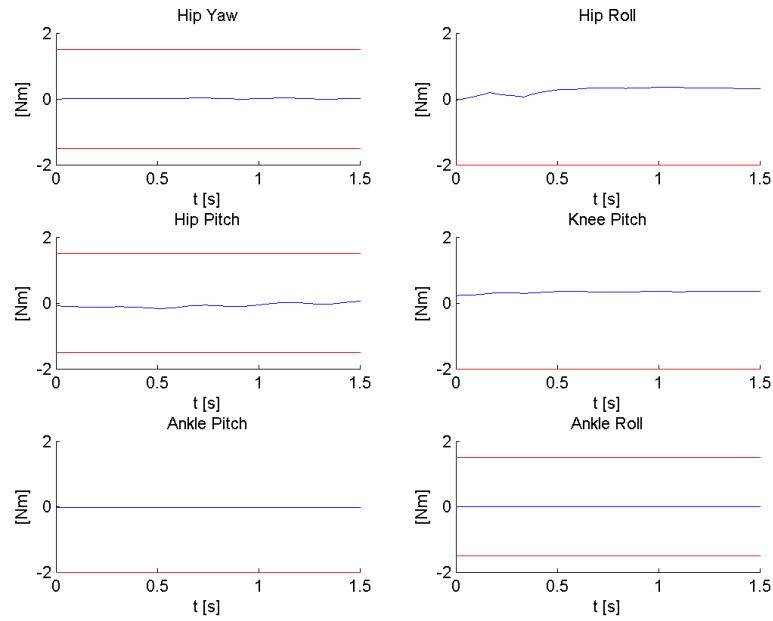


Figure 3.20: Right leg joints torques with respective torque limits

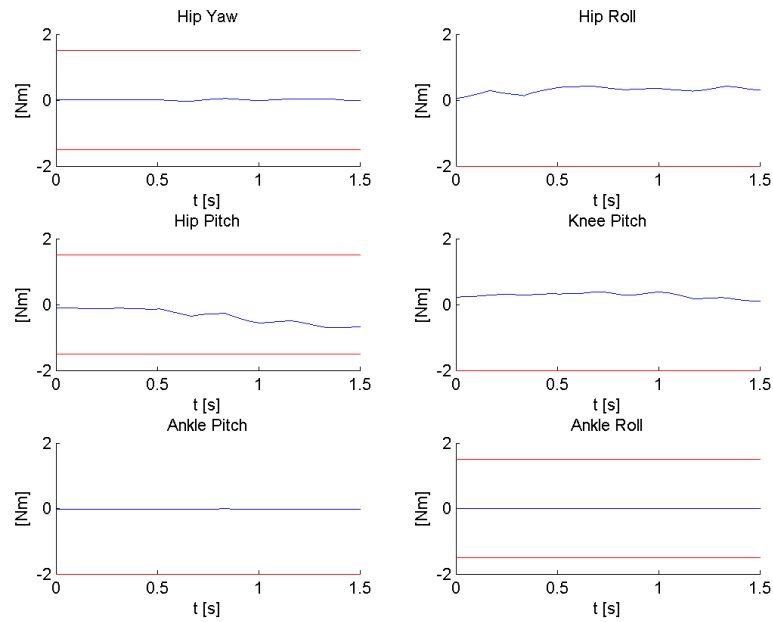


Figure 3.21: Left leg joints torques with respective torque limits

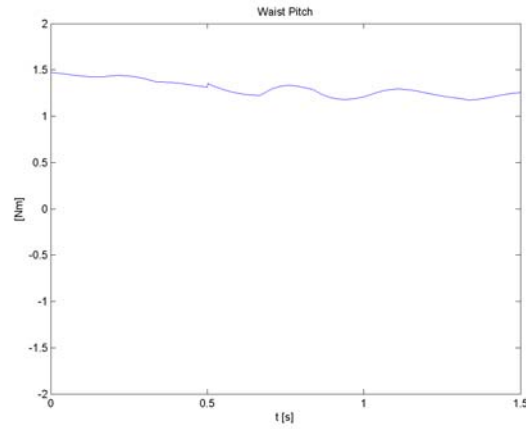


Figure 3.22: Waist pitch joint torques with respective torque limits

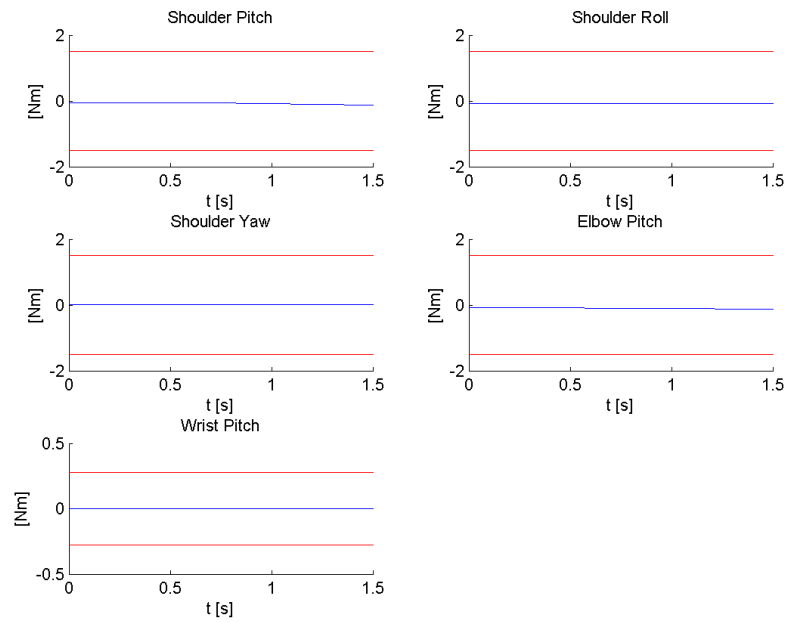


Figure 3.23: Right arm joints torques with respective torque limits

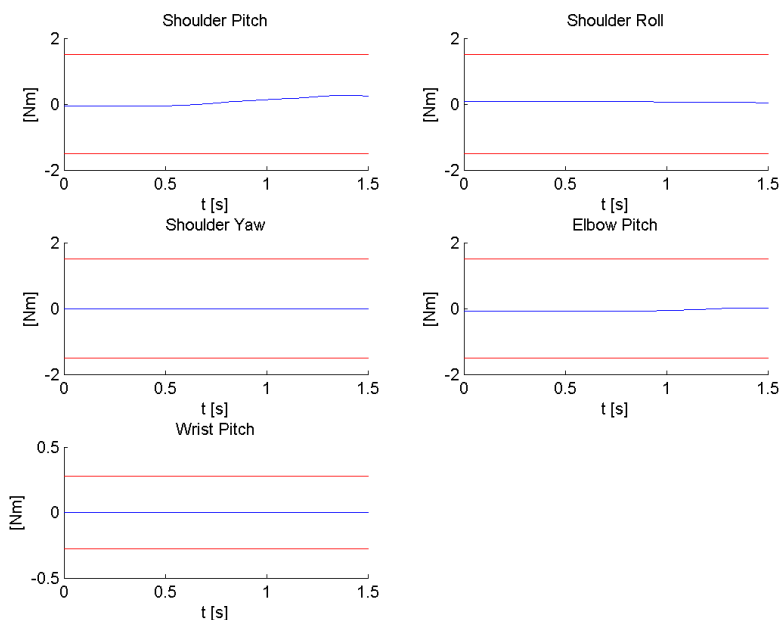


Figure 3.24: Left arm joints torques with respective torque limits

In the simplified model of Figure 3.8, joint 1 represents the left hip pitch and joint 2 the knee pitch. The mass of the whole link 1 is resumed in  $m_1$  and the remaining part in  $m_2$ . The lengths of the links are  $l_1$  and  $l_2$ .

If the same trajectory as in Figure 3.12 is used, the comparison between the full model and a simplified model is shown in Figure 3.25.

### 3.9 Floating leg trajectory generation

Most of the human size humanoid robots includes in their ankle a compliant material to absorb the force resulting from the impact when the swinging foot is landing on the floor. A controller is then generally provided to compensate the effect of this compliant material [98]. Often, on top of this controller, a walking pattern generator provides articular (or torque) trajectories ensuring that the robot is balanced.

Current real-time walking pattern generators assume a simplified inverted pendulum model to simplify the problem of finding a CoM trajectory following a given ideal ZMP trajectory or satisfy the constraint related to the ZMP [99].

This simplified model does not take into account the compliant material, and let the underlying controller compensate the passivity of this material. Although this controller works effectively for moderate walking speeds, when performing fast motion

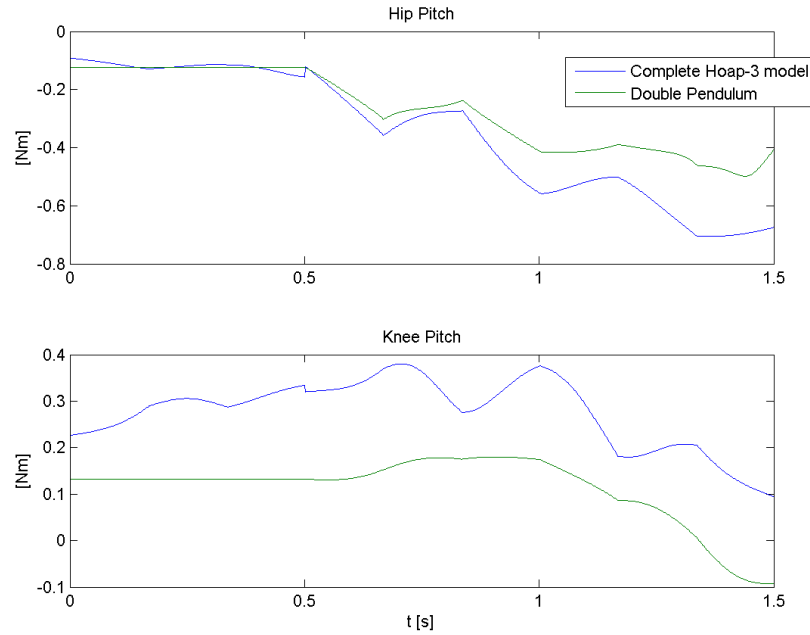


Figure 3.25: Full model compared with the double pendulum simplification

or extended stepping over an object, it is not sufficient. The compliant material deformation is such that the robot is leaning forward and might hit the floor sooner than expected, creating large impact forces.

Classically, this is addressed by adding masses to the model to take into account the inertia effect of the legs. However, instead of modifying the CoM trajectory and fixing a 3rd order polynomial trajectory for the feet, in this section the swinging foot trajectory itself is modified in order to minimize the inertia effect of the compliant material [100].

Although controllers such as the one described in [99] are designed to provide a direct-drive torque control, they also control the body posture assuming that the robot is behaving like an inverted pendulum.

Such simplified models can undermine the efficiency of the controller; this is the case of a robot that has not a mass distribution compatible with the assumption of the inverted pendulum (as for instance in Johnnie [101]), or when it is performing a fast motion.

For instance, in [102], HRP-2 robot is stepping over an obstacle and performing a step twice longer than normal standard mode. The use of the classical controller to compensate the compliant material, the inverted pendulum for the CoM trajectory, and a 3rd polynomial for the feet trajectory generate impact forces about twice the

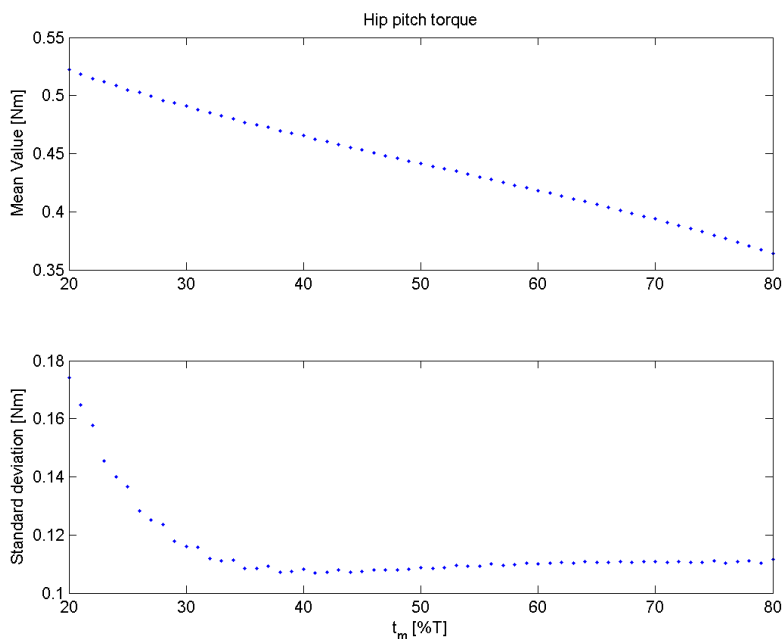


Figure 3.26: The mean and the standard deviation of the torque of the first double pendulum joint

weight of the robot.

If the trajectory for the swinging leg is chosen to connect at time  $t_m$  two trajectories of Equation (3.16), Figure 3.26 shows how the torque on the hip joint varies when this  $t_m$  varies. This example refers to the same trajectory for the floating leg used for the HOAP-3 robot.

A Newton Raphson-based algorithm has been used to choose the via point time  $t_m$  to minimize the variations through a mean value (the standard deviation) [100].

The results are presented using the HRP-2 robot since it is equipped with a good force sensorial system in its feet which permits to estimate the impacts on the ground. The kinematic model of the HRP-2 robot is presented in Appendix D.

In Figure 3.27, the force in the  $z$  direction of the right foot is shown (i.e. the direction perpendicular to the ground), representing the impact effect of the ground. As can be seen from the graph, the impact is considerably reduced using the via point. This results is almost straightforward since the trajectory is specified in order to start and arrive with null acceleration.

Using the OpenHRP platform<sup>1</sup>, the impacts of the foot on the ground are calculated. The results in Figure 3.28 show the validity of the presented strategy. In fact,

<sup>1</sup><http://www.openrtp.jp/openhrp3/en/index.html>, accessed on May 27, 2012

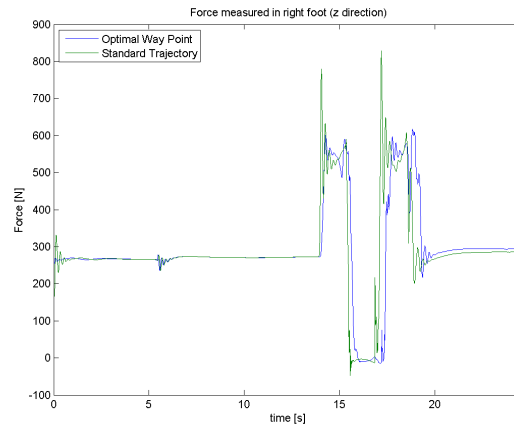


Figure 3.27: Force measurement at the right foot

the torque acting on the left foot during the right foot floating is actually related to the torque acting on the CoM. It is possible to see that this torque is greatly reduced with respect to a standard trajectory.

Actually the mean value of the standard trajectory is about 1.38 Nm with a standard deviation of 9.24 Nm, which is really more than the optimal one: 0.25 Nm with a standard deviation of 6.05 Nm.

The proposed algorithm has been tested on the robotic platform HRP-2. In Figure 3.29 the results of the impact on the ground based on [102] are presented. In this case, huge impact of about 1200 N has been reduced down to about 650 N (as shown in Figure 3.30). Also, the torque measured by the F/T sensor shows the validity of the proposed work.

## 3.10 Chapter summary

This chapter has presented the basic representations to be used throughout this research. In particular, a simple case study, the RR manipulator, is presented. This manipulator is shown to be a good simplified model of a humanoid robot during walking tasks.

The particular case of the double pendulum is used to simplify the dynamics of the floating leg while walking. Basing on this model, a trajectory that reduces the effects on the CoM, and consequently on the ZMP, is calculated. This technique has been implemented on the real HRP-2 robot.

The double inverted pendulum will be the foundation for the balance control explained afterwards.

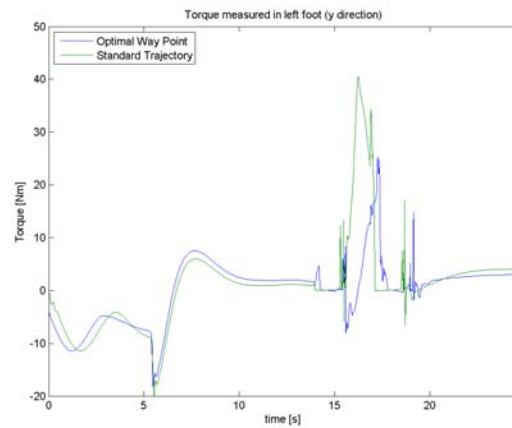


Figure 3.28: Torque measurement at the left foot

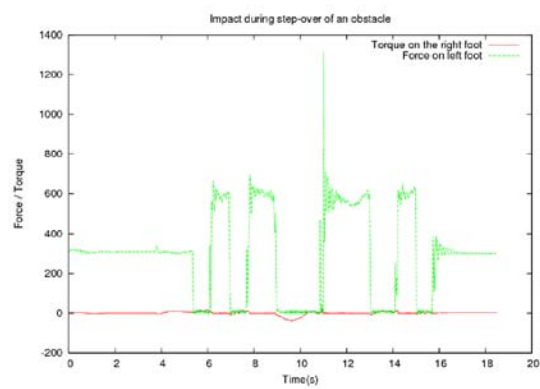


Figure 3.29: Force/torque sensor measurements in case of a standard trajectory

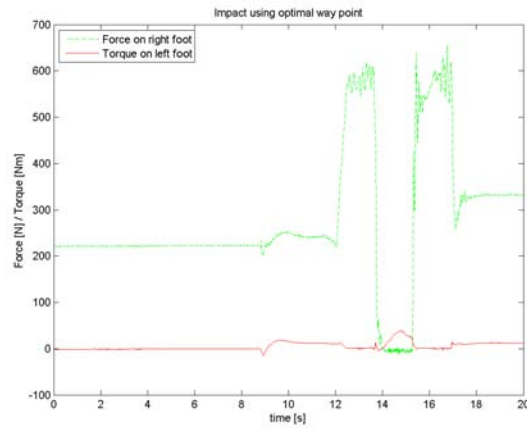


Figure 3.30: Force/torque sensor measurements in case of the trajectory with via point

Finally, a full humanoid model is presented to simulate different trajectories. A particular trajectory that permits to achieve an interpolation of position, velocity and acceleration is studied, simulated and implemented on a real robot.



## Chapter 4

# Humanoid Attitude Estimation



One fundamental requisite for the control of a humanoid is having a good state estimation of the robot. Typically the states comprise positions, velocities and orientations. Unlike classical robotics, where position and orientation can be calculated using kinematics algorithms from a fixed base, in mobile robotics such task is more complex. In particular, for the case of humanoid robots, the state estimation is important in order to detect the balance of the robot.

The robot orientation with respect to the gravity vector or with respect to the world frame is referred to as attitude. For the balance control the attitude can be described by the roll and pitch angles. Normally, the attitude estimation is achieved by combining several sensors, such as gyroscopes, inclinometers and accelerometers.

The attitude may be calculated using only the gyro output and integrating it. The problem is that the gyros measurements have usually significant noise, which may entail a great drift. Consequently, an absolute reference of the attitude can be obtained through the use of accelerometers, which provide the orientation with respect to the gravity vector. However, these are also quite sensitive to noise and, in addition, to the translational acceleration, which is usually considered as an additional noise component.

Even if the attitude estimation is a classical problem of mobile robotics [103] and of unmanned aerial vehicles (UAV) [104], several researchers have extended such techniques to legged locomotion [105] [106].

On the other hand, it is a fact the body motion for walking robots is inherently three-dimensional, making most kinematics representations nonlinear. Many researchers face this problem using Extended Kalman Filters [107]. For instance, Rehbinder and Hu have previously designed an algorithm [108] for fusing inclinometer and gyro data assuming low translational accelerations, which may not be very realistic for a walking robot. Successively, they have provided an algorithm consisting of two modes: one when accelerations are low and the other when these are high [105].

In this chapter an Extended Kalman Filter (EKF) is used in order to estimate the real state of the humanoid robot HRP-2 using the combination of the information coming from the encoders (kinematics) and from the IMU. The integration of the kinematics information into the Kalman filtering process allows a good estimation of the attitude and reduces the complexity of the problem to the use of simple kinematic transformations. The scheme for the robot state estimation is given in Figure 4.1, where:

$\mathbf{q}_a$  is the angles position vector read by encoders

$\boldsymbol{\omega}_s$  is the gyroscope measurement

$\mathbf{a}_s$  is the accelerometer measurement

$\mathbf{R}_c$  is the orientation estimation provided by kinematics

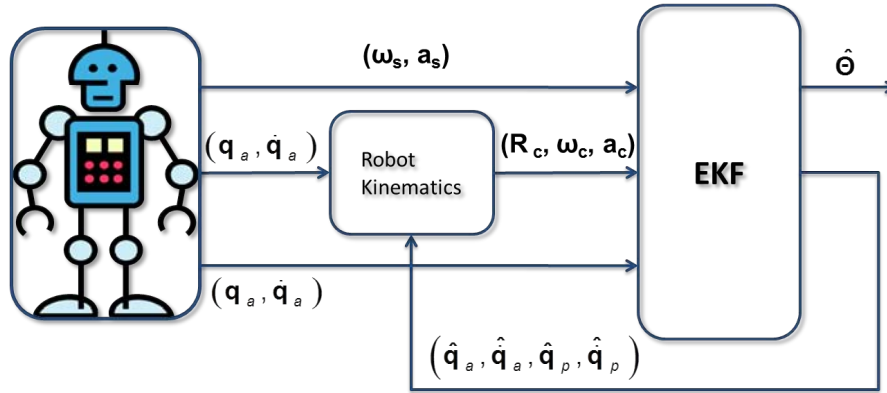


Figure 4.1: Attitude estimation scheme

$\omega_c$  is the angular velocity estimation provided by kinematics

$\mathbf{a}_c$  is the linear acceleration estimation provided by the kinematics

$\mathbf{q}_p$  is the estimation of passive DOFs, representing the mechanical flexibility

$\Theta$  is the attitude estimation

The rest of the chapter is organized as follows. First, a solution for the fusion of sensors estimations is presented. Then, an approach for the attitude estimation is detailed. The estimations are obtained without and with consideration of accelerations. Finally, some concluding remarks are briefly given.

## 4.1 Fusion of sensors estimations

This study provides a solution to fusing data from a 3-axis rate gyro and a 3-axis accelerometer in order to estimate the robot's attitude.

For the attitude representation in this system, the reference frames shown in Figure Figure 4.2 are used, where:

- $\mathcal{W}$  is an inertial world-fixed frame, with axis  $y_w$  pointing East and axis  $z_w$  pointing upward;
- $\mathcal{B}$  is a body-fixed frame attached to the sensor system in the chest of the robot, with axis  $x_b$  pointing at the forward direction of the robot and  $z_b$  pointing upward.

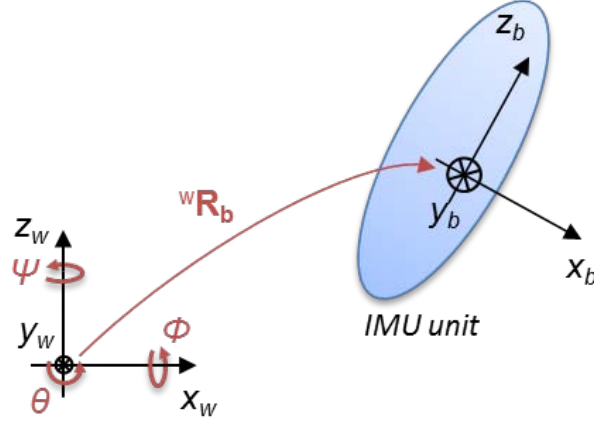


Figure 4.2: Reference frames

The 3-axis gyroscope provides the angular velocities of the body frame relative to the inertial frame, expressed in the body-fixed frame. The model of the gyroscopic measurements is given by:

$$\boldsymbol{\omega}_m = \boldsymbol{\omega} + \boldsymbol{\omega}_0 + \boldsymbol{\omega}_n \quad (4.1)$$

where  $\boldsymbol{\omega}$  is the real angular velocity and  $\boldsymbol{\omega}_0$  is the gyroscope bias that varies with a slow dynamics depending on the environment conditions. It is supposed to be constant with time, during the experiment [104]. The term  $\boldsymbol{\omega}_n$  is a Gaussian white noise.

The 3-axis accelerometer measures the difference between the inertial forces and gravity forces, expressed in frame  $\mathcal{B}$ . If the accelerometer output is  $\mathbf{y}$ , then the accelerometer model is

$$\mathbf{a}_m = {}^b\mathbf{R}_w (\mathbf{a} - \mathbf{g}) + \mathbf{a}_0 + \mathbf{a}_n \quad (4.2)$$

where  $\mathbf{a}_0$  is a bias and  $\mathbf{a}_n$  is a Gaussian white noise.

If  $\mathbf{p} = (x, y, z)$  is an arbitrary point, it will be denoted  $\mathbf{p}^w$  when expressed in frame  $\mathcal{W}$  and  $\mathbf{p}^b$  when expressed in frame  $\mathcal{B}$ , *i.e.*:

$$\mathbf{p}^w = {}^w\mathbf{o}_b + {}^w\mathbf{R}_b \mathbf{p}^b \quad (4.3)$$

where  ${}^w\mathbf{o}_b$  is the vector describing the origin of frame  $\mathcal{B}$  with respect to frame  $\mathcal{W}$ .

This equation can be rewritten as

$$\mathbf{p}^b = {}^w\mathbf{R}_b^T (\mathbf{p}^w - {}^w\mathbf{o}_b) \quad (4.4)$$

Using Equation (3.12), it is possible to write

$${}^w\dot{\mathbf{R}}_b = \mathbf{S}(\boldsymbol{\omega}^w) {}^w\mathbf{R}_b \quad (4.5)$$

which can be rewritten using Equation (3.15) as

$${}^w \dot{\mathbf{R}}_b^T = -{}^w \mathbf{R}_b^T \mathbf{S}(\boldsymbol{\omega}^w) = {}^w \mathbf{R}_b^T \mathbf{S}({}^w \mathbf{R}_b \boldsymbol{\omega}^b) = -\mathbf{S}(\boldsymbol{\omega}^b) {}^w \mathbf{R}_b^T \quad (4.6)$$

The kinematics of a rigid body is given by

$$\begin{cases} {}^w \ddot{\mathbf{o}}_b = \mathbf{a} \\ {}^w \dot{\mathbf{R}}_b^T(t) = -\mathbf{S}(\boldsymbol{\omega}^b(t)) {}^w \mathbf{R}_b^T(t) \end{cases} \quad (4.7)$$

where  $\mathbf{a}$  is the acceleration in frame  $\mathcal{W}$  and  $\mathbf{S}(\boldsymbol{\omega}^b)$  is the skew-symmetric matrix defined in Equation (3.12), whose angular velocity components are expressed in frame  $\mathcal{B}$ .

Consequently, the equation for the rotation can be written as

$${}^b \dot{\mathbf{R}}_w = -\mathbf{S}(\boldsymbol{\omega}^b) {}^b \mathbf{R}_w \quad (4.8)$$

Taking the time-derivative of Equation (3.3) and comparing with Equation (4.8), for the roll and pitch [108][105]

$$\dot{\mathbf{x}} = \begin{bmatrix} \dot{\phi} \\ \dot{\theta} \end{bmatrix} = \begin{bmatrix} 1 & \sin(\phi) \tan(\theta) & \cos(\phi) \tan(\theta) \\ 0 & \cos(\phi) & \sin(\phi) \end{bmatrix} \begin{bmatrix} \omega_x \\ \omega_y \\ \omega_z \end{bmatrix} \quad (4.9)$$

If the real acceleration is considered as a disturbance and the gravity vector  $\mathbf{g}$  as an entity to measure, the accelerometer can be used as an attitude sensor [103]. Thus

$$\mathbf{y} = {}^b \mathbf{R}_w (\mathbf{a} - \mathbf{g}) = \begin{bmatrix} -\sin(\theta) \\ \cos(\theta) \sin(\phi) \\ \cos(\phi) \cos(\theta) \end{bmatrix} g + {}^b \mathbf{R}_w \mathbf{a} \quad (4.10)$$

## 4.2 Extended Kalman Filter

The EKF evaluates the partial derivatives at the estimated state vector value and uses the full nonlinear functions on the estimate itself. The EKF assumes a model in the discrete form [106]:

$$\begin{aligned} \mathbf{x}(k+1) &= f(\mathbf{x}(k), \mathbf{u}(k)) + \boldsymbol{\nu}_k \\ \mathbf{y}(k) &= h(\mathbf{x}(k)) + \mathbf{w}_k \end{aligned} \quad (4.11)$$

The prediction phase will be

$$\mathbf{x}_{k+1|k} = f(\mathbf{x}_k, \mathbf{u}_k) \quad (4.12)$$

The predicted covariance is

$$\mathbf{P}_{k+1|k} = \mathbf{F}_k \mathbf{P}_{k|k} \mathbf{F}_k^T + \mathbf{F}_\nu \mathbf{Q} \mathbf{F}_\nu^T \quad (4.13)$$

where  $\mathbf{F}$  is the Jacobian matrix such that:

$$\mathbf{F} = \frac{\partial f}{\partial \mathbf{x}} \quad (4.14)$$

The measurement update:

$$\mathbf{x}_{k+1|k+1} = \mathbf{x}_{k+1|k} + \mathbf{K}_{k+1|k} (h(\mathbf{x}_k) - \mathbf{y}_k) \quad (4.15)$$

$$\mathbf{P}_{k+1|k+1} = \mathbf{P}_{k+1|k} + \mathbf{K}_{k+1|k} (h(\mathbf{x}_k) - \mathbf{y}_k) \mathbf{F}_k \mathbf{P}_{k|k} \mathbf{F}_k^T + \mathbf{Q} \quad (4.16)$$

### 4.3 Estimation without considering real acceleration

In the ideal case, when the accelerations are low enough to be neglected, the results are presented in the following figures. The real pitch/roll angles (estimated by a motion capture system) are compared with the OpenHRP estimation and the EKF estimation.

In Figures 4.3 and 4.4 the accelerometer noise standard deviation has been fixed to  $0.1\mathbf{I}[m/s^2]$ , to  $\mathbf{I}[m/s^2]$  in Figures 4.5 and 4.6, and to  $10\mathbf{I}[m/s^2]$  in Figures 4.7 and 4.8.

Figures 4.9 and 4.10 show the results of the estimations of the roll and pitch angles while the robot is on the crane and subjected to external pushing forces.

### 4.4 Estimation using real acceleration and mechanical flexibility

The flexibility in the ankle can be treated as a pair of passive joints:  $\mathbf{q}_p$  is the position vector of the robot flexibility in the ankle (pitch and roll) [109]. The position vector, of dimension  $n$ , of the active robot links (from the standing foot up to the IMU) is denoted as  $\mathbf{q}_a$ . The kinematic model of such system is resumed in Appendix D.

In a compact form the position vector of the joints is

$$\mathbf{q} = \begin{bmatrix} \mathbf{q}_p \\ \mathbf{q}_a \end{bmatrix} \quad (4.17)$$

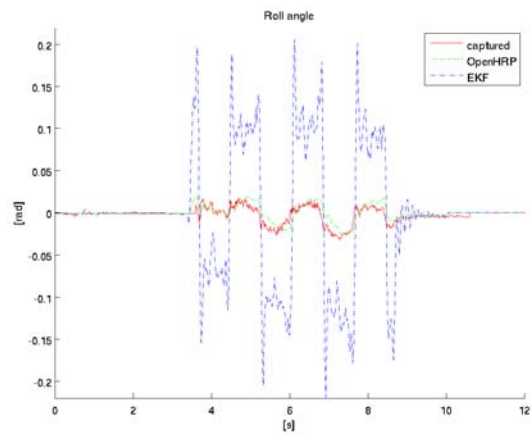


Figure 4.3: Estimation of roll angle with  $\sigma(a_n) = 0.1\mathbf{I}[m/s^2]$

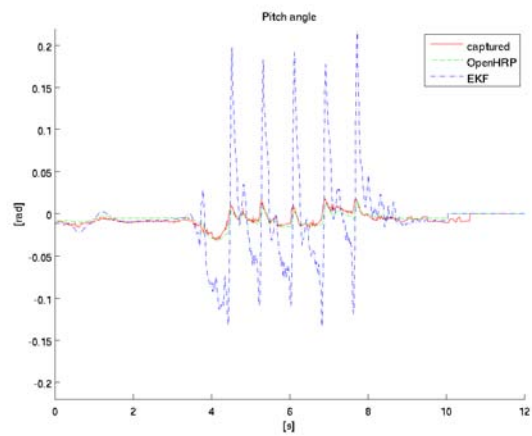


Figure 4.4: Estimation of pitch angle with  $\sigma(a_n) = 0.1\mathbf{I}[m/s^2]$

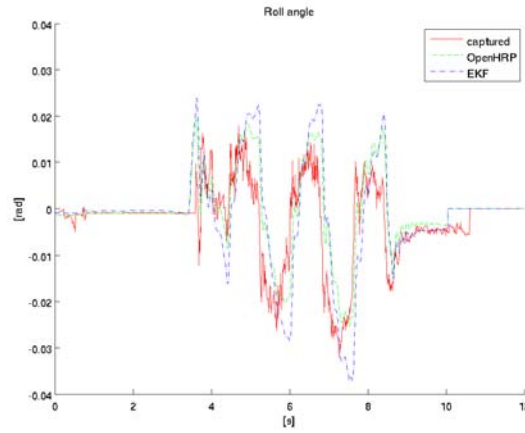


Figure 4.5: Estimation of roll angle with  $\sigma(a_n) = \mathbf{I}[m/s^2]$

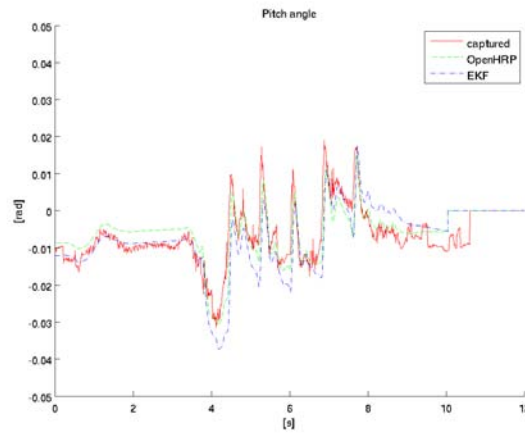


Figure 4.6: Estimation of pitch angle with  $\sigma(a_n) = \mathbf{I}[m/s^2]$

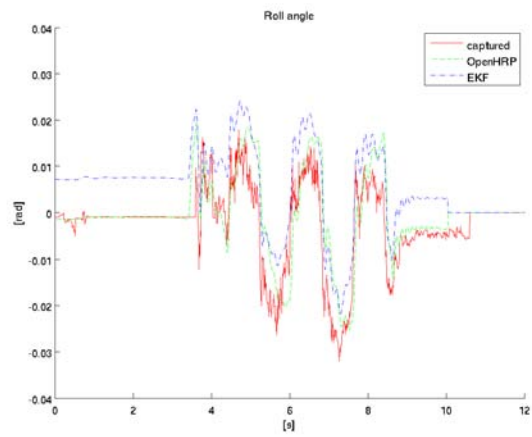


Figure 4.7: Estimation of roll angle with  $\sigma(a_n) = 10\mathbf{I}[m/s^2]$

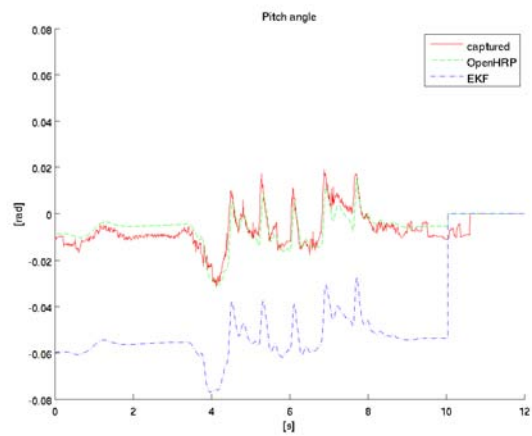


Figure 4.8: Estimation of pitch angle with  $\sigma(a_n) = 10\mathbf{I}[m/s^2]$

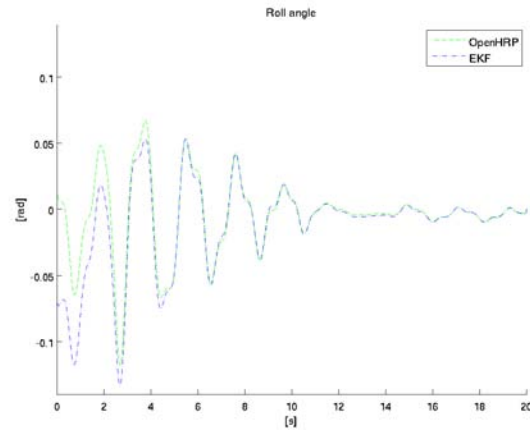


Figure 4.9: Estimation of roll angle with  $\sigma(a_n) = \mathbf{I}[m/s^2]$ . Robot on the crane and subjected to external pushing forces

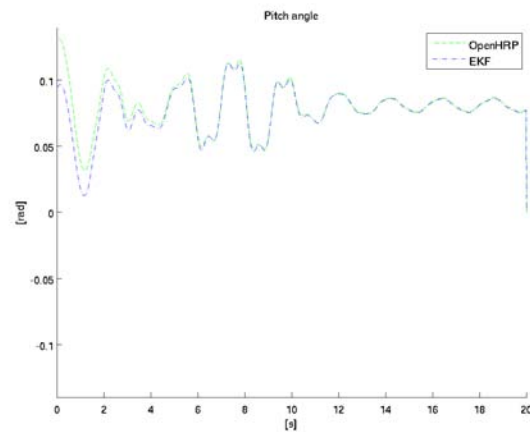


Figure 4.10: Estimation of pitch angle with  $\sigma(a_n) = \mathbf{I}[m/s^2]$ . Robot on the crane and subjected to external pushing forces

The size of such vector is  $n_p = n + 2$ . The robot state vector is selected to be

$$\mathbf{x} = \begin{bmatrix} \mathbf{q} \\ \dot{\mathbf{q}} \\ \ddot{\mathbf{q}} \\ \boldsymbol{\omega}_0 \end{bmatrix} = \begin{bmatrix} \mathbf{q}_p \\ \mathbf{q}_a \\ \dot{\mathbf{q}}_p \\ \dot{\mathbf{q}}_a \\ \ddot{\mathbf{q}}_p \\ \ddot{\mathbf{q}}_a \\ \boldsymbol{\omega}_0 \end{bmatrix} \quad (4.18)$$

where  $\mathbf{q}$  is the position vector of the robot links.

So, the state transition will be

$$\begin{bmatrix} \mathbf{q}_p(k+1) \\ \mathbf{q}_a(k+1) \\ \dot{\mathbf{q}}_p(k+1) \\ \dot{\mathbf{q}}_a(k+1) \\ \ddot{\mathbf{q}}_p(k+1) \\ \ddot{\mathbf{q}}_a(k+1) \\ \boldsymbol{\omega}_0(k+1) \end{bmatrix} = \begin{bmatrix} \mathbf{1} & \mathbf{0} & \mathbf{T}_s & \mathbf{0} & \mathbf{0} & \mathbf{0} & \mathbf{0} \\ \mathbf{0} & \mathbf{1} & \mathbf{0} & \mathbf{T}_s & \mathbf{0} & \mathbf{0} & \mathbf{0} \\ \mathbf{0} & \mathbf{0} & \mathbf{1} & \mathbf{0} & \mathbf{0} & \mathbf{0} & \mathbf{0} \\ \mathbf{0} & \mathbf{0} & \mathbf{0} & \mathbf{1} & \mathbf{0} & \mathbf{T}_s & \mathbf{0} \\ \mathbf{0} & \mathbf{0} & \mathbf{0} & \mathbf{0} & \mathbf{1} & \mathbf{0} & \mathbf{T}_s \\ \mathbf{0} & \mathbf{0} & \mathbf{0} & \mathbf{0} & \mathbf{0} & \mathbf{1} & \mathbf{0} \\ \mathbf{0} & \mathbf{0} & \mathbf{0} & \mathbf{0} & \mathbf{0} & \mathbf{0} & \mathbf{1} \end{bmatrix} \begin{bmatrix} \mathbf{q}_p(k) \\ \mathbf{q}_a(k) \\ \dot{\mathbf{q}}_p(k) \\ \dot{\mathbf{q}}_a(k) \\ \ddot{\mathbf{q}}_p(k) \\ \ddot{\mathbf{q}}_a(k) \\ \boldsymbol{\omega}_0(k) \end{bmatrix} + \begin{bmatrix} \mathbf{n}_{p,p} \\ \mathbf{n}_{a,p} \\ \mathbf{n}_{p,v} \\ \mathbf{n}_{a,v} \\ \mathbf{n}_{p,a} \\ \mathbf{n}_{a,a} \\ \mathbf{n}_\omega \end{bmatrix} \quad (4.19)$$

where  $T_s$  is the sampling time.

The measurements will be defined by the nonlinear system

$$\mathbf{y} = \begin{bmatrix} \mathbf{a}_b \\ \boldsymbol{\omega}_b \\ \dot{\mathbf{q}}_e \\ \mathbf{q}_e \end{bmatrix} = \begin{bmatrix} {}^b\mathbf{R}_w(\mathbf{a} - \mathbf{g}) \\ \boldsymbol{\omega} + \boldsymbol{\omega}_0 \\ \dot{\mathbf{q}}_a \\ \mathbf{q}_a \end{bmatrix} + \begin{bmatrix} \mathbf{a}_n \\ \boldsymbol{\omega}_n \\ \mathbf{q}_n \\ \mathbf{q}_{n,d} \end{bmatrix} \quad (4.20)$$

where  $\mathbf{q}_e$  is the position read by the encoders.

Now, defining  $\mathbf{J}_P$  as the  $(3 \times n)$  matrix relating the contribution of the joint velocities  $\dot{\mathbf{q}}$  to the linear velocity and  $\mathbf{J}_O$  as the  $(3 \times n)$  matrix relating the contribution of the joint velocities  $\dot{\mathbf{q}}$  to the angular velocity, it is possible to write

$$\mathbf{J}(\mathbf{q}) = \begin{bmatrix} \mathbf{J}_P(\mathbf{q}) \\ \mathbf{J}_O(\mathbf{q}) \end{bmatrix} \quad (4.21)$$

For  $\mathbf{a}$  being the linear acceleration, it can be written

$$\mathbf{a} = \mathbf{J}_P \ddot{\mathbf{q}} + \dot{\mathbf{J}}_P \dot{\mathbf{q}} = \mathbf{J}_P \ddot{\mathbf{q}} + \dot{\mathbf{q}}^T \mathbf{H}_P \dot{\mathbf{q}} \quad (4.22)$$

the Hessian matrix being denoted by  $\mathbf{H}_P = \frac{\partial \mathbf{J}_P}{\partial \mathbf{q}}$ .

Finally Equation (4.20) can be rewritten as

$$\mathbf{y} = \begin{bmatrix} \mathbf{a}_b \\ \boldsymbol{\omega}_b \\ \dot{\mathbf{q}}_e \\ \mathbf{q}_e \end{bmatrix} = \begin{bmatrix} {}^b\mathbf{R}_w(\mathbf{q}) (\mathbf{J}_P(\mathbf{q})\ddot{\mathbf{q}} + \dot{\mathbf{q}}^T \mathbf{H}_P(\mathbf{q})\dot{\mathbf{q}} - \mathbf{g}) \\ \mathbf{J}_O(\mathbf{q})\dot{\mathbf{q}} + \boldsymbol{\omega}_0 \\ \dot{\mathbf{q}}_a \\ \mathbf{q}_a \end{bmatrix} + \begin{bmatrix} \mathbf{a}_n \\ \boldsymbol{\omega}_n \\ \mathbf{q}_n \\ \mathbf{q}_{n,d} \end{bmatrix} \quad (4.23)$$

For the sake of simplicity, matrix  ${}^b\mathbf{R}_w$  will be denoted as  $\mathbf{R}$ . Writing the measurement function as

$$h(\mathbf{x}) = \begin{bmatrix} \mathbf{R} (\mathbf{J}_P\ddot{\mathbf{q}} + \dot{\mathbf{q}}^T \mathbf{H}_P\dot{\mathbf{q}} - \mathbf{g}) \\ \mathbf{J}_O\dot{\mathbf{q}} + \boldsymbol{\omega}_0 \\ \dot{\mathbf{q}}_a \\ \mathbf{q}_a \end{bmatrix} \quad (4.24)$$

its Jacobian matrix can be written as:

$$\mathbf{H} = \frac{\partial h}{\partial \mathbf{x}} = [ \mathbf{H}_q \quad \mathbf{H}_{\dot{q}} \quad \mathbf{H}_{\ddot{q}} \quad \mathbf{H}_{\boldsymbol{\omega}_0} ] \quad (4.25)$$

where

$$\mathbf{H}_q = \begin{bmatrix} \frac{\partial \mathbf{R}}{\partial \mathbf{q}} (\mathbf{J}_P\ddot{\mathbf{q}} + \dot{\mathbf{q}}^T \mathbf{H}_P\dot{\mathbf{q}} - \mathbf{g}) + \mathbf{R} (\mathbf{H}_P\ddot{\mathbf{q}} + \dot{\mathbf{q}}^T \mathbf{K}_P\dot{\mathbf{q}}) \\ \mathbf{H}_O\dot{\mathbf{q}} \\ \mathbf{0}_{2,n} \\ \mathbf{0}_{n,n} \\ \mathbf{0}_{2,n} \\ \mathbf{I}_n \end{bmatrix} \quad (4.26)$$

where  $\mathbf{K}_P = \frac{\partial \mathbf{H}_P}{\partial \mathbf{q}}$  is the second-derivative of the Jacobian  $\mathbf{J}_P$ .

$$\mathbf{H}_{\dot{q}} = \begin{bmatrix} \mathbf{R} (\mathbf{H}_P\dot{\mathbf{q}} + \dot{\mathbf{q}}^T \mathbf{H}_P) \\ \mathbf{J}_O \\ \mathbf{0}_{2,n} \\ \mathbf{I}_n \\ \mathbf{0}_{2,n} \\ \mathbf{0}_{n,n} \end{bmatrix} \quad (4.27)$$

$$\mathbf{H}_{\ddot{q}} = \begin{bmatrix} \mathbf{R}\mathbf{J}_P \\ \mathbf{0}_{3,n+2} \\ \mathbf{0}_{n+2,n+2} \\ \mathbf{0}_{n+2,n+2} \end{bmatrix} \quad (4.28)$$

$$\mathbf{H}_{\boldsymbol{\omega}_0} = \begin{bmatrix} \mathbf{0}_{3,3} \\ \mathbf{I}_3 \\ \mathbf{0}_{n,3} \\ \mathbf{0}_{n,3} \end{bmatrix} \quad (4.29)$$

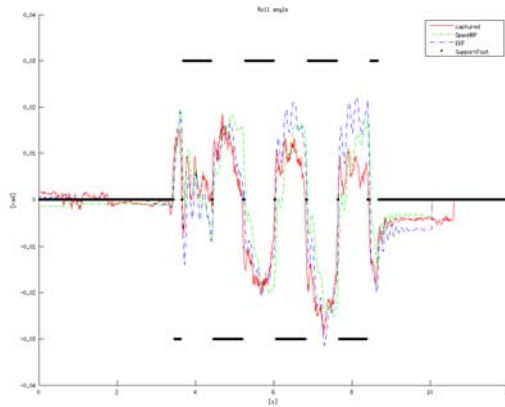


Figure 4.11: Roll angle estimation

denoting  $\mathbf{O}_{i,j}$  as the zero matrix of size  $i \times j$  and  $\mathbf{I}_i$  as the identity matrix of size  $i \times i$ .

In Figures 4.11 to 4.13 the results of the estimation during a standard forward walking are presented. The captured data is compared with the OpenHRP estimation and the EKF estimation.

Finally, Figure 4.14 presents an estimation of the flexibility in the robot ankle.

## 4.5 Chapter summary

This chapter has studied a major problem when dealing with the control of humanoid platforms: the attitude estimation.

While most authors estimate the robot attitude combining acceleration and gyroscope measurements through the use of EKF, in this approach the kinematics information is also integrated in order to improve the filtering. Using the information coming from the robot encoders and simple kinematic transformations, this method allows obtaining a good estimation of the robot attitude with respect to the world frame, even considering the existence of accelerations and mechanical flexibilities in the robot.

This method has been implemented on the humanoid robot HRP-2, comparing the results with the information obtained from the robot inner stabilizer and showing the better performance of the proposed approach.

It is important to stress that the comparison between the EKF with kinematics information and the EKF running in OpenHRP is made considering that the real robot attitude is the one calculated through the Motion Capture System. Anyway, it is not clearly known how the OpenHRP estimates the robot attitude, since it is a

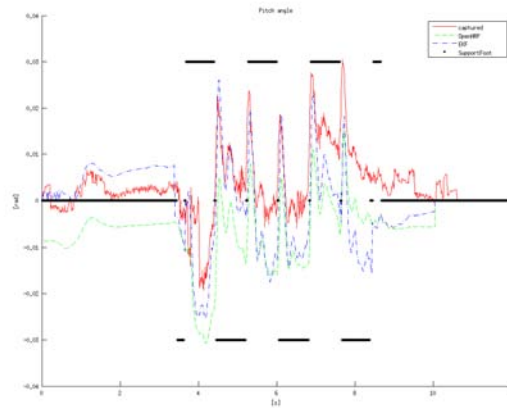


Figure 4.12: Pitch angle estimation

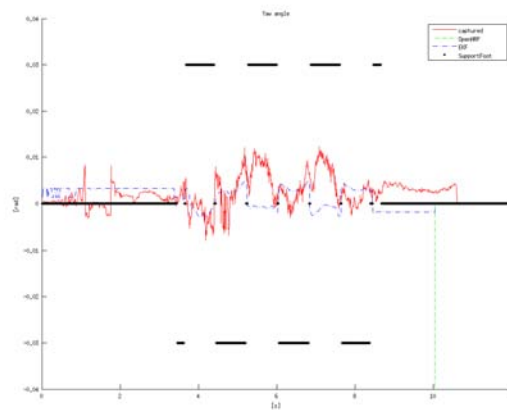


Figure 4.13: Yaw angle estimation

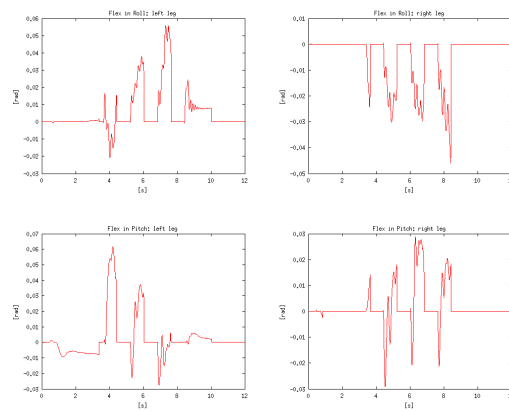


Figure 4.14: Estimation of the flexibility in the ankle

closed system. On the contrary, the estimation presented in this chapter is open and can be extended to any robot.

## Chapter 5

# Stabilizer Architecture for a Humanoid Robot



The study presented in this chapter focuses on a novel technique for the humanoid control, based on a very well-known and simplified model: the double inverted pendulum. This model permits to have a real-time control on the structure while submitted to external forces/disturbances. The control actions are strongly dependent on three stability regions, which are determined by the position of the ZMP in the support polygon.

The stabilizing control algorithm for a humanoid robot may be faced in several ways. This work tries to solve the problem of maintaining the humanoid in an upright position, using two types of controllers. The attitude controller is actually regulating the roll and pitch angles of the robot CoM, whereas the balance controller is balancing the robot, controlling the ZMP.

Two kinds of balancers are proposed, the use of which depends on the degree of severity of the situation. When the robot is subjected to small disturbances, a static low-gained controller is used. In the critical case of a large disturbance, a dynamical controller is used which properly generates fast control actions.

## 5.1 Task definition

A task may be defined as explained in Chapter 3, as a vector  $\mathbf{x}$  in the operational space. As in Equation (3.19), the solution may be found as [1]:

$$\ddot{\mathbf{q}} = \mathbf{J}^\dagger (\mathbf{K}\mathbf{x} - \dot{\mathbf{q}}^T \mathbf{H}\dot{\mathbf{q}}) + (\mathbf{I} - \mathbf{J}^\dagger \mathbf{J}) \ddot{\mathbf{q}}_0 \quad (5.1)$$

In this case, vector  $\ddot{\mathbf{q}}_0$  may be used to fulfil a secondary solution, which can be chosen so as to optimize an objective function. In classical robotics, such solution is used to move away from the joints limits or from obstacles.

For instance, when the robot is walking, only the robot legs and waist of the task Jacobian  $\mathbf{J}$  will of interest; so it would be useful to use the remaining DOFs to reduce the ZMP distance from the foot origin.

## 5.2 ZMP regions

In this section, the concept of ZMP regions is introduced. In particular, three regions are defined depending on the position of the ZMP, as suggested in [29].

The control action applied by the stabilizer will strongly depend on the position of the ZMP with respect to the support area. In the balanced area (safe region), the control action will not actuate, leaving the vector of the secondary solution being used for other purposes.

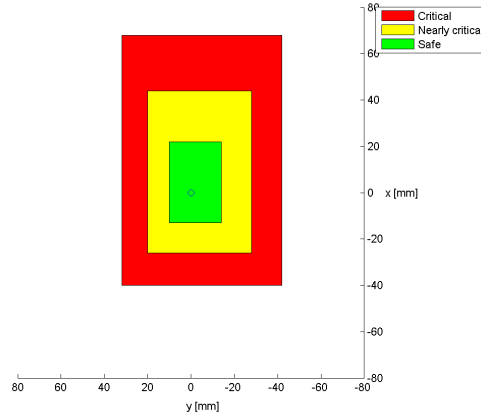


Figure 5.1: Graphical example for stability regions: humanoid standing on right foot

In the nearly critical region, the control action will actuate as a secondary solution. This may be the case of a walking task. As humans do, the robot may use its arms in order to reduce the zero-moment point position closer to the safe region.

Finally, in the critical region, the stabilizer will actually disconnect the ongoing task and actuate on the full body. Even if this region is still stable, the balance may be easily lost. In order to avoid control discontinuities which may even further undermine robot balance, adequate trajectories have to be used which permit continuity in the acceleration domain.

In Figure 5.1, an example of such regions is given for the humanoid robot HOAP-3 standing on the right foot. The foot origin is graphically represented by a blue circle.

### 5.3 The full humanoid body as a composition of inverted pendulums

The full humanoid robot may be simplified using a combination of different double inverted pendulums. If the state of the robot is considered to be as  $\boldsymbol{\chi} = [\boldsymbol{\chi}_{sl}, \boldsymbol{\chi}_{fl}, \boldsymbol{\chi}_{ra}, \boldsymbol{\chi}_{la}]^T$ , where  $\boldsymbol{\chi}_i = [\alpha_i, \gamma_i]^T$ , being  $i = sl, fl, ra, la$ , representing the state (roll and pitch angles) of the standing leg, the floating leg and right and left arms, respectively, the equations of motion (3.58) can be used to calculate the position of the ZMP:

$$\mathbf{p}_{ZMP} = \frac{1}{gM} \left( \begin{bmatrix} \boldsymbol{\beta}_{sl} & \boldsymbol{\beta}_{fl} & \boldsymbol{\beta}_{ra} & \boldsymbol{\beta}_{la} \end{bmatrix} \ddot{\boldsymbol{\chi}} + \begin{bmatrix} \mathbf{0} & \boldsymbol{\kappa}_{fl} & \boldsymbol{\kappa}_{ra} & \boldsymbol{\kappa}_{la} \end{bmatrix} \dot{\boldsymbol{\chi}} + \boldsymbol{\iota} \right) \quad (5.2)$$

where the total mass of the robot is  $M = m_b + m_l + 2m_a$ ,  $m_b$  being the standing bodies masses,  $m_l$  the leg mass and  $m_a$  the arm mass. Such equation is calculated using the

sum of the effects of every inverted pendulum. The acceleration contribution of the standing leg is:

$$\boldsymbol{\beta}_{sl} = l_b^2 M \begin{bmatrix} 0 & -1 \\ 1 & 0 \end{bmatrix} \quad (5.3)$$

The acceleration contribution for the floating leg, right or left arm, is  $\boldsymbol{\beta}_i(\boldsymbol{\chi}_{sl}, \boldsymbol{\chi}_i)$ , with  $i = fl, ra, la$ :

$$\boldsymbol{\beta}_i = m_i l_b l_i \begin{bmatrix} 0 & -\cos(\gamma_{sl} - \gamma_i) \\ \cos(\alpha_{sl} - \alpha_i) & 0 \end{bmatrix} \quad (5.4)$$

The velocity contribution of the floating leg and right and left arms  $\boldsymbol{\kappa}_i(\boldsymbol{\chi}_{sl}, \boldsymbol{\chi}_i, \dot{\boldsymbol{\chi}}_i)$  is:

$$\boldsymbol{\kappa}_{sl} = m_i l_{sl} l_i \begin{bmatrix} 0 & -\sin(\gamma_{sl} - \gamma_i) \dot{\gamma}_i \\ \sin(\alpha_{sl} - \alpha_i) \dot{\alpha}_i & 0 \end{bmatrix} \quad (5.5)$$

And  $\boldsymbol{\nu}(\boldsymbol{\chi}_{sl})$ :

$$\boldsymbol{\nu} = M l_b g \begin{bmatrix} \sin(\gamma_{sl}) \\ -\sin(\alpha_{sl}) \end{bmatrix} \quad (5.6)$$

It has to be noted that  $\boldsymbol{\chi}$  is function of the pendulum position:

$$\boldsymbol{\chi} = \begin{bmatrix} -\arctan\left(\frac{y}{z}\right) \\ \arctan\left(\frac{x}{z}\right) \end{bmatrix} \quad (5.7)$$

$$\mathbf{J}_p = \begin{bmatrix} 0 & -\frac{z}{y^2+z^2} & \frac{y}{y^2+z^2} \\ \frac{z}{x^2+z^2} & 0 & -\frac{x}{x^2+z^2} \end{bmatrix} \quad (5.8)$$

## 5.4 Attitude control

The robot attitude may be easily controlled using the inverse kinematics with the Jacobian of the supporting leg regarding the roll and pitch rows.

Using the control scheme of Figure 3.2, the roll and pitch angles of the CoM with respect to the world frame are controlled.

In particular, in Figure 5.2 there are the roll and pitch errors for a humanoid robot standing on the right foot. The algorithm is using the remaining DOFs of the right leg and the waist in order to move away from joints limits. The reference positions for joints angles are in Figure 5.3 and Figure 5.4.

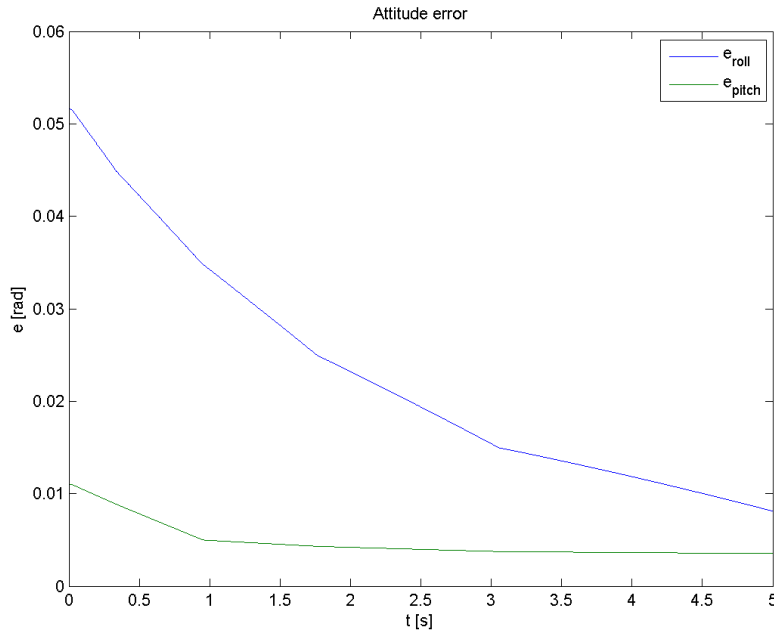


Figure 5.2: Attitude control error

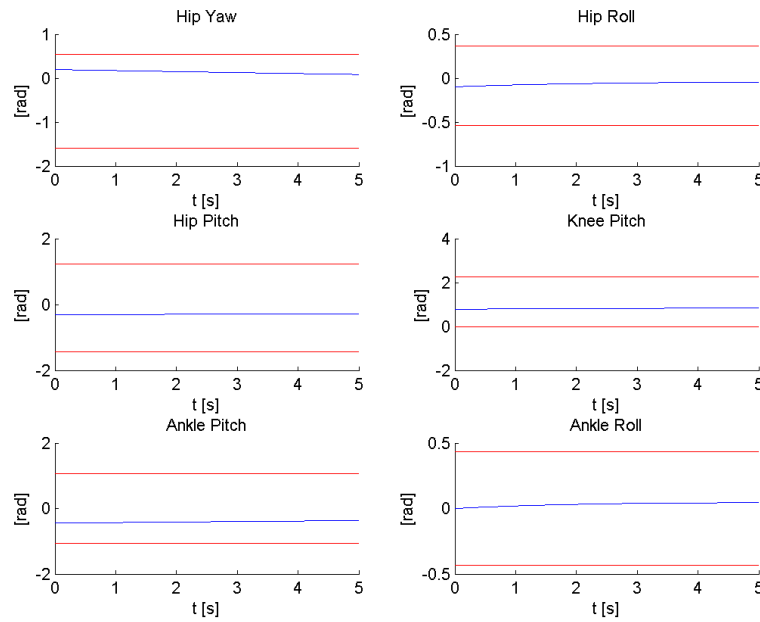


Figure 5.3: Right leg joints angles for the attitude control

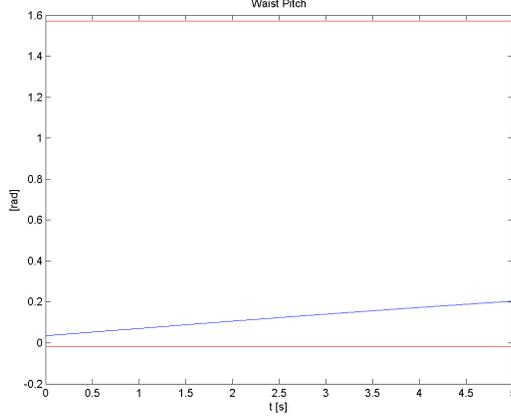


Figure 5.4: Waist angles for the attitude control

## 5.5 Static balance control

The objective of the balance control is finding a proper control action for reducing the distance of the ZMP from the foot center. For a static balance, *i.e.* for balancing the humanoid platform without taking into account CoM accelerations, the stability may be achieved using the standing leg and waist joints, considering that:

$$\dot{\mathbf{p}}_{ZMP} = \frac{\partial \mathbf{p}_{ZMP}}{\partial \boldsymbol{\chi}_{sl}} \frac{\partial \boldsymbol{\chi}_{sl}}{\partial \mathbf{p}_{sl}} \frac{\partial \mathbf{p}_{sl}}{\partial \mathbf{q}_{sl}} \dot{\mathbf{q}}_{sl} = \mathbf{J}_{ZMP}(\boldsymbol{\chi}_{sl}) \mathbf{J}_{\boldsymbol{\chi}_{sl}}(\mathbf{p}_{sl}) \mathbf{J}_{\mathbf{p}_{sl}}(\mathbf{q}_{sl}) \dot{\mathbf{q}}_{sl} \quad (5.9)$$

From such equation, it is possible to determine the desired control actions for the joints under consideration.

The static balance control is used when the ZMP is in the safer regions. The simulated results for the ZMP control are in Figure 5.5. The reference positions for joints angles are in Figure 5.6 and Figure 5.7. In Figure 5.8 and Figure 5.9 the submitted joints torques are depicted, showing the feasibility of the control actions.

## 5.6 Dynamic balance control

In the most critical case, the simple solution of a static balance controller is not enough. In this case, it is necessary to use the pendulums accelerations efficiently in order to achieve the balance.

The control action for the humanoid balance may be found using Equation (5.2) in order to set the ZMP position:

$$\hat{\mathbf{p}}_{ZMP} \approx \mathbf{J}_c \ddot{\mathbf{q}}_c + \boldsymbol{\eta}(\boldsymbol{\chi}, \dot{\boldsymbol{\chi}}, \ddot{\boldsymbol{\chi}}_{fl}) \quad (5.10)$$

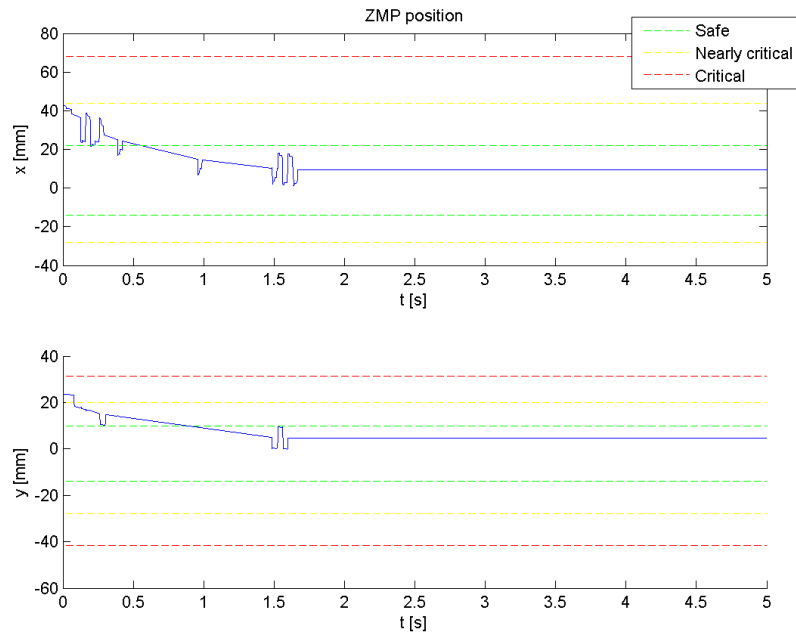


Figure 5.5: ZMP position for the static balance control

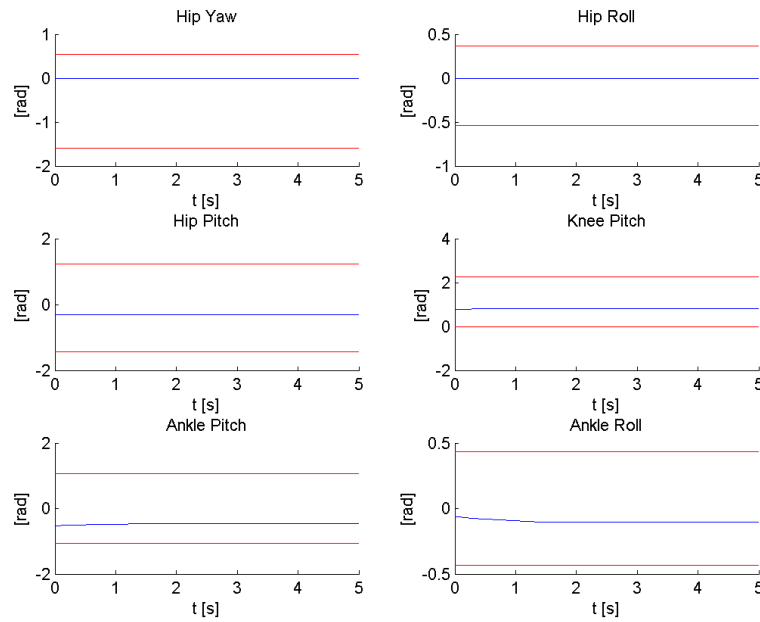


Figure 5.6: Right leg joints angles for the static balance control

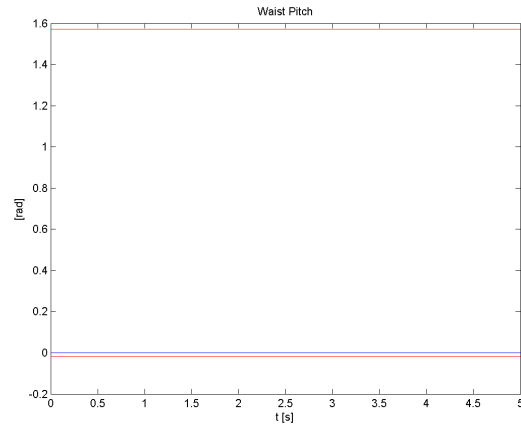


Figure 5.7: Waist angles for the static balance control

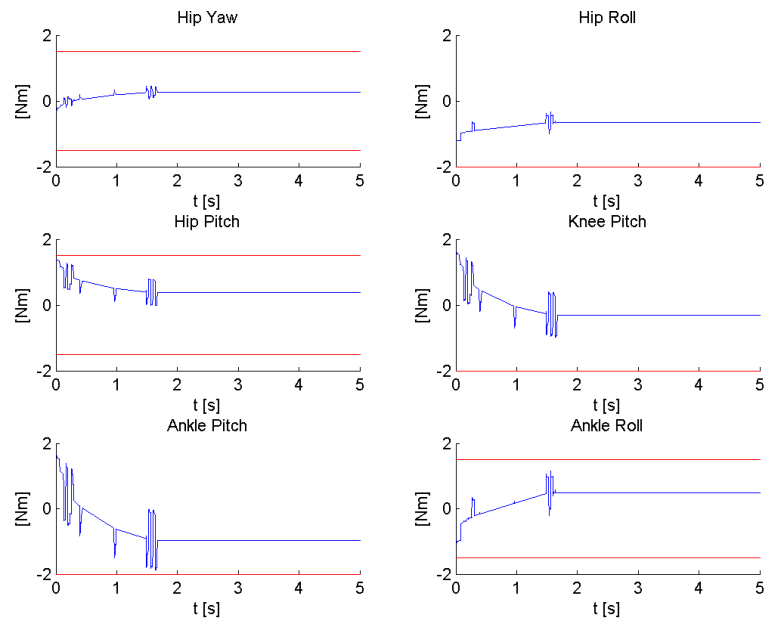


Figure 5.8: Right leg joints torques for the static balance control

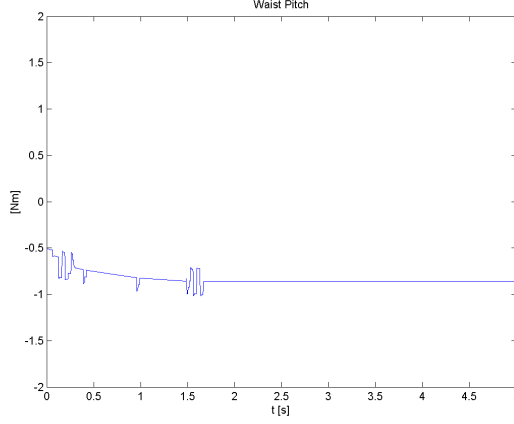


Figure 5.9: Waist torques for the static balance control

The approximation in such equation is due to the fact that second order derivatives are neglected.

The  $\boldsymbol{\eta}(\boldsymbol{\chi}, \dot{\boldsymbol{\chi}}, \ddot{\boldsymbol{\chi}}_{fl})$  term takes into account the velocity and gravity contributions of the double pendulums together with the acceleration contribution of the pendulums which are not being controlled. In this case, the floating leg is not controlled for the balance:

$$\boldsymbol{\eta}(\boldsymbol{\chi}, \dot{\boldsymbol{\chi}}, \ddot{\boldsymbol{\chi}}_{fl}) = \frac{1}{gM} (\boldsymbol{\beta}_{fl} \ddot{\boldsymbol{\chi}}_{fl} + [\mathbf{0} \quad \boldsymbol{\kappa}_{fl} \quad \boldsymbol{\kappa}_{ra} \quad \boldsymbol{\kappa}_{la}] \dot{\boldsymbol{\chi}} + \boldsymbol{\iota}) \quad (5.11)$$

In this case the Jacobian  $\mathbf{J}_c$  is:

$$\mathbf{J}_c = \frac{1}{gM} \left( [\boldsymbol{\beta}_{sl} \quad \boldsymbol{\beta}_{ra} \quad \boldsymbol{\beta}_{la}] \begin{bmatrix} \mathbf{J}_{sl} & \mathbf{0} & \mathbf{0} \\ \mathbf{J}_{sl} & \mathbf{J}_{ra} & \mathbf{0} \\ \mathbf{J}_{sl} & \mathbf{0} & \mathbf{J}_{la} \end{bmatrix} \right) \ddot{\mathbf{q}} \quad (5.12)$$

and a generic  $\mathbf{J}_i$  is:

$$\mathbf{J}_i = \mathbf{J}_{ZMP}(\boldsymbol{\chi}_i) \mathbf{J}_{\boldsymbol{\chi}_i}(\mathbf{p}_i) \mathbf{J}_{\mathbf{p}_i}(\mathbf{q}_i) \quad (5.13)$$

The simulation results for the ZMP for the case of the dynamic controller are in Figure 5.10. The dynamic controller responds to disturbances randomly created and controls using joints accelerations. The feasibility of the control actions is shown in Figure 5.11 and Figure 5.12, where the joints torques are depicted.

## 5.7 Walking pattern generation

The humanoid dynamics when the robot is standing on one leg can be simplified using an inverted pendulum.

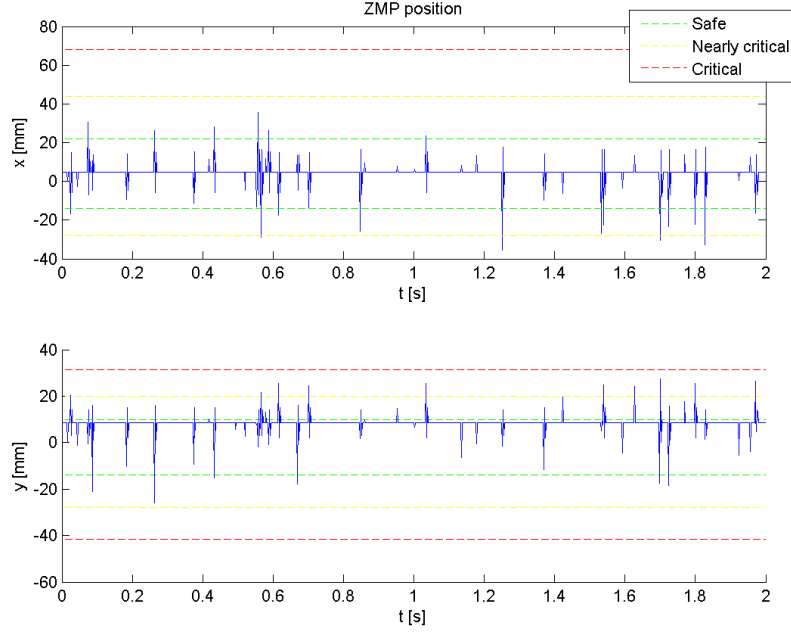


Figure 5.10: ZMP position for the dynamic balance control by right standing leg

Such model can be used as a walking generator, as suggested by Kajita *et al* in [110].

In particular, the motion can be described by the differential equation

$$\ddot{\mathbf{p}}_{CoM} = \frac{g}{z_c} (\mathbf{p}_{CoM} - \mathbf{p}_{ZMP}) \quad (5.14)$$

If  $\mathbf{p} = {}^{ZMP}\mathbf{p}_{CoM}$ , the general solution is:

$$\begin{aligned} \mathbf{p} &= \mathbf{p}_i \cosh\left(\frac{t-t_i}{T_c}\right) + \dot{\mathbf{p}}_i T_c \sinh\left(\frac{t-t_i}{T_c}\right) \\ \dot{\mathbf{p}} &= \mathbf{p}_i \frac{1}{T_c} \sinh\left(\frac{t-t_i}{T_c}\right) + \dot{\mathbf{p}}_i \cosh\left(\frac{t-t_i}{T_c}\right) \end{aligned} \quad (5.15)$$

given the initial conditions  $(\mathbf{p}_i, \dot{\mathbf{p}}_i)$  at time  $t = t_i$ .

Defining  $T_c$  as  $\sqrt{\frac{z_c}{g}}$ , from Figure 5.13 and from Equation (5.15), the following conditions hold:

$$\begin{aligned} \beta &= \alpha \cosh\left(\frac{T_{SS}}{2T_c}\right) \\ v_{ds(y)} &= \frac{\alpha d}{T_c} \sinh\left(\frac{T_{SS}}{2T_c}\right) \\ T_{DS} &= 2 \frac{1-\beta}{v_{ds(y)}} d \end{aligned} \quad (5.16)$$

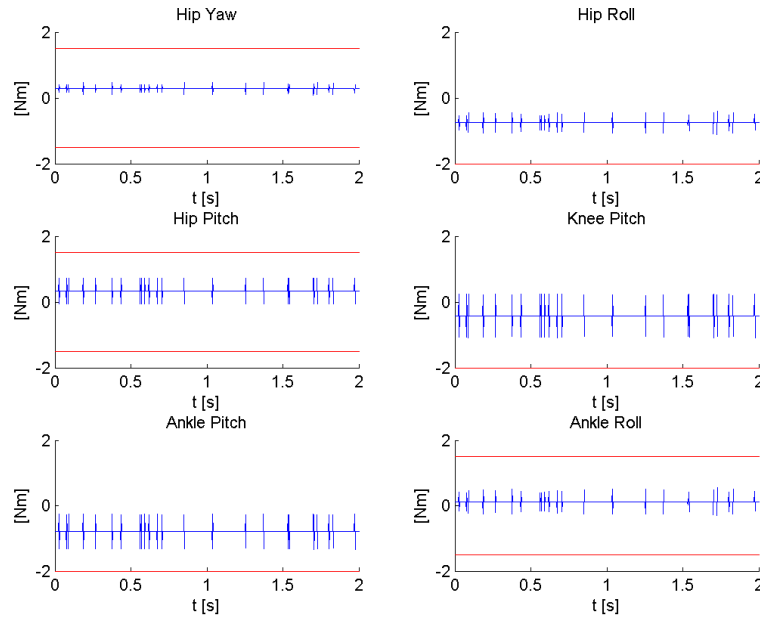


Figure 5.11: Right leg joints torques for the dynamic balance control by right standing leg

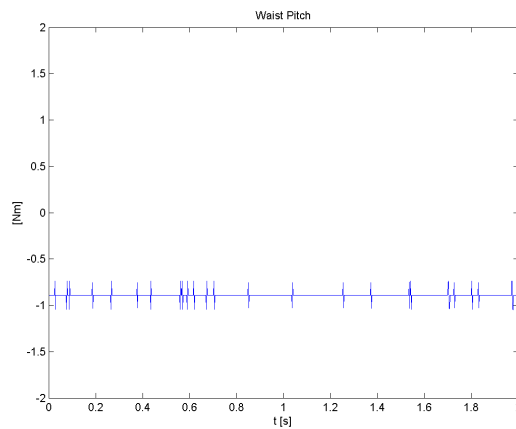


Figure 5.12: Waist torques for the dynamic balance control by right standing leg

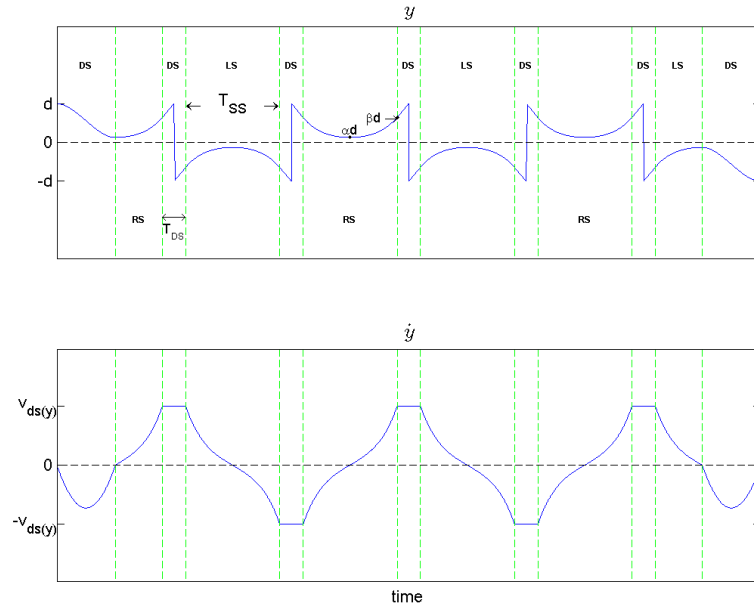


Figure 5.13: Position and velocity of the CoM in the lateral plane

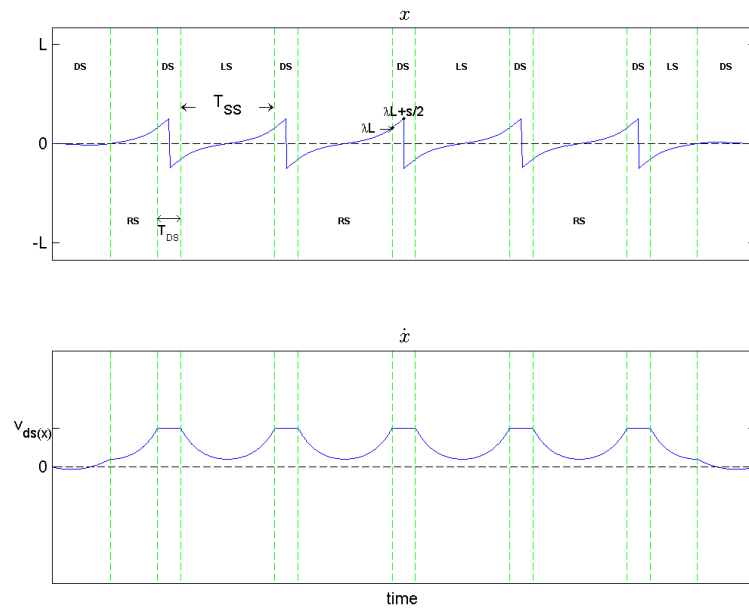


Figure 5.14: Position and velocity of the CoM in the step direction

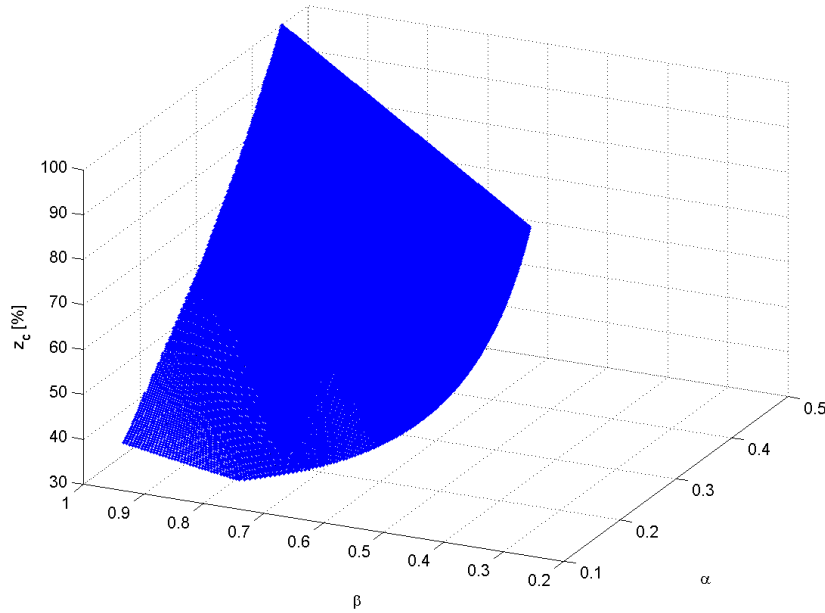


Figure 5.15: Relationship between lateral displacements and CoM height

The position and velocities trajectories using this model are presented in Figure 5.13 and Figure 5.14.

The relationship between the displacements in lateral motions and the CoM height is presented in Figure 5.15.

### 5.7.1 Walking generation with velocity continuity

In order to properly join the different walking phases, it is possible to use a different strategy for the double-support phase. In this phase the initial and final positions may be interpolated using a third order polynomial giving position and velocity continuity.

The step generation is divided into three phases: a first double-support phase used to carry the robot on single-support, the single-support phase and a last double-support phase used to finish the step.

Given the exact displacements with a mean velocity in the sagittal plane to be executed by the robot, the duration of these three phases are univocally determined giving continuity among them. The results are given in Figure 5.16 and Figure 5.17.

Using this continuity in the position and velocity, this algorithm can be used for generating a fast step when a large disturbance is affecting the robot. In particular, when the robot is moving for a grasping task, a large disturbance may undermine

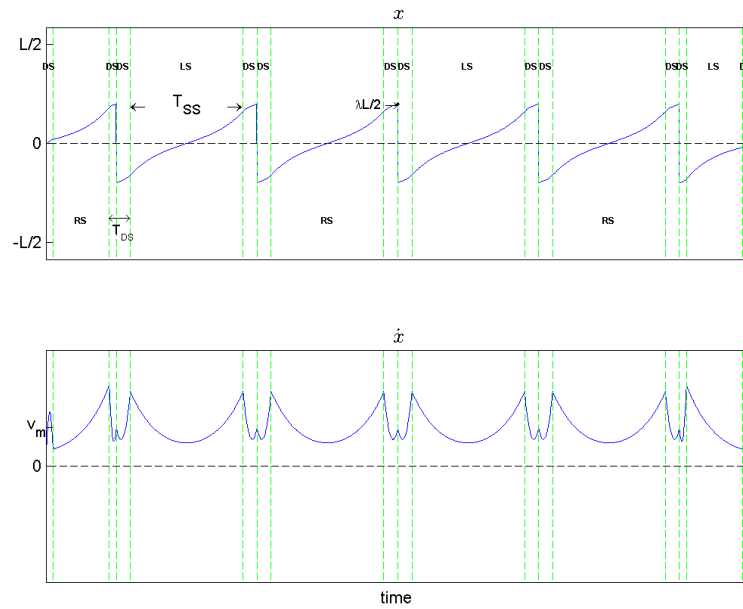


Figure 5.16: Position and velocity of the CoM in the step direction using third polynomial interpolation

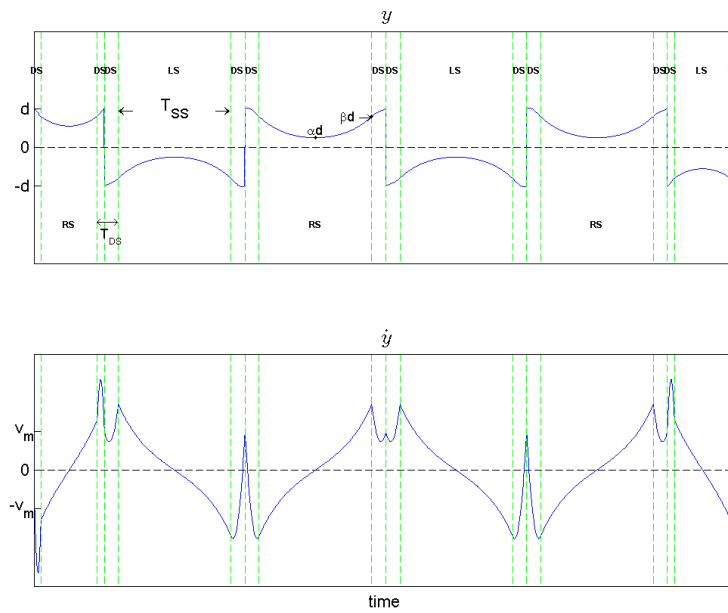


Figure 5.17: Position and velocity of the CoM in the lateral plane using third polynomial interpolation

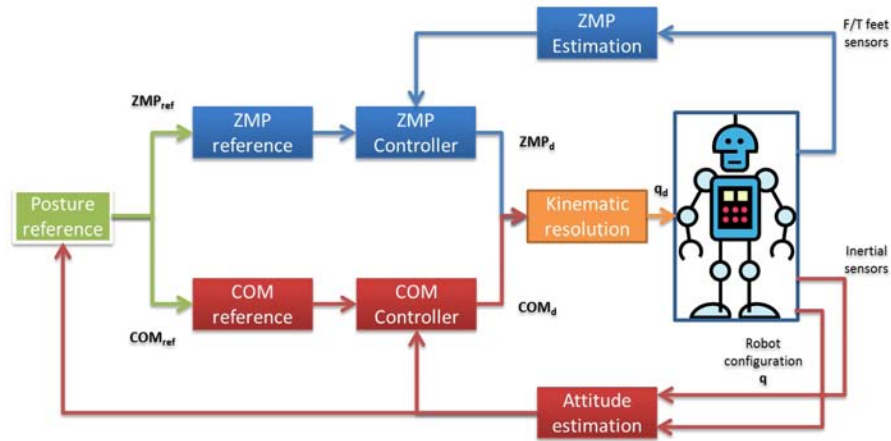


Figure 5.18: Attitude and balance control scheme

the robot stability. In such case, a step in the direction of the disturbance may be executed.

## 5.8 Attitude and balance control

The full humanoid control is achieved using the scheme in Figure 5.18.

The attitude estimation is achieved using the information of the motor encoders and the IMU sensors, using the algorithm presented in Chapter 4.

The force/torque sensors in the robot feet are used to estimate the ZMP position that feeds the ZMP controller, which is actually working as a switch between the static controller and the dynamic one.

In the case of a large and impulsive disturbance, the ZMP controller switches to the dynamic controller, whereas in the other cases, a static controller is used.

The online measurements are simulated adding a Gaussian noise at every iteration. Such noise is filtered limiting the control peaks.

The ZMP measurements are shown in Figure 5.19, and the impulsive disturbances occurring at  $t = 2.112$  and  $t = 2.258$  are highlighted in Figure 5.20.

The joints angles are depicted in Figure 5.22 and Figure 5.23 for the right standing leg and the waist joint, respectively.

The feasibility of the control actions is shown in Figure 5.24, Figure 5.25, Figure 5.26 and Figure 5.27, where the joints torques are depicted.

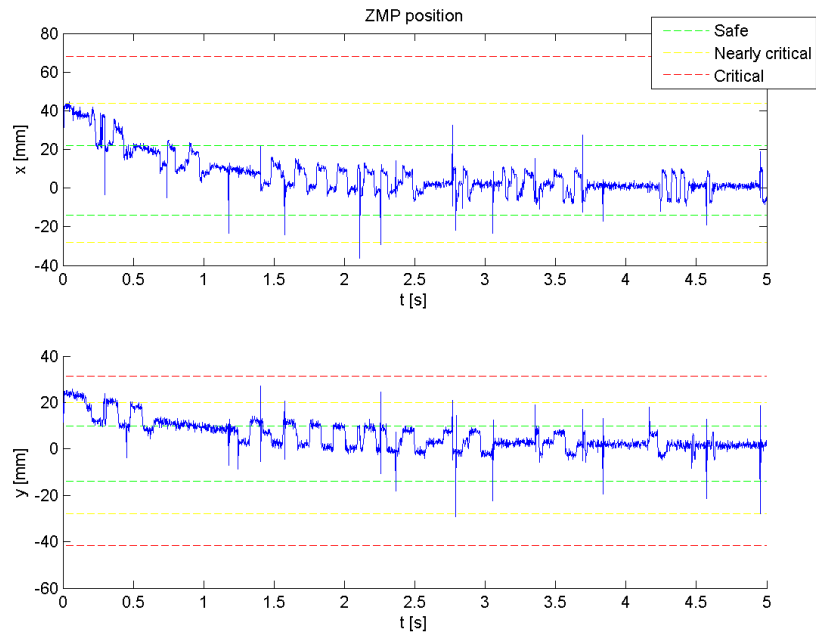


Figure 5.19: ZMP position for the attitude and balance control



Figure 5.20: Detail of the ZMP position for the attitude and balance control

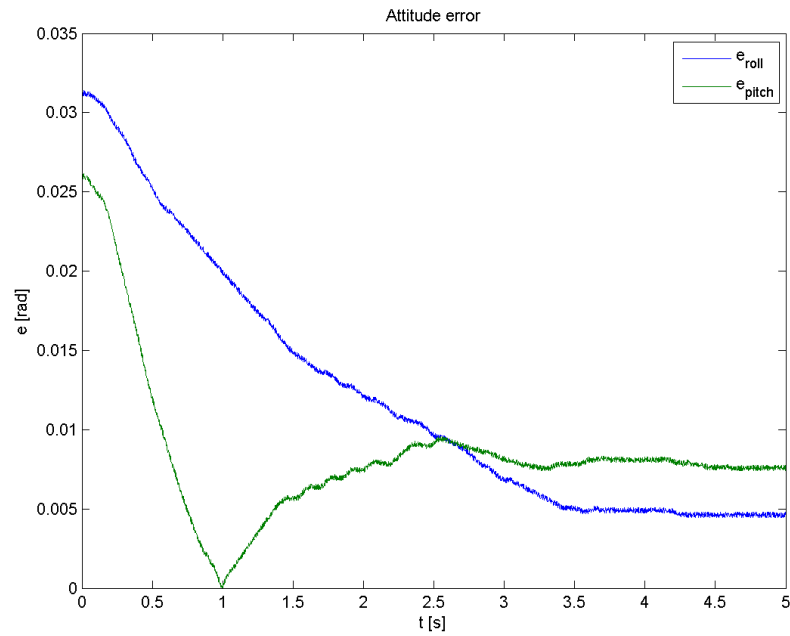


Figure 5.21: Attitude error for the attitude and balance control

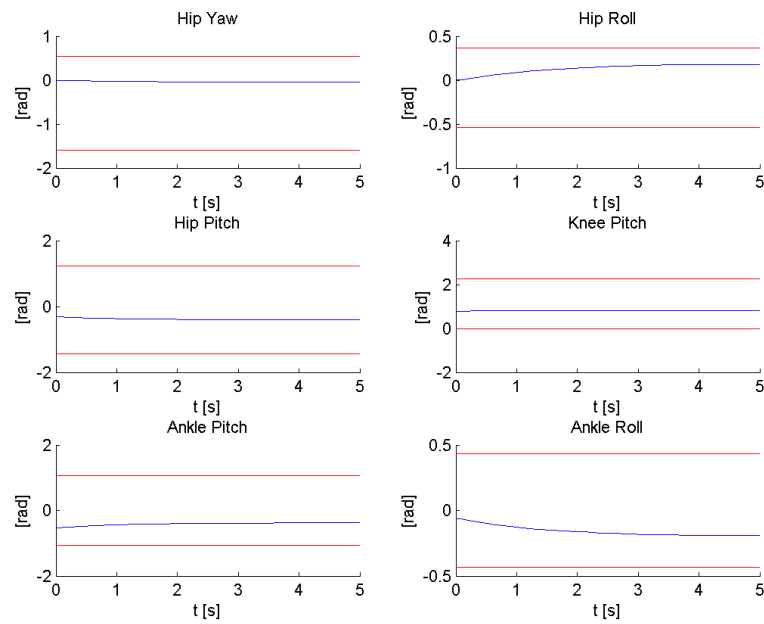


Figure 5.22: Right leg joints angles for the attitude and balance control

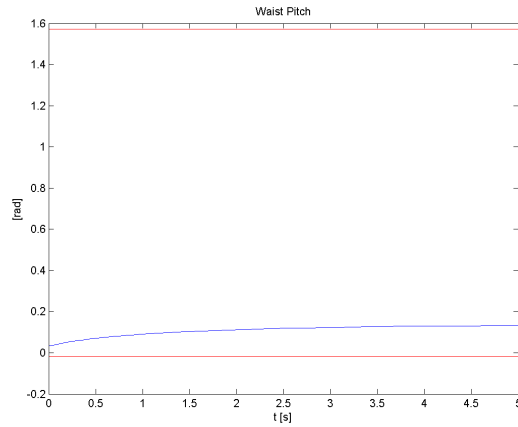


Figure 5.23: Waist angles for the attitude and balance control

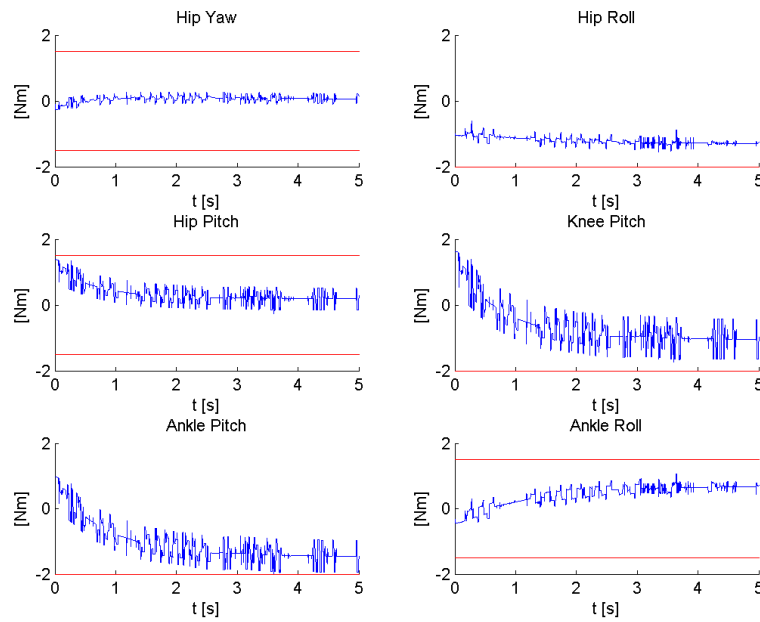


Figure 5.24: Right leg joints torques for the attitude and balance control

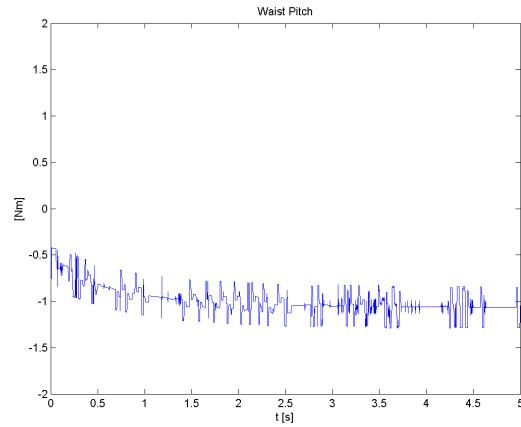


Figure 5.25: Waist torques for the attitude and balance control

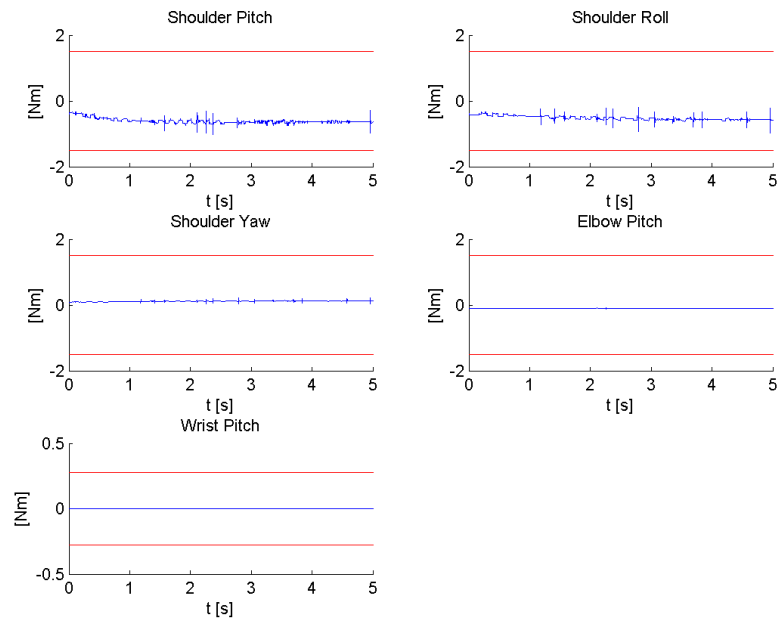


Figure 5.26: Right arm joints torques for the attitude and balance control

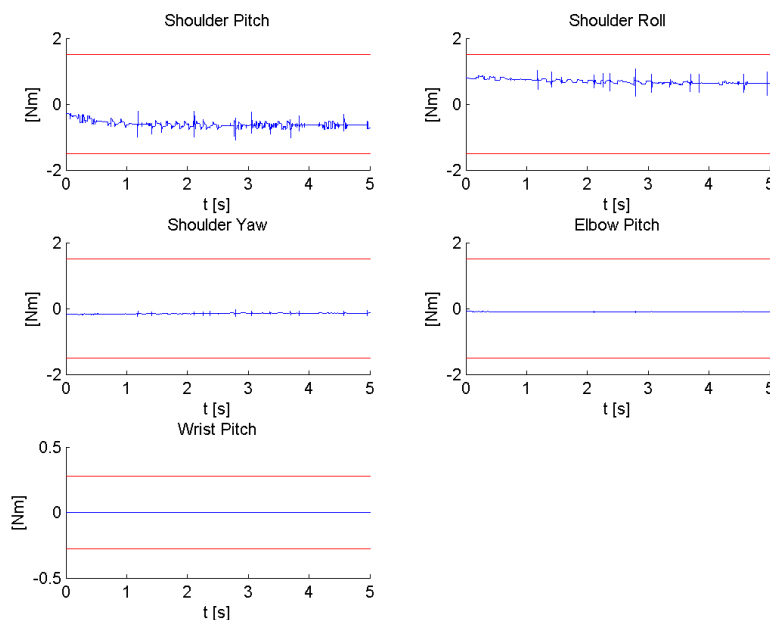


Figure 5.27: Left arm joints torques for the attitude and balance control

## 5.9 Chapter summary

This chapter has presented three types of controllers for the humanoid stability. An attitude controller which aims at controlling the roll and pitch angles of the CoM with respect to the world frame permits the robot to be always in a upright configuration.

Then, two balance controllers are presented. The use of one or another strongly depends on the definition of the stability regions. Three stability regions are statically defined, basing on the support polygon: a first inner region is considered safe in terms of the robot balance. The outer regions are less stable and require the use of a controller in order to avoid the drift of the ZMP away from the support polygon.

The robot stabilizer selects the controller that best fits the situation. In particular, when a small disturbance is present, the static controller is used. The static controller is actually controlling the configuration of the robot, without taking into account inertial terms. For large and impulsive disturbances, the inertial effects have to be used to dynamically control the robot. Thus, the robot reacts immediately to the disturbance and then, using the proposed walking pattern generator, moves one step in order to enlarge the support polygon in the direction of the step.

The effectiveness and feasibility of the presented controllers are shown in simulation, adding a small continuous Gaussian noise and an additive larger disturbance

---

Controller	Elapsed time [s]
Attitude controller	$8.16 \cdot 10^{-4}$
Static balance controller	0.042
Dynamic balance controller	0.044

---

Table 5.1: Elapsed times for the attitude and balance controllers on a dual-core 1.86GHz processor

randomly.

Anyway, even if the whole humanoid structure is simplified using the double pendulums, the complexity of the algorithms do not permit their use in real-time applications. In Table 5.1, the elapsed times for the different controllers are presented. The calculation of the dynamical parameters and the subsequent control action to be taken cause the times for the balance controllers to be very high. An algorithm optimization is mandatory but possible in order to permit its effective use on a real robot.



## **Chapter 6**

# **Human–robot Collaboration**



We humans can interact with the world surrounding us using our arms and hands. In this sense, the research in humanoid platforms tends to reproduce our arms and hands in order to achieve a good manipulation. The term manipulation means to operate with the hands in order to move or act on an object. For manipulation tasks, the transfer of objects between humans and robots is a fundamental way to coordinate the activity and cooperatively perform a useful work.

The objective of this section is to analyze the different methodologies proposed in the research field regarding manipulation in collaboration with a human.

One of the most interesting works in collaborative manipulation is presented in [111]. This method has been tried on the NASA Robonaut platform. The issues addressed in this work are several and the most interesting ones, when operating in conjunction with a human operator, are:

**Vision system:** The objective for the vision system is to provide the robot with object recognition.

**Pose estimation:** The estimation of the object orientation is a real problem when acting on real objects having a non-featured shape.

**Grasping:** The Robonaut robot employs a tactile glove for autonomous grasping which is equipped with several low-resolution force sensors [112].

One interesting idea used in the field of collaborative manipulation is presented in [113]. In this work, the idea is having different levels of autonomy for the humanoid robot HRP-2.

When the robot is operating in a known environment, the human collaborator can use only a few high-level commands in order to command the robot. In this case, in fact, the definite knowledge of the environment permits the robot to move in it almost autonomously.

On the contrary, when the robot is moving in a new environment, the human will actually teleoperate it, having access to a lower level in the system architecture.

The problem of cooperative manipulation is simplified and successfully tested on the 29 DOFs humanoid robot Domo, developed at MIT Computer Science and Artificial Intelligence Laboratory (Cambridge, Massachusetts). When handing an object to the robot, the problem of controlling the position and orientation of the object is shifted to the human [114]. The robot detects when an object has been placed in its hand, then tries to grasp it and can detect whether the grasp has been successful or not.

In the robotic community there is a great interest in the field of human-robot interaction. Many researchers are studying and developing several ways to permit robots to easily and explicitly communicate with a human by gestures or speech.

But this type of interaction, which is actually suitable for tasks in social robotics, may become inappropriate for human–robot cooperative works in terms of the user cognitive load because it forces the user to become familiar with explicit communication protocols.

On the other hand, in cooperative human–robot tasks different kinds of interactions have been studied, such as an implicit and physical interaction for handling objects, carrying objects and for outdoor tasks<sup>1</sup>.

In any case, these studies lack of a general architecture for the human–robot collaboration and are limited to the information of force and vision.

In this section, one possible classification of the different types of modalities in a collaborative context is presented:

**Direct control:** it refers to the most classical possibility of controlling the robot, which is accessing directly to the PC onboard.

**Visual and vocal interaction:** this type of interaction is what in the research on human–robot interaction is known as dialog management and gesture recognition.

**Tablet PC and PDA system:** it is the possibility to communicate with the control PC via a notebook, or a personal digital assistant (PDA) equipped with a touch screen giving the possibility to work with a fingertip, instead of a keyboard or mouse.

**Remote control:** this indicates the possibility to operate the robot at a distance, using teleoperation methodologies.

Taking the cue from the classification presented in [115], it is possible to define the following parameters in order to characterize the different modalities of interaction in collaborative systems:

**Communication security:** it refers to the possible errors that can appear during the communication between the interface and the robotic systems.

**Precision:** it is the modality quality of being reproducible in amount or performance giving the same result.

**Adaptability to different tasks:** if the interaction modality can be easily adapted to several tasks.

**Available computational resources:** the interface has some processing capabilities.

---

<sup>1</sup><http://www.phriends.eu>, accessed on May 27, 2012

**Composition of robot teams:** the possibility of using the same interface for different robots and different types.

**Interaction roles:** the roles that a human may have when interacting with a robot: supervisor, operator, teammate, mechanic/programmer, and bystander [116].

**Human–robot physical proximity:** depending on the task and the type of the interaction, robots and people may have different distances.

**Decision support for operators:** it is related to the type of information that is provided to the operators to help them to decide.

**Time/space taxonomy:** humans and robots may share the same time (synchronous) or different ones (asynchronous) and share the same place (collocated) or different ones (non–collocated) [117].

**Required autonomy level of the robot:** it studies if an intervention of the human is present and at which level.

**Ease of use:** during collaborative tasks, different interaction modalities may be impossible, complex or easy.

Table 6.1 compares the different modalities based on the characterizing parameters.

Two cases of collaboration are analyzed in this chapter: a) the case in which the human and the robot collaborate by means of an object is studied (close collaboration), and b) the case of a collaboration in which the human and the robot do not share the same environment (remote collaboration).

## 6.1 Architecture for human–robot collaboration

Within a collaborative working environment, it is possible to define a functional architecture as the set of basic information processing capabilities available to the system. In this section, the general architecture for the collaboration is presented, which can be organized as shown in Figure 6.1.

The general network can have different local networks. For instance, a local network can be a closed room, where different sub–networks are present: one sub–network can be a robot. Every sub–network may have different services.

The possible services can be:

- Perception, *i.e.* vision, sound, force, detection, etc.
- Action, *i.e.* walk, manipulate, etc.

	<i>Direct control</i>	<i>Visual and vocal interaction</i>	<i>Tablet PC</i>	<i>PDA system</i>	<i>Remote control</i>
<b>Communication security</b>	high	low	medium	medium	low
<b>Precision</b>	high	low	high	medium	medium
<b>Adaptability to different tasks</b>	low	low	medium	medium	high
<b>Available computational resources</b>	high	low	high	low	high
<b>Composition of Robot Teams</b>	homogeneous	heterogeneous	heterogeneous	heterogeneous	heterogeneous
<b>Interaction Roles</b>	operator	teammate	teammate	teammate	operator
<b>Human–Robot Physical Proximity</b>	close	close	relatively close	relatively close	far
<b>Decision Support for Operators</b>	high availability of sensors	no availability of sensors	medium availability of sensors	low availability of sensors	high availability of sensors
<b>Time/space taxonomy</b>	synchronous–collocated	synchronous–collocated	synchronous–non–collocated	synchronous–non–collocated	asynchronous–non–collocated
<b>Required autonomy level of the robot</b>	no autonomy	high autonomy	semi–autonomy	reduced high autonomy	autonomy
<b>Ease of use</b>	complex	easy	medium	easy	medium

Table 6.1: Comparison between the different interaction modalities possible in a collaborative working environment

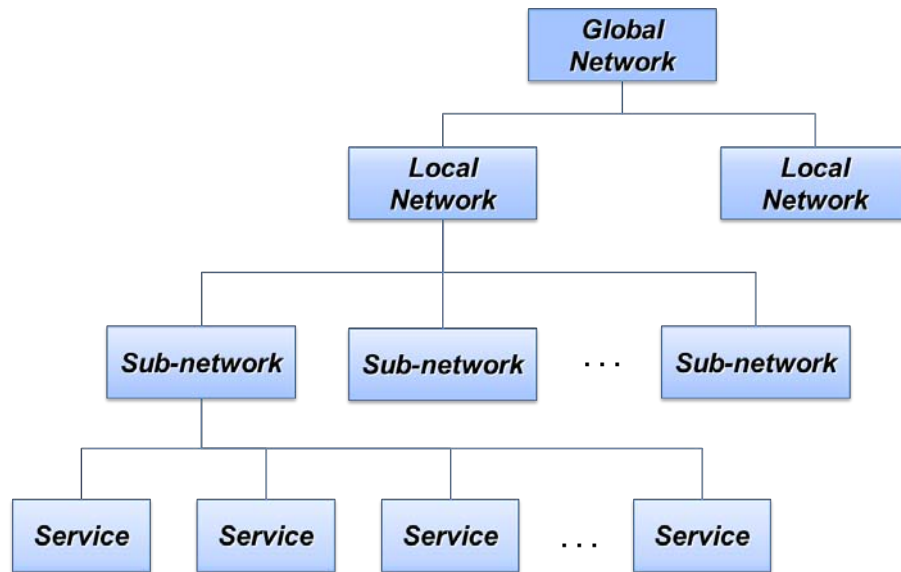


Figure 6.1: The general architecture for collaboration

- Decision taking, *i.e.* computational services.

For example, a camera in the room provides a perception service, whereas a robot may only have action services.

Different ways to carry out the human–robot interaction, for instance through direct contact, via PDA or a joystick, are graphically explained in Figure 6.2.

First of all a robot partner has to recognize what the human users are doing and perceive their intentions or goals [118]. For inferring and reasoning these intentions the integration of a sensorial system in the robot is especially important. For instance, in order to achieve a collaborative transportation or an assembly task, the robot should be provided with different types of sensors, such as force/torque ones and cameras.

The information from the sensorial system will be used by a control algorithm that allows carrying out the collaborative task, ensuring the stability of the whole system during the activity.

## 6.2 Close collaboration

When it is desired to attain the aim of coordinating a task between a human and a humanoid robot such as transporting a long or a heavy object (like in the case depicted in Figure 6.3), the problem can be studied modeling the robot arms and the object as a closed chain.

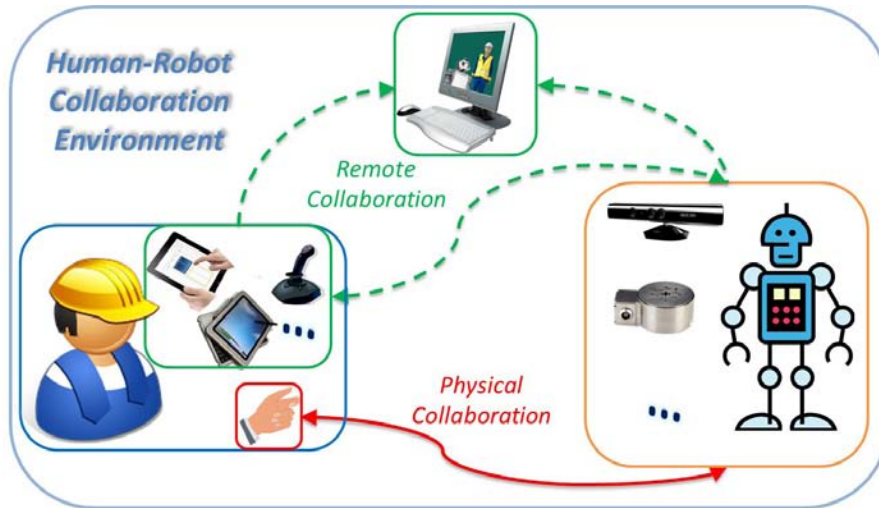


Figure 6.2: Modalities of the human-robot collaboration



Figure 6.3: An example of a human and a robot jointly transporting a table

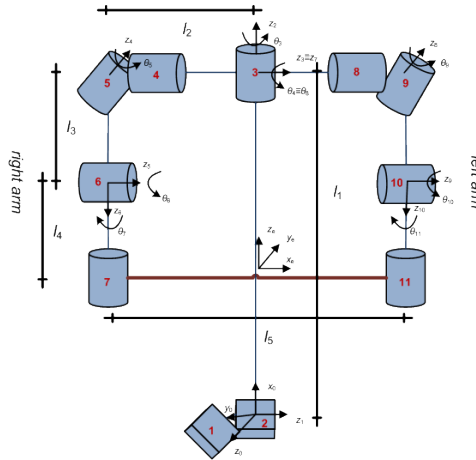


Figure 6.4: Kinematic model of the arms

For this kind of collaboration, the first version of the humanoid robot TEO (presented in Appendix A) is used: the RH-1 robot. RH-1 arms present several limitations related to the robot mechanics. Each arm of the humanoid robot has only four joints and the two arms share a common neck joint.

The drawback of such a model is that only the structure of the humanoid arms is considered in the problem of joint manipulation. Of course, this is a strong simplification, since the whole platform has actually 21 DOFs which are sufficient to achieve locomotion and manipulation at the same time.

Khatib has solved this problem in [119] using a task-oriented framework for whole-robot dynamic coordination and control.

But, in order to reduce computational complexity, it is possible to consider a structure like the one in Figure 6.4, where the arms of the humanoid robot RH-1 are presented in a schematic way. Two virtual joints, representing the movement of the CoM in the horizontal and sagittal plane, have been added. This model has been defined as the Virtual CoM Joints approach in [120].

These two virtual prismatic joints resume the kinematics of the robot legs. If the position of this point is placed in the CoM of the robot, the solution of the inverse kinematics becomes a reference for the mobile legged part.

Being  $\mathbf{x}_r$  and  $\mathbf{x}_l$  the position and orientation of the right and left arms, respectively, the solutions  $\mathbf{q}_r$  and  $\mathbf{q}_l$  referring to the joint angles of the right and left arms must be found.

The tasks to be implemented are the following ones:

- *Task 1:* the EE of the right and left arms should coincide in position and orientation.

- *Task 2*: the EE must follow a desired trajectory.

The first task can be written as:

$$\dot{\mathbf{x}}_r = \dot{\mathbf{x}}_l \Rightarrow \mathbf{J}_r \dot{\mathbf{q}}_r = \mathbf{J}_l \dot{\mathbf{q}}_l \quad (6.1)$$

where  $\mathbf{J}_r$  and  $\mathbf{J}_l$  are the Jacobian matrices of the right and left arms, respectively, and  $\dot{\mathbf{q}}_r$  and  $\dot{\mathbf{q}}_l$  the joints velocities of the two arms.

Now, a consideration has to be done. Every arm is constituted by a part that is shared with the other arm (*i.e.* the CoM virtual joints and the neck joint) and a distinctive one. Denoting by  $\dot{\mathbf{q}}_C$  the common part and by  $\dot{\mathbf{q}}_R$  and  $\dot{\mathbf{q}}_L$  the distinctive parts of right and left arm, respectively, it is possible to rewrite Equation (6.1) as:

$$\begin{aligned} \dot{\mathbf{x}}_r &= \mathbf{J}_r \dot{\mathbf{q}}_r = \mathbf{J}_C \dot{\mathbf{q}}_C + \mathbf{J}_R \dot{\mathbf{q}}_R \\ \dot{\mathbf{x}}_l &= \mathbf{J}_l \dot{\mathbf{q}}_l = \mathbf{J}_C \dot{\mathbf{q}}_C + \mathbf{J}_L \dot{\mathbf{q}}_L \end{aligned} \quad (6.2)$$

$\mathbf{J}_C$  being a 6 by 3 matrix, and  $\mathbf{J}_R$  and  $\mathbf{J}_L$  two  $6 \times 4$  matrices, related to the common and the distinctive parts, respectively.

It is possible to write the objectives as follows:

- *Task 1*:  $\dot{\mathbf{e}}_1 = \mathbf{0} = \mathbf{J}_R \dot{\mathbf{q}}_R - \mathbf{J}_L \dot{\mathbf{q}}_L$
- *Task 2*:  $\dot{\mathbf{e}}_2 = \dot{\mathbf{x}}_r = \mathbf{J}_C \dot{\mathbf{q}}_C + \mathbf{J}_R \dot{\mathbf{q}}_R$

Writing the tasks in a conventional way, that is:

$$\dot{\mathbf{e}} = \mathbf{J} \dot{\mathbf{q}} \quad (6.3)$$

Equation (6.3) can be written in matrix form:

$$\begin{bmatrix} \dot{\mathbf{e}}_1 \\ \dot{\mathbf{e}}_2 \end{bmatrix} = \begin{bmatrix} \mathbf{0} & \mathbf{J}_R & -\mathbf{J}_L \\ \mathbf{J}_C & \mathbf{J}_R & \mathbf{0} \end{bmatrix} \begin{bmatrix} \dot{\mathbf{q}}_C \\ \dot{\mathbf{q}}_R \\ \dot{\mathbf{q}}_L \end{bmatrix} \quad (6.4)$$

In the most general case, matrix  $\mathbf{J}$  in Equation (6.3) is composed by two matrices  $6 \times 11$ . This means that with these assumptions, using 6 DOFs for the closed kinematic chain, it is only possible to specify the position and two orientations for the EE.

Now, if position and orientation along axis  $z_0$  is only being considered, the unused rows of the Jacobian  $\mathbf{J}$  can be removed, resulting a  $10 \times 11$  matrix:

$$\dot{\mathbf{q}} = \mathbf{J}^\dagger \dot{\mathbf{e}} = \mathbf{J}^\dagger \begin{bmatrix} \mathbf{0} \\ \dot{\mathbf{p}}_d \\ \omega_{z,d} \end{bmatrix} \quad (6.5)$$

where  $\dot{\mathbf{p}}_d$  and  $\omega_{z,d}$  are the derivatives of the desired position and orientation (along  $z$  axis) of the EE, respectively. In this equation the notation  $\mathbf{J}^\dagger$  is used to denote the right pseudo-inverse matrix of  $\mathbf{J}$ .

Since the manipulator is redundant, the following solution for the inverse kinematics has been used [1]:

$$\dot{\mathbf{q}} = \mathbf{J}^\dagger (\dot{\mathbf{e}} + \mathbf{K}\mathbf{e}) + (\mathbf{I} - \mathbf{J}^\dagger \mathbf{J}) \dot{\mathbf{q}}_0 \quad (6.6)$$

where  $\dot{\mathbf{q}}_0$  is an homogeneous solution, used to satisfy the additional constraint of the distance from mechanical joint limits.

The task vector  $\mathbf{e}$  is defined as

$$\mathbf{e} = \begin{bmatrix} \mathbf{e}_1 \\ \mathbf{e}_1 \end{bmatrix} = \begin{bmatrix} \mathbf{e}_{p,1} \\ \mathbf{e}_{O,1} \\ \mathbf{e}_{p,2} \\ \mathbf{e}_{O,2} \end{bmatrix} \quad (6.7)$$

where  $\mathbf{e}_{p,i}$  and  $\mathbf{e}_{O,i}$  denote the position and orientation tasks, respectively, these being referred to by the  $i$  subscript and defined as

$$\begin{aligned} \mathbf{e}_{p,i} &= \mathbf{p}_{d,i} - \mathbf{p}_i \\ \mathbf{e}_{O,i} &= \eta_i \varepsilon_d - \eta_d \varepsilon_i - \mathbf{S}(\varepsilon_d) \varepsilon_i \end{aligned} \quad (6.8)$$

For  $i = 1$ , the desired position is  $\mathbf{x}_{d,1} = \mathbf{0}$  and the desired quaternion is  $Q_{d,1} = \{1, \mathbf{0}\}$ :

$$\mathbf{e}_{P,1} = \mathbf{p}_l - \mathbf{p}_r \quad (6.9)$$

$$\mathbf{e}_{O,1} = -\varepsilon_1 \quad (6.10)$$

where  $\varepsilon_1$  is the vector part of the quaternion related to the matrix  $\mathbf{R}_r \mathbf{R}_l^{-1}$ , which depends on the matrices giving the reference of the EE for both arms.

For  $i = 2$ , the desired position is  $\mathbf{x}_{d,2} = \mathbf{p}_d$  and the desired quaternion  $Q_{d,2} = \{\eta_d, \varepsilon_d\}$  is defined by the rotation matrix  $\mathbf{R}_d$ , which represents a rotation along the  $z_0$  axis.

### 6.2.1 Simulation Results

The Virtual COM Joints algorithm presented here has been implemented using Matlab®. While the trajectory for the end-effector has been specified as a sinusoid, it has been checked that the algorithm is always maintaining the same position and same orientation for both arms.

The reference for the COM is shown in Figure 6.5, while the joints angles for both arms are in Figure 6.6. The position and orientation errors for the closed chain are in Figure 6.7, demonstrating the solution to the problem of the closed kinematic chain.

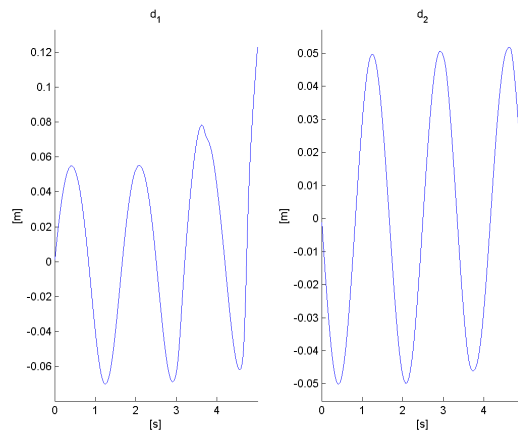


Figure 6.5: Desired COM position in the horizontal plane

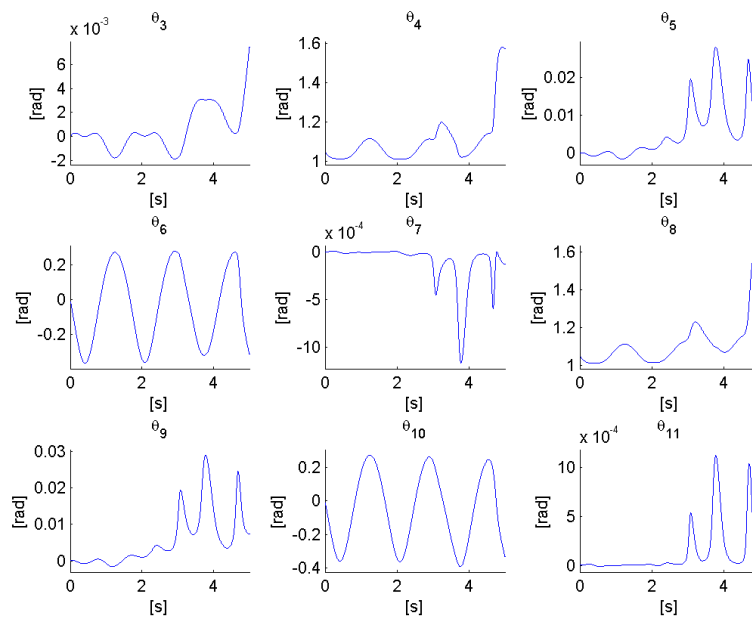


Figure 6.6: Joint angles of the arms

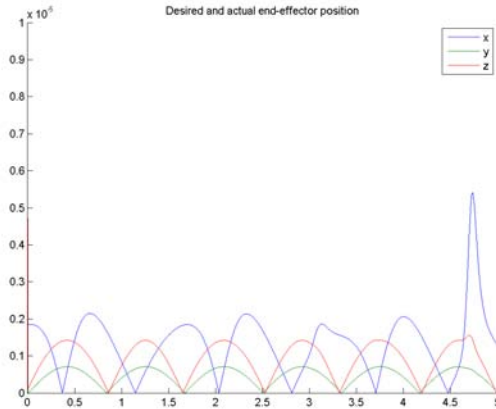


Figure 6.7: Position and orientation errors between left and right arm

## 6.3 Remote collaboration

A kind of collaboration which does not imply a close interaction between the robot and the user is what has been defined as remote collaboration. This could be the case of a collaboration between humanoid robots and humans in order to achieve tasks in space environments.

The user and the robot do not share the same physical environment but they work together in order to accomplish a specific goal.

The robot has to be able to explore the surroundings and detect an object that is placed in the scenario. The robot can go towards the object and take it.

One human–machine interface (HMI) permits the user and the robot to communicate, sending and receiving commands and data.

### 6.3.1 System architecture

A DH $\leftrightarrow$ DR collaborative architecture has been developed for a human operator to interact with a robot located at a remote location. Such architecture is based on the concept: “what is Difficult or Dangerous for the Human (DH) will be Done by the Robot (DR)” and “what is Difficult and Devious for the Robot (DR) would be better Done by the Human (DH)”. Figure 6.8 shows the proposed human–robot DH $\leftrightarrow$ DR collaborative architecture.

A human operator monitors the state of the humanoid robot HOAP–3 in the remote collaborative task. By means of an HMI the human operator will supervise the robot, send instructions and provide assistance to the robot for the completion of the tasks.

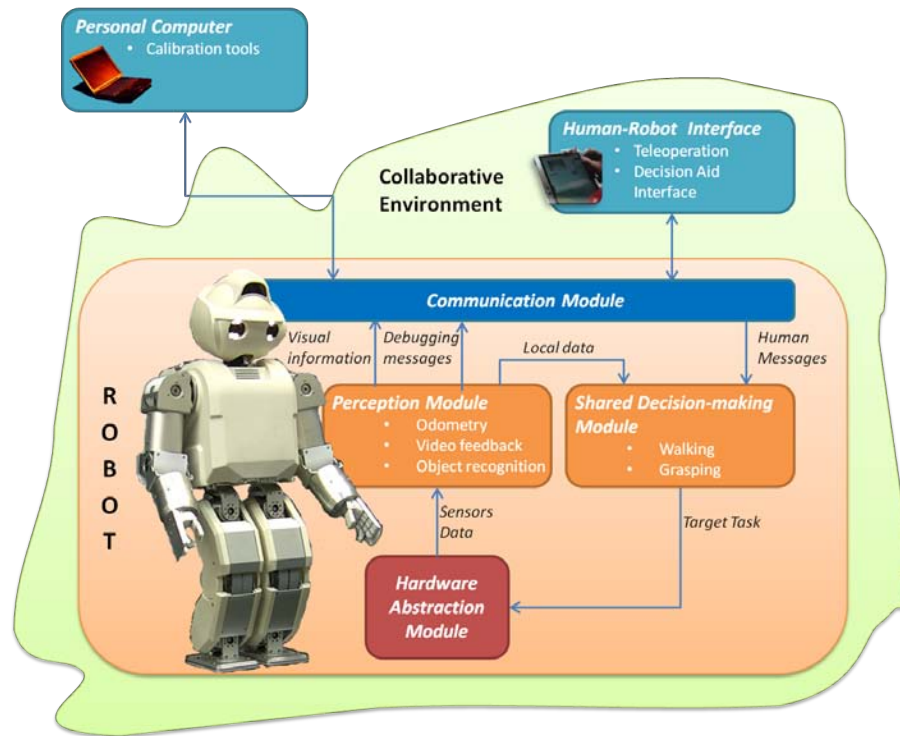


Figure 6.8: DH↔DR collaborative architecture

The HOAP-3 software server handles the robot movements and motions and maintains the communication with the operator through the HMI regarding the status of the tasks.

The software architecture is composed of four basic modules: a Perception module for vision and sensory perception, a Shared decision-making module, the Hardware Abstraction module and the Communication module.

The Perceptual module receives the sensor data from the robot sensory system. It handles the vision services and the object recognition capabilities of the HOAP-3. The Perceptual module provides the users with video feedback and visual cues, related to what the robot is seeing. It detects and traces objects in their environment and gives detailed information about recognized objects (such as distance and orientation measurements).

The Shared decision-making module, based on local information provided by the Perceptual module, will provide the Communication module with high level information that can be useful for the human operator. Anyway, it is the user who, by means of the Communication module, will select the action to be taken for a devious task, whereas the robot will execute a standard task autonomously.

The third module is in charge of converting high level task references in motor

commands: the Hardware Abstraction module implements the controller for the joint actuators and generates appropriate trajectories for the walking, turning and grasping motions.

Finally, a fourth module handles the communication protocol between the HMI and the human operator: the Communication module is responsible for establishing a collaborative dialog between the human operator and the robot working together. Such module translates the Robot Command Protocol (RCP) to forward the instructions from the operator back to the other services and gives the adequate responses to the operator and the HMI.

### 6.3.2 Shared decision-making module

This module is in charge of switching between an autonomous task and a supervised task and, in any case, generates high level decisions which, to the purposes of this research, represent tasks for the robot.

The decisions may be taken with or without the help of the human depending on the task itself.

The state machine corresponding to such module is represented in Figure 6.9. The transition color is blue if the condition is coming from the Communication module and red if it depends on the Hardware Abstraction module (HAM).

The module is waiting for a Control Request from the communication module (transition 0.1). Once a user has taken control of the robot, the system is waiting for the commands. A standard command will be put at the end of the queue (transition 1.2).

If the command is a direct command, it will by-pass the queue and will be sent directly to the Hardware Abstraction module (transition 1.1). In this case the DM bit (which stands for Direct-Mode) is activated (state 2).

If the user asks for disconnection (transition 1.3), the robot server is disconnected from the user.

The queue resolution is graphically explained in Figure 6.10.

If the command read from the queue is an autonomous command (i.e. it does not need human intervention), it is directly converted into a task for the Hardware Abstraction module.

If the command is a shared-decision command (transition 0.2), the server will provide the user with different strategies. Once a strategy is selected (transition 2.1), the command is converted into a task for the HAM.

In the case of a walking command, this module will generate an abstract task which is plugged into the Hardware module.

On the contrary, if the command is a grasping, the first problem to be considered

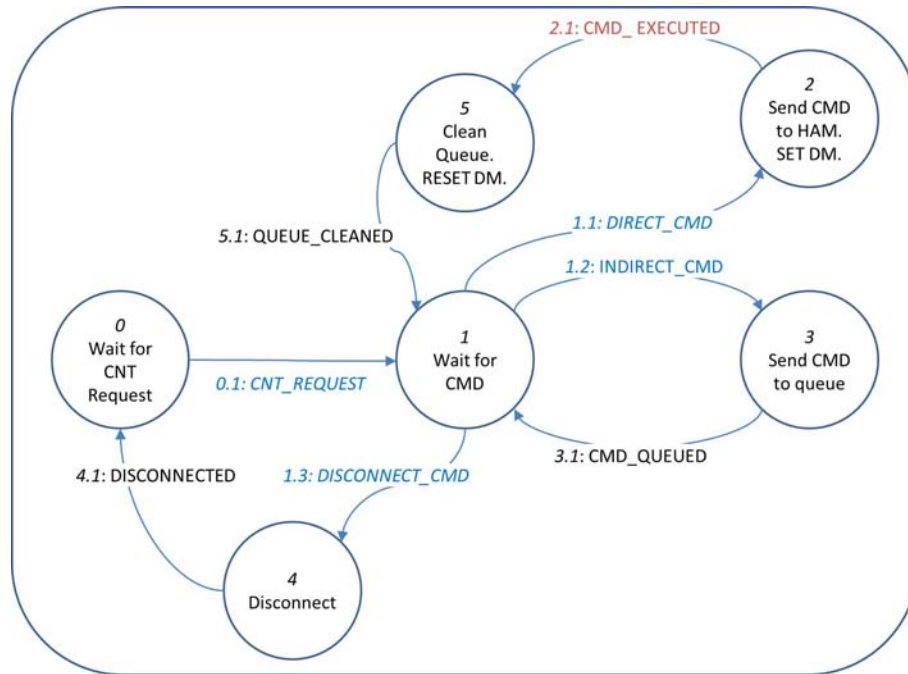


Figure 6.9: State machine for the Shared decision-making server

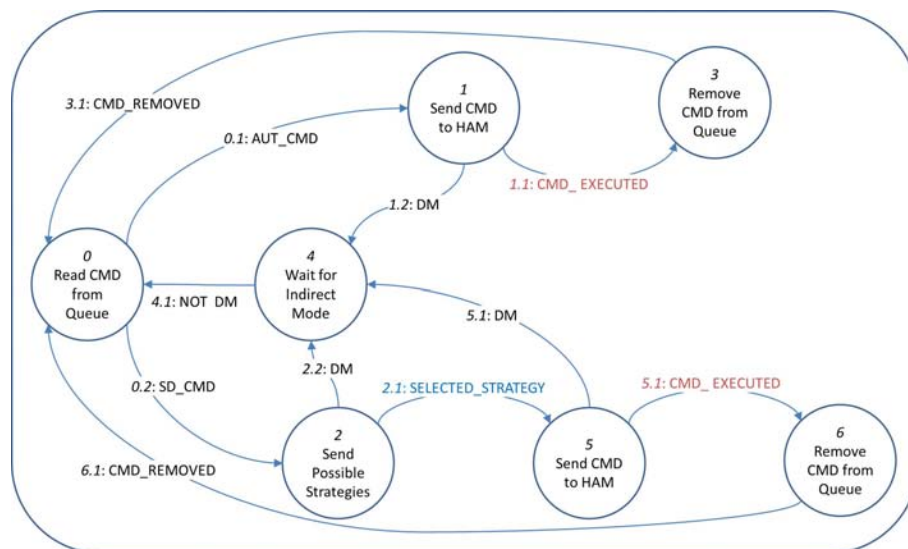


Figure 6.10: State machine for the Shared decision-making queue resolution

is the selection of the suitable arm. The robot, according to the local information provided by the Perception module, will generate the workspace and the manipulability for each arm that can reach the object. Then, it will wait for the decision taken by the human for the best manipulator (left or right arm) for grasping operations. In fact, even if one hand is closer to the object than the other, the human may take another choice according to the visual information showing, for instance, that an obstacle can be on the trajectory.

The sensing system provides information about objects and a notion about the uncertainty in such measurements, which is mandatory to decide whether the estimation is accurate enough for performing the grasping operation or some cognitive action should be taken for improving it.

In order to achieve the grasping using one of the arms, the decision about the best one to perform that operation is supervised by an operator using the information about the robot's capabilities, object location in robot's coordinates and information about the manipulability. The whole system has been integrated using a layer architecture that makes a functional decomposition of the different tasks.

### 6.3.3 Experimental results

For the experiments, an operator must connect to the robot, and a connection negotiation according to predefined users and protocols ensue. Once the robot has granted the connection, the operator would be able to see the remote scenario through the eyes of the robot, receiving continuous vision feedback from the robot cameras. Figure 6.11 shows a human operator using the HMI and the HOAP-3 at the remote environment.

The human-robot team are requested to look for an antenna and restore communications. An efficient way to do this is that the operator requests the robot to walk around the environment until it sees an object. Since the human vision capabilities to recognize objects are greater than the ones that can be implemented on a robot platform, it would be on the operator side the responsibility to look on the video feedback and tell the robot when the antenna has been found. Once the target object is localized, the robot can autonomously walk towards the object up to a close enough distance so that it can grab it when requested by the human operator. Depth estimation using stereo vision allows reaching the objective and placing the robot in a feasible location for the grasping operation. This operation is currently autonomous, given the *a priori* known object.

Once the robot receives the operator strategy indication, the humanoid robot would proceed to perform the requested action. Figure 6.12 shows the sequence of a grasping operation tracking the object to manipulate. In order to accelerate the convergence of the tracking, the grid-based method is initialized with a density quite

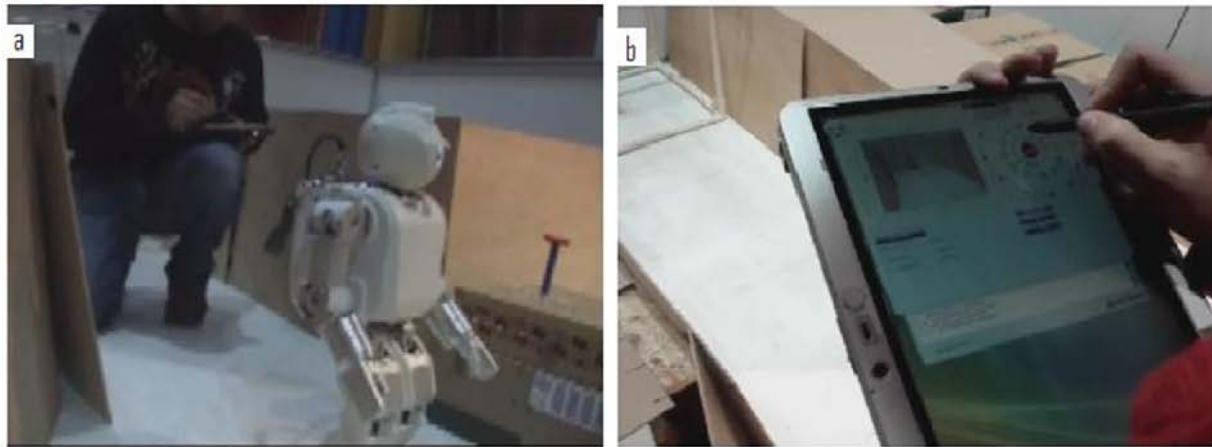


Figure 6.11: Demonstration of the proposed teleoperated system on a ‘lunar scenario’ a) Robot HOAP–3 and a human operator work collaboratively on finding and moving the antenna. b) The operator teleoperates the robot with the HMI using a pocket PC.

similar to the actual location of the object.

## 6.4 System assessment

At the RoboticsLab of the University Carlos III of Madrid (UC3M) a lunar scenario has been built to simulate the operation of a robotic agent working in collaboration with a human in a space environment.

The task to be performed consists of teleoperating the robot HOAP–3, first walking through an enclosed hall and finding an object, in this case an antenna, then grasping the object and placing it in a different location.

For the teleoperation task, the communication between the robot and the HMI is performed over a standard Wi–Fi 802.11 network.

In order to evaluate the teleoperated system proposed here, several tests have been conducted with HOAP–3. The robot walks in an enclosed corridor while being teleoperated by a human agent. Through the HMI the operator sends walking and turning movement commands. Video feedback from the robot cameras indicates the operator that the robot has localized the antenna. Then, the robot approaches the object up to a close enough distance so that it can grab it when requested by the human operator.

A first development of the HMI (Figure 6.13) has been evaluated by the ICT&S center, from the University of Salzburg, partner of the Robot@CWE project.

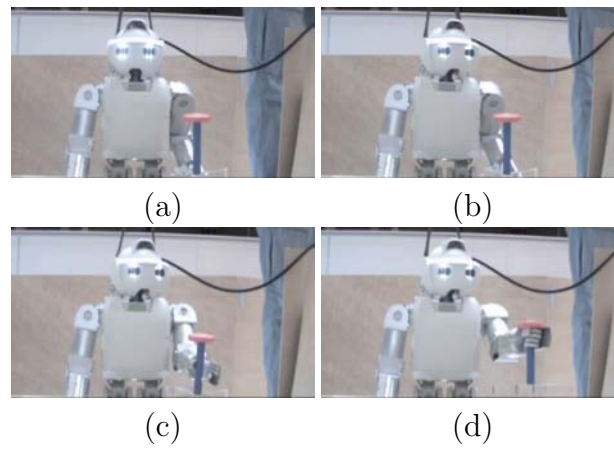


Figure 6.12: Sequence of grasping operation using the techniques described in this chapter.

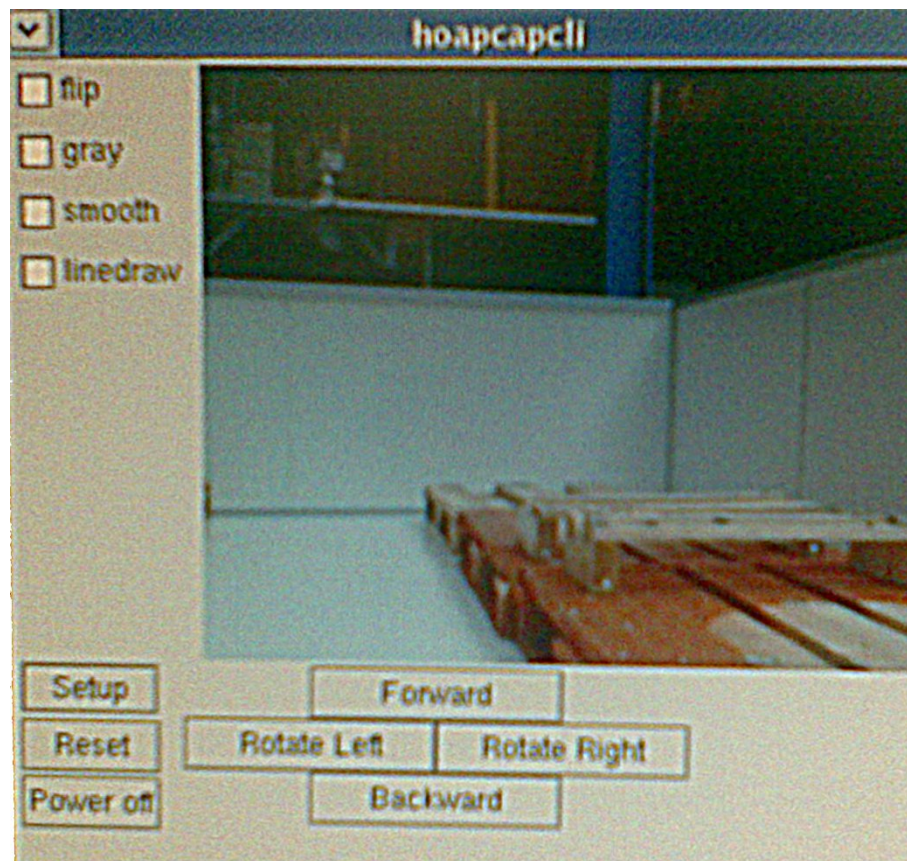


Figure 6.13: First development of the HMI

The HMI has been tested with HOAP–3 and the evaluation took place at the RoboticsLab at the UC3M from 28th to 30th of October 2008.

Twelve people (6 females, 6 males) with an average age of 23.75 years participated in the study; the youngest participant was aged 16, the oldest participant was aged 26. The nationalities of the participants were the following: Spanish (9), Columbian (1), Italian (1) and Guatemalan (1). All participants use the PC and the internet every day, and most of them (9 out of 12) use their mobile phone daily or at least several times a week. All participants except one use a MP3 Player several times a week.

The following research questions were investigated:

- How does the user experience the collaboration with the humanoid robot HOAP–3 when interacting via remote control?
- How do users perceive the system in terms of usability?
- Does the general attitude towards robotics change because of the interaction with the robot?
- How did the users experience interacting with HOAP–3?
- How did the interaction with HOAP–3 affect participants?
- How do people imagine a future society with humanoid robots as co–workers, after interacting with the robot?

Two tasks dealing with remote control of HOAP–3 via a computer interface had to be accomplished by the participants.

Before starting with the tasks, participants got to know HOAP–3, the movements it is capable of as well as vision and navigation through the interface in a learning phase.

Afterwards, two tasks were performed by the means of a computer interface which enabled participants to see through HOAP–3’s eyes and control its movements.

The users discovered several problems among which [121]:

- Feedback about the position of the head is missing
- The robot was considered too slow
- The interface does not provide any information about the distance to the wall
- Information about the global movement of the robot is missing
- The users did not like to use buttons

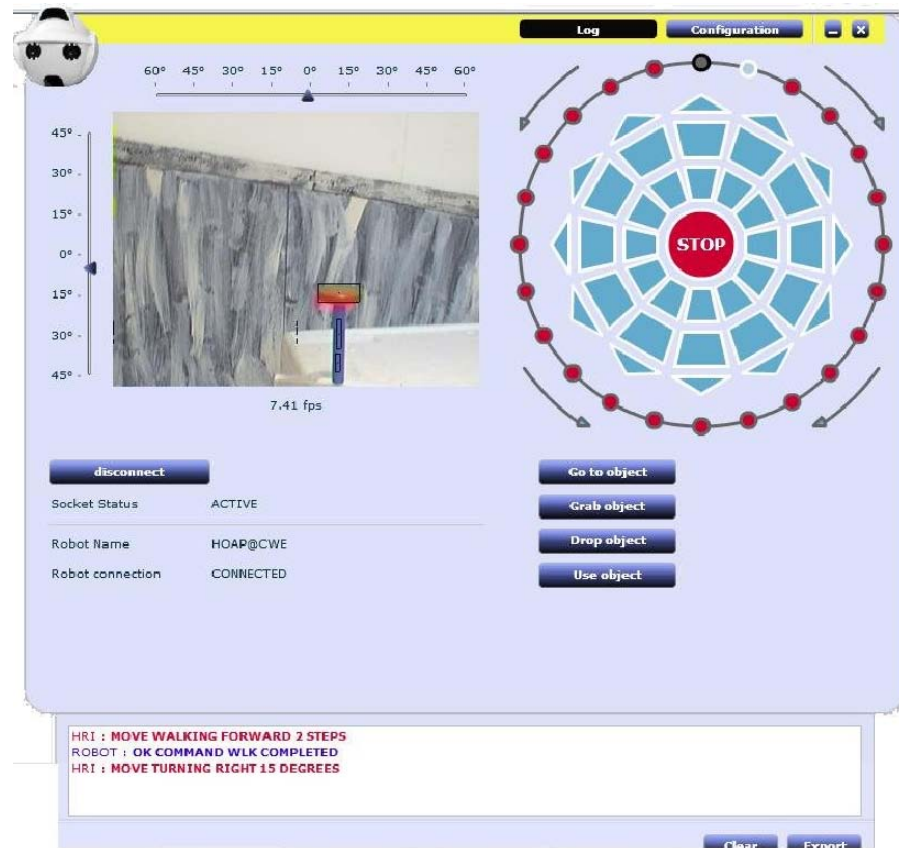


Figure 6.14: New version of the HMI

- The users did not understand when a movement is finished

Based on the considerations of this evaluation, a new HMI has been developed, shown in Figure 6.14.

Finally, the robot computes the best trajectory for the grasping movement and performs accordingly to the operator decisions.

Figure 6.15 shows the experimental setup for the demonstration conducted with the proposed teleoperated system. A human agent works collaboratively with a humanoid robot by supervising, controlling and helping in the decision taken by the robot.

A virtual scenario representing the real one has been designed, as shown in Figure 6.16. The idea is to use this scenario in order to provide the HMI with the global position of the robot and give a visual and virtual information, that helps the user understand the movements of the robot.



Figure 6.15: Real scenario at RoboticsLab



Figure 6.16: The recreation of lunar scenario

## 6.5 Chapter summary

This chapter has introduced and studied two kinds of human-robot collaboration, that depend on the proximity between the two agents.

Even if a generic architecture is presented, two distinct cases has to be analyzed.

A first case, defined as close collaboration, has been analyzed under the kinematics point of view, allowing a possible joint collaboration. Such study has been implemented in simulation using the RH-1 robot, a predecessor of the TEO robot. The study has been used as an input for the future realization of the new platform.

Then, a second kind of collaboration is presented: the remote collaboration. This is the case when the two agents do not share the same environments and need a different kind of communication which is not physical one.

Using an HMI a human agent can work collaboratively with the robot in the achievement of the proposed tasks.

The HMI allows an operator to see the environment from the robot cameras, as well as to control various movements of the robot and give orders for doing some tasks, *e.g.* “grab an object”.

The HMI provides several functionalities to the human agent working with the robot:

- video feedback from robot cameras and visual cues of object recognition;
- control of movements of the robot head (pan and tilt);
- control of walking and turning movements of the robot;
- command the robot to perform higher order tasks, such as go to a specific location, grab an object or drop an object;
- communication feedback with a log of the commands between the operator and the robot.

The HMI should also give the operator more feedback from the robot environment and the state of the robot actions.

The HMI and the robot communicate using an application-level protocol which specifies how the client HMI application talks with the server in the robot. It is a hierarchical protocol, structured in several and specific sub-protocols. Such a protocol has been defined as Robot Command Protocol (RCP) and designed within the project Robot@CWE [122]. The RCP is presented and defined in Appendix E.

The remote collaboration system has been tested with human non-technical users.



## Chapter 7

### Conclusions and Future Works



## 7.1 Conclusions

This research has focused on the aspects of the humanoid control when collaborating with human agents. The concepts of collaboration and interaction among human and robot agents have several features in common, but they may differ in the achievement of the goal. A robot which is collaborating with a human partner shares his same goal and it is required to actively participate to the particular executing task. In addition, when referring to humanoid robots further requirements must be fulfilled in order to realize an efficient system architecture.

The use of humanoid robots that can support human daily activities are expected to significantly help people in work sites, especially in dangerous and emergency situations. Before this vision becomes a reality, many important challenges need to be addressed. For such reason, a human–conceivable interaction is essential.

Although many barriers have been overcome, the intelligence and autonomy of robots is not even close to mankind. Humanoid robots still depend on human guidance. Thus, since robots are not fully autonomous, many applications rely on a direct teleoperation which is now actually converging to telepresence, in which the human feels the interaction in several ways. This concept can actually be extended to the use of robots which share the command of the operation with the human. This means that robots may guide the human in some situations, and still be teleoperated in other ones.

Clearly, there is a growing need for research on human-robot collaboration and models of communication between human and robotic systems. Such communication can be explicit, in the common sense we humans intend, but it can be also implicit: this could be a case, still common among humans, in which the partners are physically in contact. It is evident that such situations must be faced in two different ways, but they still share a common background.

Humanoid robots may be the perfect tool for collaborating with humans, since they are physically complex like human bodies and, this way, they can achieve similar tasks. Anyway, such robots still lack many basic capabilities which could permit their use in collaboration with humans.

The collaboration between a robotic and a human agent has special requirements from a control point of view and for the interaction modalities. The agents may interact having special interfaces or directly through a physical contact. In this case, a special control technique has to be used which takes into account the disturbances that arise from the contact.

The humanoid robot is a high–dimensional space, but when a stabilization control is required, there is a need for using a model close as much as possible to the reality, like any other system. In this research, a very simplified model is shown to be suitable in many situations which could be common in collaborative human–environments.

The advantages of a simplified model result in the possibility of being used in real-time applications.

In Chapter 3, a full humanoid model has been used to validate the simplified models. In particular, this Thesis has used the double (inverted) pendulum as a basic model.

The non-inverted case has been used on the HRP-2 robot in order to reduce the dynamical effects provoked by the floating leg in walking tasks.

In fact, among different trajectories it is possible to choose the one which allows reducing the impacts on the ground. This is made possible through interpolating polynomials that produce continuity in acceleration, velocity and position.

Using the simplified model of the floating leg, the mean torque on the CoM is reduced finding two appropriate via-points through which the floating foot has to pass.

The full humanoid model is used for the robot attitude estimation. The typical estimation is done using the EKF, combining the information of the accelerometer and the gyroscope.

In Chapter 4, the attitude estimator (still based on the EKF) also uses the information coming from motor encoders. In fact, using the robot kinematics and identifying the support phase from the force sensors in the robot feet, when the robot is balanced, it is possible to calculate the orientation of the CoM with respect to the world frame. The robot attitude estimation is achieved using an EKF which combines the IMU measurements with the predicted kinematics due to the robot joints. The inclusion of kinematics information has reduced the error in the estimation especially during the impacts, where an acceleration peak occurs.

A good attitude estimation is used by the balance control, which is based on the double inverted pendulum simplified model. In particular, the robot is simplified as four pendulums, one for each leg and arm.

The combination of these pairs of inverted pendulums is used in order to get an estimated model for predicting the ZMP.

A balance and attitude controller is proposed in Chapter 5 in order to stabilize the robot. An attitude controller is controlling the roll and pitch angles of the CoM. The balance controller is working basing on the concept of the stability regions. The support polygon is actually divided into three regions which represent three different stable situations: the inner region is the most stable, whereas the outer region needs an effective control in order to avoid the loss of balance. When a small disturbance is affecting the ZMP, a static balancer is sufficient in order to reduce the difference between the foot center and the ZMP. The static balancer is working as a secondary-priority controller while the robot is moving.

The dynamic balance controller acts when a large and impulsive disturbance takes place. In this case, the inertial effects due to the acceleration of the CoM and the

arms are used to respond. In such case, the controller priority is the highest, thus the robot leaves the present task and then makes a step which is used to enlarge the support polygon.

The step generator needs a continuity in velocity in order to reduce additional inertial effects which can further undermine the robot stability. For such reason a walking pattern generator is presented which interpolates position and velocity for the CoM.

Chapter 6 has focused on aspects of human–robot collaborative work in unstructured scenarios. Two kinds of human–robot collaboration are presented. First, a physical human–robot collaboration is analyzed when the human and the robot share the same workspace and a common object, as in the case of a joint transportation.

In the case of a humanoid that should sustain an object together with a human, the problem from a kinematical approach has been faced. This has exhibited the mechanical limitations of humanoid robot RH–1, encouraging the RoboticsLab research group at the UC3M to investigate a different structure for the upper part, which is currently being developed for their new version of humanoid robot TEO.

A second collaboration case is named remote collaboration: the human and robot agents do not share the same environment and need communication capabilities. The collaborative architecture is based on the DH $\leftrightarrow$ DR concept allowing a human–robot team to interact and cooperate during the execution of a task.

By means of an HMI, a human operator can teleoperate the robot and choose, among different approaches, the way then robot can perform an action such as, for instance, “grab an object”. The HMI also includes a video streaming of the robot cameras: the roll and pitch nuisance has been reduced conveniently filtering the images. The HMI design is critical since it is the unique way the human operator can supervise and command the robot: its design should be simple, usable and efficient.

The communication between the two agents is achieved through the RCP, a text–based protocol, simple to understand and debug. As a result of its generality, such protocol can be used for a generic target robot described by a high–level model as well as the designed HMI can also be reused for other humanoid platforms.

A hypothetical lunar scenario has been used for testing the proposed architecture: the commercial Fujitsu HOAP–3 humanoid platform was teleoperated until it could recognize an antenna and grasp it after an exchange of messages with the human.

In conclusion, the proposed architecture could result troublesome for long and repetitive tasks: this system is particularly convenient only if the time efficiency is not an essential parameter. Additionally, non–specialist users could encounter the system unpleasant due to the lack of familiarity with teleoperation issues and with concepts such as manipulability or workspace.

## 7.2 Main contributions

The main contributions of this work can be synthetically described as:

- humanoid attitude estimation, presented in Chapter 4
- balance control, shown in Chapter 5
- human–robot collaborative approach, introduced in Chapter 6

The attitude estimation has been performed and compared with the estimation done by the HRP–2 stabilizer.

Several experiments have been carried out with the HRP–2 robot and the real attitude has been measured using a motion capture system. The comparison between the proposed algorithm and the HRP–2 stabilizer shows that the first one is getting a reduced error in the estimation and is more robust to robot impacts.

The balance controller is working based on the concept of the stability regions. The novel concept of the stability regions permits to determine the level of invasiveness of the control algorithm. For the most stable region, no action is required for the balance. The second region needs a balance action: in this case, a static balancer is proposed which is actually working ‘behind’ the task controller using the unused DOFs. Finally the most critical case is managed by the dynamic balancer which has been proposed to act on the joints acceleration achieving a fast controller.

Finally, the DH $\leftrightarrow$ DR concept is a general collaborative scheme which can be extended to any kind of robot that has to be used with human teams. It has been tried and tested on the real HOAP–3 robotic platform by non–technical human agents. This concept, based on the simple idea which is behind any kind of organization, where all the agents contribute for the same goal and provide their own skills, has several advantages that permit to use the robot in complex tasks that are normally not achievable by a full–autonomous robot.

## 7.3 Future works

This work has open many issues in the framework of humanoid robot collaborating with humans. Some possible consequent studies are as follows:

- A comparative evaluation of the attitude estimation is necessary, based on different robot motion tasks.
- Other kinds of algorithms for the estimation can be exploited, such as particle filtering. A good extension of the algorithm may be the use of an  $n$ –states estimator, in which a different estimator is used for each robot phase (single– and double–support).

- 
- A complete state machine needs to be designed: the states have to take into account the particular posture of the robot together with the prediction of the next one. This way the controller may act depending on the particular task the robot is executing.
  - As previously stated, the main issue regarding the balance controller is the algorithm complexity. An optimization of such algorithm is necessary in order to reduce the computational cost and thus improve the real-time response to abrupt external disturbances.
  - A distributed system may help in calculating the complete humanoid dynamics and correct the control action for the balancer.
  - A whole controller that combines the advantages of the static and dynamic controllers may still be necessary, making use of a preview controller.
  - Such controller may also be used for the physical collaboration. An external force or torque due to the interaction with the human can be estimated using the robot simplified dynamics and generate a control action.
  - The information of force/torque sensors in robot wrists is necessary in order to predict human movements.
  - An impact controller, acting when the robot is impacting the ground with one foot, needs to be implemented.
  - A virtual external force may be used as input for the robot control in particular situations, such as the case the robot wants to move an object whose mass is comparable with its mass.
  - Virtual forces may also be used as a motion generator for the robot.
  - A vision system able to predict human movements may provide further information for the robot reaction to the interaction.
  - The collaborative scheme still lacks many functionalities, such as a direct stop that should move the robot to the closest stable configuration.



**Appendix A**

**TEO Robot**



---

Humanoid robot TEO (Task Environment Operator) is the successful result of several years of research carried out by the robotics group RoboticsLab at the UC3M. The RoboticsLab researchers have been working for many years on the RH project, realizing the RH-0 and RH-1 platforms. They are robust and open humanoid platforms for research on biped walking, balancing control, and human-robot interaction.

The RH-1 humanoid robot platform of 1.45m and 50Kg has been designed completely at the UC3M [123]. This robot has been thought to work in human-robot collaboration tasks in indoor and outdoor environments, *e.g.* mounting panels or transporting objects with human cooperation. The sensorial system of the robot, divided into two parts, has been designed to allow collaboration tasks: 1) sensors for locomotion (accelerometers and inclinometers) and 2) sensors for interaction (camera and microphones). The HMI of the robot could work through the friendly-oriented menus of the central computer or via voice commands [124].

Nevertheless, the main research objectives of this platform have been limited to the stability of the robot and the gait generation [123] without considering upper part movements related to physical collaboration. As a main problem, the mechanical structure of this prototype has not been very robust and has presented limitations regarding the flexibility of the whole body, which has hardly complicated the balance control, and thus reducing the applications range. The RH-1 has also presented strong limitations in the energy efficiency due to its weight and its limited power capabilities.

The research team at RoboticsLab is now working on the development of the new platform TEO, which better suits the needs for using this platform in a human environment, equipping it with as special sensors system, composed of force/torque sensors in the wrists the feet together with cameras in the head, and accelerometer and gyroscope sensors in the chest [125].

Basing on the previous experience, an optimal mechanical design of the structure has been realized. This entails a lighter structure which can be better introduced in human environments. Additionally, the use of a fuel cell as a battery is supposed to improve the energy efficiency, increasing the autonomy of the robot.

TEO addresses challenges in the fields of motion, safety, energy efficiency, and power autonomy performance. The mechatronics of this structure has been inspired to be capable of realizing the human adaptable locomotion and to physically achieve complex tasks with humans. Whereas the upper part of RH-1 robot presented several limitation, TEO arms and waist were added two DOFs each in order to extend the workspace and to raise the manipulability in the different configurations. This way, TEO robot has now 26 DOFs. A tangible difference concerns the structure: RH-1 was skeleton-like where electronics was attached to. This strongly limited the possibility of adding new components. Thus, TEO has a box-like structure which includes inside all the electronics.

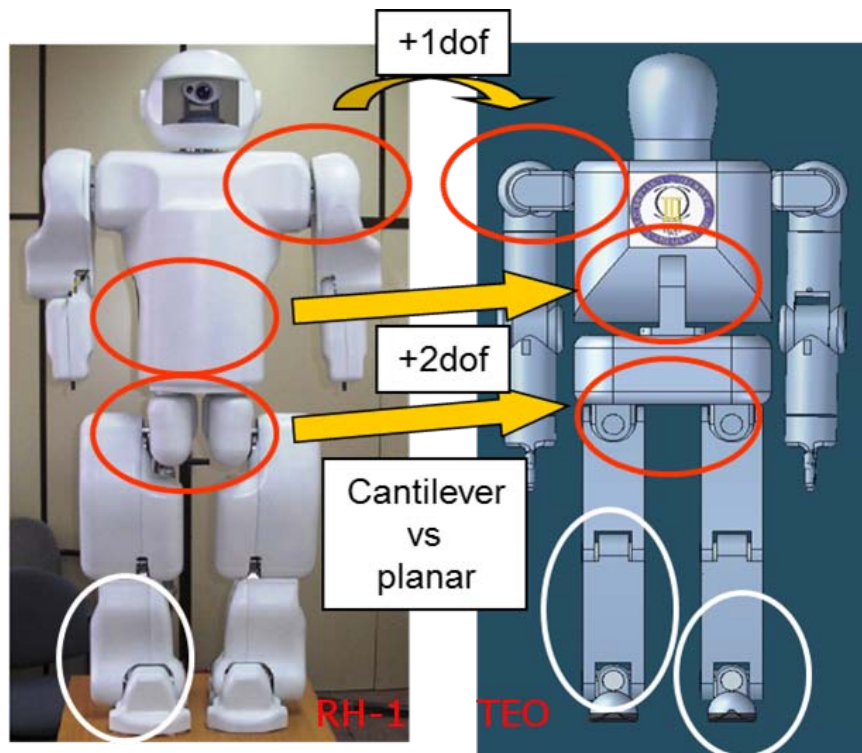


Figure A.1: RH-1 and TEO platforms

A schematic comparison between the two platform is presented in Figure A.1.

# Appendix B

## HOAP-3 Robot



The HOAP series robots have been an advanced humanoid robot platform manufactured by Fujitsu Automation in Japan<sup>1</sup>. HOAP is an abbreviation for “Humanoid for Open Architecture Platform”.

In 2001, Fujitsu realized its first commercial humanoid robot named HOAP-1. The HOAP-2 was released in 2003 followed by the HOAP-3 in 2005. Hoap-3 Robot has been the last humanoid platform realized by Fujitsu Automation.

The small humanoid robot HOAP-3 [126] is about 60cm in height; therefore it is easy to treat since it is small and lightweight (the weight is about 8kg if the battery is removed).

The HOAP system consists of the robot body, a control PC and the power supplies.

The control architecture operates on RT-Linux mounted on a personal computer and communicates with the robot main part via a USB interface or wi-fi communication.

HOAP-3 robot (Figure B.1) has a total of 28 joints, distributed as:

- 6 DOFs in each arm
- 6 DOFs in each leg
- 3 DOFs in the head
- 1 DOF in the body

The sensors onboard the robot are:

- Posture sensors: a gyroscope and an accelerometer
- Contact sensors: in every corner of each foot
- Grip sensor: in the thumb of the hands
- Two USB cameras in the head

Its structure and sensor system permit to try different control architecture thought to be used in a collaborative system.

---

<sup>1</sup>[http://jp.fujitsu.com/group/labs/techinfo/techguide/list/robotics\\_p11.html](http://jp.fujitsu.com/group/labs/techinfo/techguide/list/robotics_p11.html), accessed on May 27, 2012



Figure B.1: The HOAP-3 platform

# Appendix C

## HRP-2 Robot



The HRP series robots are part of the Japanese Humanoid Robotics Project headed by the Manufacturing Science and Technology Center (MSTC), which is sponsored by the Ministry of Economy, Trade and Industry (METI) through New Energy and Industrial Technology Development Organization (NEDO). Recently Kawada<sup>1</sup>, that is actually designing and integrating these platforms, has released the forth platform (HRP-4), but the platform used as a reference for this work is the HRP-2.

The height of the HRP-2 robot (Figure C.1) is 154 cm and its width is 62 cm. Its weight (including batteries) is 58kg. The robot has 30 DOFs and can walk up to 2 Km/h. Its force/torque sensors placed in the feet and wrists allow using it as a platform for the collaborations.

The main characteristics of HRP-2 are the cantilevered crotch joint which allows walking in a restricted area and its compact electrical system which avoids the “backpack”, that is typical in many humanoids.

The combination of different functional control elements is made possible thanks to the OpenRTM-AIST, a special middleware implementation.

HRP-2 has been used for experiments to further develop robotic technologies in the areas of “walking on uneven surfaces”, “lying down and getting up” [24], and “human-interactive operations in open spaces” [10].

Several applications have been studied using the HRP robot in collaborative tasks. For instance, the HRP-3 robot has been utilized in teleoperation [127]. This way, it could be used in maintenance tasks for energy plants, where the robot semi-autonomy will help to perform the operation it has been assigned.

---

<sup>1</sup><http://global.kawada.jp/mechatronics>, accessed on May 27, 2012



Figure C.1: The HRP-2 platform

# Appendix D

## Humanoid Models



Here the kinematic models for the complete humanoid robots are presented. This models are based on DH convention and they are shown to be unique for all the platforms that have been used in this research. Finally, Figure D.6 represents the dynamical model of HOAP-3, realized in SimMechanics<sup>TM</sup>.

Table D.1: DH parameters for a humanoid floating leg (Figure D.1)

Name	Joint type	number	$\mathbf{a}_i$	$\alpha_i$	$\mathbf{d}_i$	$\theta_i$
<i>Right hip</i>	Yaw	1	0	$\frac{\pi}{2}$	0	$\theta_1 + \frac{\pi}{2}$
	Roll	2	0	$-\frac{\pi}{2}$	0	$\theta_2 - \frac{\pi}{2}$
	Pitch	3	Leg_Link2	0	0	$\theta_3$
<i>Right knee</i>	Pitch	4	Leg_Link3	0	Leg_Link4	$\theta_4$
<i>Right ankle</i>	Pitch	5	0	$\frac{\pi}{2}$	0	$\theta_5$
	Roll	6	Leg_Link5	0	0	$\theta_6$

Table D.2: DH parameters for a humanoid standing leg (Figure D.2)

Name	Joint type	number	$\mathbf{a}_i$	$\alpha_i$	$\mathbf{d}_i$	$\theta_i$
<i>Right ankle</i>	Roll	1	0	$\frac{\pi}{2}$	0	$\theta_1$
	Pitch	2	Leg_Link3	0	Leg_Link4	$\theta_2$
<i>Right knee</i>	Pitch	3	Leg_Link2	0	0	$\theta_3$
<i>Right hip</i>	Pitch	4	0	$-\frac{\pi}{2}$	0	$\theta_4$
	Roll	5	0	$-\frac{\pi}{2}$	0	$\theta_5 + \frac{\pi}{2}$
	Yaw	6	Leg_Link1	0	0	$\theta_6$

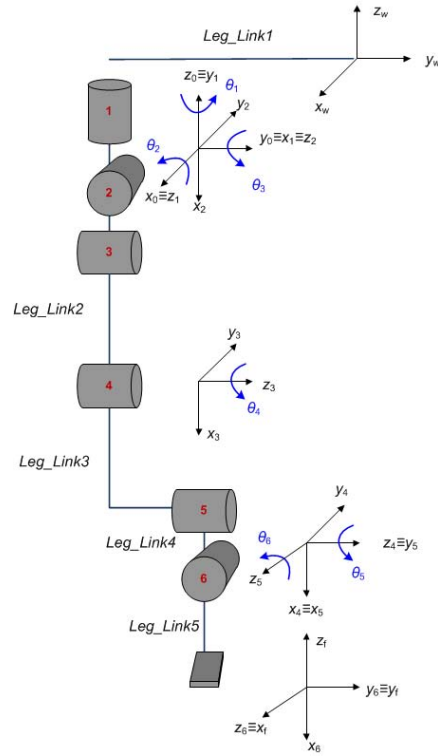


Figure D.1: Kinematic model for a humanoid floating leg

Table D.3: Dimensions for humanoid legs

Name	Symbol	Length [m]		
		TEO	HOAP-3	HRP-2
<i>Waist</i>	Leg_Link1	0.146	0.039	0.06
<i>Femur</i>	Leg_Link2	0.33	0.105	0.3
<i>Tibia</i>	Leg_Link3	0.3	0.105	0.3
<i>Patella</i>	Leg_Link4	0.033	0	0.035
<i>Astragalus</i>	Leg_Link5	0.124	0.040	0.105

Table D.4: DH parameters for a humanoid flexible ankle (Figure D.3)

Name	Joint type	number	$a_i$	$\alpha_i$	$d_i$	$\theta_i$
<i>Flexibility</i>	Roll	1	0	$\frac{\pi}{2}$	0	$\theta_1$
	Pitch	2	0	$-\frac{\pi}{2}$	0	$\theta_2 - \frac{\pi}{2}$

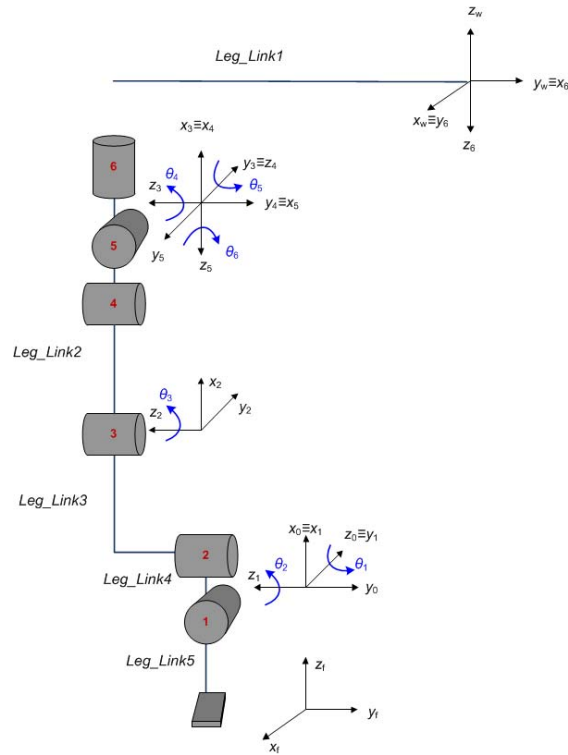


Figure D.2: Kinematic model for a humanoid standing leg

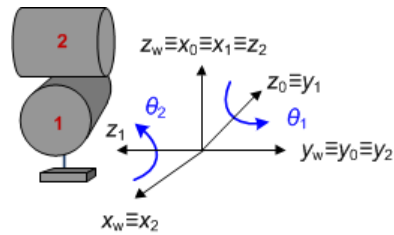


Figure D.3: Kinematic model for a humanoid flexible ankle

Table D.5: DH parameters for a humanoid torso (Figure D.4)

Name	Joint type	number	$a_i$	$\alpha_i$	$d_i$	$\theta_i$
Torso	Yaw	1	0	$-\frac{\pi}{2}$	0	$\theta_1$
	Pitch	2	-Torso_Link1	0	0	$\theta_2$

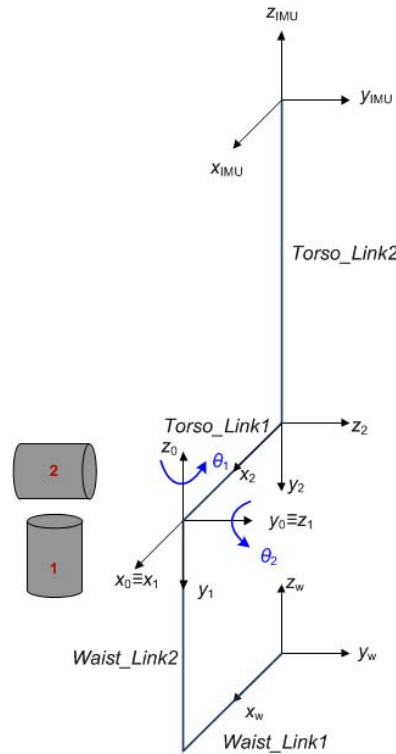


Figure D.4: Kinematic model for a humanoid torso

Table D.6: Dimensions for humanoid torso

Name	Symbol	Length [m]		
		TEO	HOAP-3	HRP-2
<i>Waist</i>	Waist_Link1	0	0.035	0.032
	Waist_Link2	0.287	0.055	0.351
<i>Torso</i>	Torso_Link1	0	0.035	0.130
	Torso_Link2	0.060	0.070	0.118

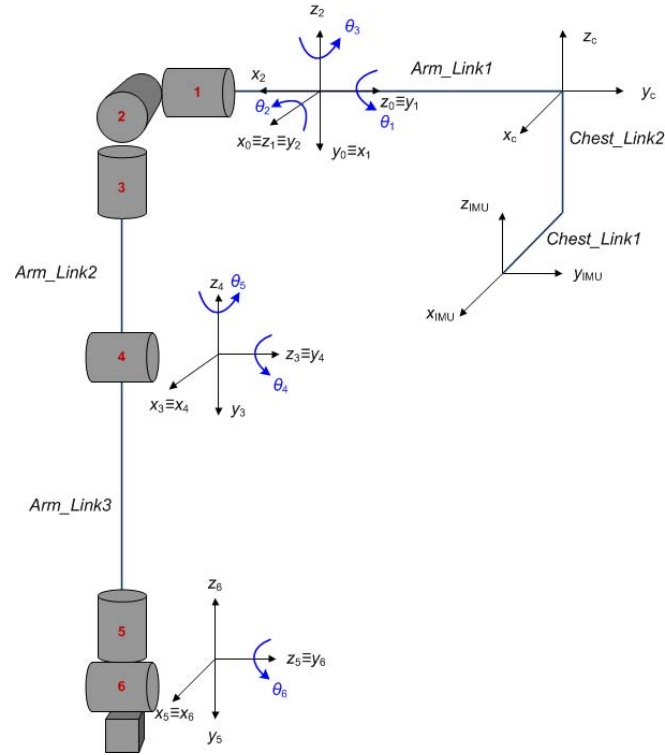


Figure D.5: Kinematic model for a humanoid arm

Table D.7: DH parameters for a humanoid arm (Figure D.5)

Name	Joint type	number	$a_i$	$\alpha_i$	$d_i$	$\theta_i$
<i>Right shoulder</i>	Pitch	1	0	$\frac{\pi}{2}$	0	$\theta_1 + \frac{\pi}{2}$
	Roll	2	0	$\frac{\pi}{2}$	0	$\theta_2 - \frac{\pi}{2}$
	Yaw	3	0	$-\frac{\pi}{2}$	-Arm_Link2	$\theta_3 + \frac{\pi}{2}$
<i>Right elbow</i>	Pitch	4	0	$\frac{\pi}{2}$	0	$\theta_4$
<i>Right wrist</i>	Yaw	5	0	$-\frac{\pi}{2}$	-Arm_Link3	$\theta_5$
	Pitch	6	0	$\frac{\pi}{2}$	0	$\theta_6$

Table D.8: Dimensions for humanoid arms

Name	Symbol	Length [m]		
		TEO	HOAP-3	HRP-2
<i>Chest</i>	Chest_Link1	0	0	0.093
	Chest_Link2	0.245	0.055	0.063
<i>Clavicle</i>	Arm_Link1	0.340	0.111	0.250
<i>Humerus</i>	Arm_Link2	0.337	0.111	0.250
<i>Ulna</i>	Arm_Link3	0.210	0.171	0.250

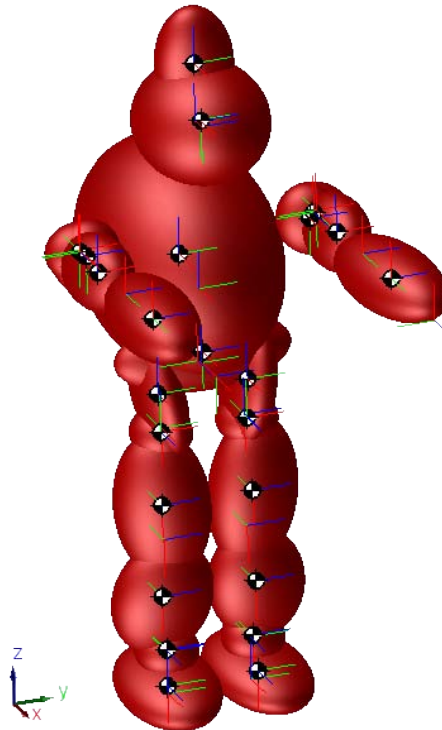


Figure D.6: HOAP-3 dynamical model

## Appendix E

### The Robot Command Protocol (RCP)



The Robot Command Protocol (RCP) was originally defined in [128] and can be decomposed into several sub-protocols, and, as for the RoboLink protocol [129], is organized into “profiles”. Each sub-protocol contains a set of commands used for a single purpose. The list of RCP sub-protocols is shown in Table E.1.

Design goals for the protocol are: simplicity, generality, flexibility and expressiveness. The protocol should be simple in the sense that no unneeded features should be added; the protocol should be general and flexible enough to be used for several use cases without modifications. A powerful characteristic that leads to both flexibility and expressiveness can be identified as orthogonality, which can be achieved by clearly separating disconnected functionalities while at the same time allowing their combination without unneeded constraints.

**RCP** is a text-based protocol which has its roots in Unix protocols like SMTP or FTP. Each **RCP** command is a text string terminated by a newline character. The RCP protocol presents various attractive characteristics:

- The resulting protocol is simple to understand and implement.
- Support for robot control can also be easily added to programs different from this HMI.
- The protocol is lightweight; since the robot has limited computational resources that can be dedicated to command parsing, this was an important design goal.
- The human-readable text commands make debugging easy.
- The protocol is also general in that it has not been designed for a specific target robot, but for a generic target robot described by a high-level robot model.

One can start and end a communication with the robot using the connection sub-protocol. Once connected, you can use any of the other sub-protocols, for example the sensor reading sub-protocol, which allows operator access to the output of robot sensors.

The sub-protocols summarized so far could be used by multiple users connected to the robot at the same time, since they are mostly composed of query commands, but other sub-protocols which really control robot movements need exclusive access to it. Thus it is necessary for the operator to acquire a sort of “exclusive lock” using the control negotiation sub-protocol before issuing action commands. This ensures only one user at a time can control the robot. Once a user has acquired exclusive control over the robot, he/she can use the basic movement sub-protocol to translate or rotate it.

A basic movement sub-protocol is detailed as an example. The basic movement sub-protocol defines movements of the body and head for teleoperation of the robot. A general **MOVE** command presents the following structure:

```
MOVE <movement_type><direction><count><unit>
```

Currently three movement types of the command are supported:

```
MOVE WALKING [FORWARD|BACKWARD] <count> STEPS
MOVE TURNING [LEFT|RIGHT] <count> DEGREES
MOVE HEAD [UP|DOWN|LEFT|RIGHT] <count> DEGREES
```

The **MOVE** command is a good example of the flexibility of the protocol, in that its structure allows adding new movement types easily. For example a new BOWING movement could be added. As movements are not an instant action, the robot can send multiple replies in response to a **MOVE** command:

```
OK COMMAND <command_id> QUEUED
OK COMMAND <command_id> STARTED
OK COMMAND <command_id> COMPLETED
```

The first reply is sent as soon as the command is accepted; the second one when the command is considered for execution and the third one after the movement has been completed.

Robot movements depend on parameters such as speed and step length. These (and other) parameters can be read or set via the configuration sub-protocol.

The generic robot model includes a command queue, where commands are inserted before being executed. So, even if commands are sent by the user before the current movement has been completed, they are put into the queue and executed sequentially. However, while the robot is moving the user may notice he/she has made a mistake (*e.g.* the robot is going too far away) and want to stop the robot immediately, without waiting for all commands in the queue to complete. This is a situation in which the direct command execution sub-protocol is useful, because it allows sending a command which is executed immediately, bypassing the queue. For example the user will issue the command

#### DIRECT STOP

The robot executes the **STOP** command immediately. It terminates the current movement by reaching the nearest stable position, clears out the queue and sends a reply to the user. The **DIRECT** command described above is a good example of orthogonality because it can be combined with any other command, used as a parameter, to make it bypass the queue. Also the **STOP** command is orthogonal because it can be used to terminate any command, not only movements. The reply sent by the robot after executing the **STOP** command is:

---

```
OK COMMAND <cmd_id> INTERRUPTEDBY <cmd_id>
```

From the above line it can be noted that IDs are used to refer to commands. Every command is assigned an ID by its receiver (*i.e.* the robot or the HMI). Then the receiver sends the counterpart a reply indicating whether the command has been accepted or not. Successful replies always start with “OK”, while unsuccessful ones start with “KO”.

The goal-setting sub-protocol presents a more advanced way of controlling robot’s movements. This sub-protocol allow for higher order request to be send to the robot with a task goal oriented movement in mind. In order to tell the robot to go towards, grab or drop an object the user issues the commands:

```
GOTO OBJECT(<object_id>)
GRAB OBJECT(<object_id>)
DROP OBJECT(<object_id>)
```

The protocol allows defining the robot’s target position in two ways; one is to define the position with a pair of coordinates, while the other is to indicate an object as a target.

The relevant command is GOTO, which is shown below in its two variants:

```
GOTO OBJECT(<object_id>)
GOTO <x><y>
```

If the target position is occupied by an object, the robot cannot stop exactly there; in this case the robot stops within a certain range (defined by a configuration parameter) from the target.

The same target-object specification of the goal-setting sub-protocol is also used in the object grabbing sub-protocol. In order to tell the robot to grab or drop an object the user issues the commands:

```
GRAB OBJECT(<object_id>)
DROP OBJECT(<object_id>)
```

Typically these kind of high-level operations are not unambiguously defined by the target object only, but involve some decision about which strategy should be used for executing the operation. For this purpose a specific strategy selection sub-protocol has been defined with which both the robot and the user collaborate in deciding which strategy to use for the operation at hand.

The strategy selection dialogue is initiated from the robot side with a request listing the possible strategies:

```
SELECT STRATEGY FOR <cmd_id> [<strategy_1>, <strategy_2>...  
                               <strategy_n>]
```

Then the user chooses a strategy and communicates his/her decision with the command:

```
USE STRATEGY FOR <command_id><strategy>
```

After the strategy has been selected, the robot can actually grab or drop the object.

In this work a subset of the full protocol described above has been implemented. A reference of all the commands currently defined in the RCP protocol is shown in Table E.2.

A final remark has to be done: the transmission of the video stream from the robot camera is not defined as part of the command protocol, as it happens on a separate channel using an *ad-hoc* streaming protocol.

---

<b>Name</b>	<b>Number of commands</b>
Connection	2
Control negotiation	2
Basic movement	3
Direct command execution	1
Configuration	2
Sensor reading	1
Positioning	2
Notification	tbd
Goal-setting	1
Object grabbing	2
Strategy selection	2

Table E.1: RCP Sub-protocols

Sub-protocol	Command
Connection	CONNECT <profile> DISCONNECT
Control negotiation	CONTROL BEGIN CONTROL END
Basic movement	MOVE <movement_type><direction><count><unit> STOP
Direct command execution	DIRECT <command>
Configuration	QUERY PARAM <parameter_name> SET <parameter_name><parameter_value>
Sensor reading	QUERY SENSOR [<label>, ... , <label>]
Positioning	QUERY POSITION POSITION <x><y><confidence>
Notification	tbd
Goal-setting	GOTO OBJECT(<object_id>) GOTO <x><y>
Object grabbing	GRAB OBJECT(<object_id>) USE OBJECT(<object_id>) DROP OBJECT(<object_id>)
Strategy selection	SELECT STRATEGY FOR <cmd_id>[<strategy_1>, ..., <strategy_n>] USE STRATEGY FOR <cmd_id><strategy>

Table E.2: RCP commands

# Bibliography

- [1] B. Siciliano, L. Sciavicco, L. Villani, and G. Oriolo, *Robotics: Modelling, planning and control*. London: Springer-Verlag, 2009.
- [2] M. E. Bratman, “Shared cooperative activity,” *The Philosophical Review*, vol. 101, no. 2, pp. 327–341, 1992.
- [3] B. J. Grosz and S. Kraus, “The evolution of SharedPlans,” in *Foundations and Theories of Rational Agency* (A. Rao and M. Woolridge, eds.), (Dordrecht), pp. 227–262, Kluwer Academic Publishers, 1999.
- [4] N. R. Jennings, “Controlling cooperative problem solving in industrial multi-agent systems using joint intentions,” *Artificial Intelligence*, vol. 75, no. 2, pp. 195–240, 1995.
- [5] C. Breazeal, A. G. Brooks, J. Gray, G. Hoffman, C. D. Kidd, H. Lee, J. Lieberman, A. Lockerd, and D. Chilongo, “Tutelage and collaboration for humanoid robots,” *International Journal of Humanoid Robotics*, vol. 1, no. 2, pp. 315–348, 2004.
- [6] K. Kroemer and E. Grandjean, *Fitting the task to the human: A textbook of occupational ergonomics*. London: Taylor & Francis, 5th ed., Apr. 1997.
- [7] A. M. Steinfeld, “Human-robot interaction,” in *International Encyclopedia of Ergonomics and Human Factors* (W. Karwowski, ed.), vol. 3, London: CRC Press, 2nd ed., Mar. 2006.
- [8] R. Brooks, L. Aryananda, A. Edsinger, P. Fitzpatrick, C. Kemp, U.-M. O’Reilly, E. Torres-Jara, P. Varshavskaya, and J. Weber, “Sensing and manipulating built-for-human environments,” *International Journal of Humanoid Robotics*, vol. 1, no. 1, pp. 1–28, 2004.

- 
- [9] K. Yokoi, K. Nakashima, M. Kobayashi, H. Mihune, H. Hasunuma, Y. Yanagihara, T. Ueno, T. Gokyyuu, and K. Endou, "A tele-operated humanoid operator," *The International Journal of Robotics Research*, vol. 25, pp. 593–602, May 2006.
- [10] K. Yokoi, N. Kawauchi, N. Sawasaki, T. Nakajima, S. Nakamura, K. Sawada, I. Takeuchi, K. Nakashima, Y. Yanagihara, K. Yokoyama, T. Isozumi, Y. Fukase, K. Kaneko, and H. Inoue, "Humanoid robot applications in HRP," *International Journal of Humanoid Robotics*, vol. 1, no. 3, pp. 409–428, 2004.
- [11] C. Bartneck, J. Reichenbach, and J. Carpenter, "Use of praise and punishment in human-robot collaborative teams," in *Proceedings of the IEEE International Workshop on Robot and Human Communication*, (Hatfield, United Kingdom), pp. 177–182, IEEE, Sept. 2006.
- [12] K. Yokoi, N. E. Sian, T. Sakaguchi, O. Stasse, Y. Kawai, and K. Maruyama, "Humanoid robot HRP-2 with human supervision," in *Experimental Robotics* (O. Khatib, V. Kumar, and D. Rus, eds.), vol. 39 of *Springer Tracts in Advanced Robotics*, pp. 513–522, Berlin/Heidelberg, Germany: Springer Berlin Heidelberg, 2008.
- [13] E. Gambao and C. Balaguer, "Robotics and automation in construction," *IEEE Robotics and Automation Magazine*, vol. 9, pp. 4–6, Mar. 2002.
- [14] R. A. Jarvis, "Sensor rich teleoperation of an excavating machine," in *Proceedings of the International Conference on Field and Service Robotics*, (Pittsburgh, Pennsylvania, USA), pp. 238–243, 1999.
- [15] K. Tanie, "Humanoid robot and its application possibility," in *Proceedings of the IEEE International Conference on Multisensor Fusion and Integration for Intelligent Systems*, (Tokyo, Japan), pp. 213–214, IEEE, 2003.
- [16] W. Bluethmann, R. O. Ambrose, M. A. Diftler, S. Askew, E. Huber, M. Goza, F. Rehnmark, C. Lovchik, and D. Magruder, "Robonaut: a robot designed to work with humans in space," *Autonomous Robots*, vol. 14, pp. 179–197, Mar. 2003.
- [17] D. J. Bruemmer, D. A. Few, R. L. Boring, J. L. Marble, M. C. Walton, and C. W. Nielsen, "Shared understanding for collaborative control," *IEEE Transactions on Systems, Man, and Cybernetics - Part A: Systems and Humans*, vol. 35, pp. 494–504, July 2005.

- [18] T. W. Fong, C. Thorpe, and C. Baur, "Collaboration, dialogue, and human-robot interaction," in *Proceedings of the International Symposium of Robotics Research*, (Lorne, Australia), July 2001.
- [19] T. W. Fong and I. Nourbakhsh, "Interaction challenges in human-robot space exploration," *Interactions*, vol. 12, no. 1, pp. 42–45, 2005.
- [20] Y. Ogura, H. Aikawa, K. Shimomura, H. Kondo, A. Morishima, H. Lim, and A. Takanishi, "Development of a humanoid robot WABIAN-2," in *Proceedings of the IEEE International Conference on Robotics and Automation*, (Orlando, Florida, USA), pp. 76 –81, IEEE, 2006.
- [21] M. Zecca, N. Endo, S. Momoki, K. Itoh, and A. Takanishi, "Design of the humanoid robot KOBIAN - preliminary analysis of facial and whole body emotion expression capabilities," in *Proceedings of the IEEE-RAS International Conference on Humanoid Robots*, (Daejeon, South Korea), pp. 487–492, IEEE, Dec. 2008.
- [22] H. Kimura, T. Horiuchi, and K. Ikeuchi, "Task-model based human robot cooperation using vision," in *Proceedings of the IEEE/RSJ International Conference on Intelligent Robots and Systems*, (Kyongju, South Korea), pp. 701–706, IEEE, 1999.
- [23] M. D. Johnston and K. J. Rabe, "Integrated planning for telepresence with time delays," in *Proceedings of the IEEE International Conference on Space Mission Challenges for Information Technology*, (Pasadena, California, USA), pp. 140–148, IEEE, 2006.
- [24] K. Kaneko, F. Kanehiro, S. Kajita, H. Hirukawa, T. Kawasaki, M. Hirata, K. Akachi, and T. Isozumi, "Humanoid robot HRP-2," in *Proceedings of the IEEE International Conference on Robotics and Automation*, vol. 2, (New Orleans, Louisiana, USA), pp. 1083 – 1090 Vol.2, IEEE, 2004.
- [25] N. Freedman, "The analysis of movement behavior during the clinical interview," in *Studies in Dyadic Communication* (A. Siegman and B. Pope, eds.), pp. 153–175, New York, NY, USA: Pergamon Press, 1972.
- [26] J. M. Hollerbach, "Some current issues in haptics research," in *Proceedings of the IEEE International Conference on Robotics and Automation*, (San Francisco, California, USA), pp. 757–762, IEEE, 2000.
- [27] S. Lauria, G. Bugmann, T. Kyriacou, and E. Klein, "Mobile robot programming using natural language," *Robotics and Autonomous Systems*, vol. 38, no. 3-4, pp. 171–181, 2002.

- [28] A. Kheddar, "Teleoperation based on the hidden robot concept," *IEEE Transactions on Systems, Man, and Cybernetics - Part A: Systems and Humans*, vol. 31, no. 1, pp. 1–13, 2001.
- [29] M. Vukobratović, B. Borovac, and V. Potkonjak, "Towards a unified understanding of basic notions and terms in humanoid robotics," *Robotica*, vol. 25, pp. 87–101, 2007.
- [30] P. Sardain and G. Bessonnet, "Forces Acting on a Biped Robot. Center of Pressure - Zero Moment Point," *IEEE Transactions on Systems, Man, and Cybernetics - Part A: Systems and Humans*, vol. 34, pp. 630–637, Sept. 2004.
- [31] A. Goswami, "Postural stability of biped robots and the Root-Rotation Indicator (FRI) point," *The International Journal of Robotics Research*, vol. 18, pp. 523–533, June 1999.
- [32] M. Vukobratović and B. Borovac, "Zero-Moment Point - thirty five years of its life," *International Journal of Humanoid Robotics*, vol. 1, no. 1, pp. 157–173, 2004.
- [33] M. Vukobratović and D. Juričić, "Contribution to the synthesis of biped gait," in *Proceeding of the I.F.A.C. International Symposium on Technical and Biological Problem of Control*, (Yerevan, USSR), 1968.
- [34] M. Vukobratović and D. Juričić, "Contribution to the synthesis of biped gait," *IEEE Transactions on Biomedical Engineering*, vol. 16, pp. 1–6, Jan. 1969.
- [35] M. Vukobratović, A. A. Frank, and D. Juričić, "On the stability of biped locomotion," *IEEE Transactions on Biomedical Engineering*, vol. 17, pp. 25–36, Jan. 1970.
- [36] M. Vukobratović and Y. Stepanenko, "On the stability of anthropomorphic systems," *Mathematical Biosciences*, vol. 15, pp. 1–37, 1972.
- [37] A. Goswami, "Foot Rotation Indicator (FRI) point: A new gait planning tool to evaluate postural stability of biped robots," in *Proceedings of the IEEE International Conference on Robotics and Automation*, (Detroit, Michigan, USA), pp. 47–52, IEEE, 1999.
- [38] K. Yoneda and S. Hirose, "Tumble stability criterion of integrated locomotion and manipulation," in *Proceedings of the IEEE/RSJ International Conference on Intelligent Robots and Systems*, (Osaka, Japan), pp. 870–876, IEEE, 1996.

- [39] S. Kagami, T. Kitagawa, K. Nishiwaki, T. Sugihara, M. Inaba, and H. Inoue, "A fast dynamically equilibrated walking trajectory generation method of humanoid robot," *Autonomous Robots*, vol. 12, no. 1, pp. 71–82, 2002.
- [40] S. Kaneko, K. Mitobe, M. Yamano, and Y. Nasu, "Control of the walking robots considering locally defined Zero Moment Points," in *Proceedings of the Annual Conference of the Robotics Society in Japan*, (Tokyo, Japan), pp. 829–830, The Robotics Society of Japan, 2001.
- [41] K. Harada, S. Kajita, K. Kaneko, and H. Hirukawa, "Dynamics and balance of a humanoid robot during manipulation tasks," *IEEE Transactions on Robotics*, vol. 22, pp. 568–575, June 2006.
- [42] T. Saida, Y. Yokokohji, and T. Yoshikawa, "FSW (feasible solution of wrench) for multi-legged robots," in *Proceedings of the IEEE International Conference on Robotics and Automation*, (Taipei, Taiwan), pp. 3815–3820, IEEE, 2003.
- [43] H. Hirukawa, S. Hattori, K. Harada, S. Kajita, K. Kaneko, F. Kanehiro, K. Fujiiwara, and M. Morisawa, "A universal stability criterion of the foot contact of legged robots - adios ZMP," in *Proceedings of the IEEE International Conference on Robotics and Automation*, (Orlando, Florida, USA), pp. 1976–1983, IEEE, 2006.
- [44] A. Michel, "Quantitative analysis of simple and interconnected systems: Stability, boundedness, and trajectory behavior," *IEEE Transactions on Circuit Theory*, vol. 17, no. 3, pp. 292–301, 1970.
- [45] B. Borovac, M. Vukobratović, and D. Stokić, "Stability analysis of mechanisms having unpowered degrees of freedom," *Robotica*, vol. 7, pp. 349–357, Oct. 1989.
- [46] F. Gubina, H. Hemami, and R. B. McGhee, "On the dynamic stability of biped locomotion," *IEEE Transactions on Biomedical Engineering*, vol. BME-21, no. 2, pp. 102–108, 1974.
- [47] S. Kajita, T. Yamaura, and A. Kobayashi, "Dynamic walking control of a biped robot along a potential energy conserving orbit," *IEEE Transactions on Robotics and Automation*, vol. 8, no. 4, pp. 431–438, 1992.
- [48] J. H. Park and K. D. Kim, "Biped robot walking using gravity-compensated inverted pendulum mode and computed torque control," in *Proceedings of the IEEE International Conference on Robotics and Automation*, (Leuven, Belgium), pp. 3528–3533, IEEE, 1998.

- [49] J. H. Park and H. Chung, “Hybrid control for biped robots using impedance control and computed-torque control,” in *Proceedings of the IEEE International Conference on Robotics and Automation*, (Detroit, Michigan, USA), pp. 1365–1370, IEEE, 1999.
- [50] S.-H. Hyon, “Compliant terrain adaptation for biped humanoids without measuring ground surface and contact forces,” *IEEE Transactions on Robotics*, vol. 25, pp. 171–178, Feb. 2009.
- [51] K. Jung-Hoon and O. Jun-Ho, “Walking control of the humanoid platform KHR-1 based on torque feedback control,” in *Proceedings of the IEEE International Conference on Robotics and Automation*, (New Orleans, Louisiana, USA), pp. 623–628, IEEE, 2004.
- [52] Y. Okumura, T. Tawara, K. Endo, T. Furuta, and M. Shimizu, “Realtime ZMP compensation for biped walking robot using adaptive inertia force control,” in *Proceedings of the IEEE/RSJ International Conference on Intelligent Robots and Systems*, (Las Vegas, Nevada, USA), pp. 335–339, IEEE, 2003.
- [53] S. Lohmeier, T. Buschmann, and H. Ulbrich, “System design and control of anthropomorphic walking robot LOLA,” *IEEE/ASME Transactions on Mechatronics*, vol. 14, pp. 658–666, Dec. 2009.
- [54] J. H. Park, “Impedance control for biped robot locomotion,” *IEEE Transactions on Robotics and Automation*, vol. 17, no. 6, pp. 870–882, 2001.
- [55] K. J. Waldron, “Force and motion management in legged locomotion,” *IEEE Journal on Robotics and Automation*, vol. 2, pp. 214–220, Dec. 1986.
- [56] M. Mistry, J. Nakanishi, G. Cheng, and S. Schaal, “Inverse kinematics with floating base and constraints for full body humanoid robot control,” in *Proceedings of the IEEE-RAS International Conference on Humanoid Robots*, (Daejeon, South Korea), pp. 22–27, IEEE, 2008.
- [57] M. Mistry, J. Buchli, and S. Schaal, “Inverse dynamics control of floating base systems using orthogonal decomposition,” in *Proceedings of the IEEE International Conference on Robotics and Automation*, (Anchorage, Alaska, USA), pp. 3406–3412, IEEE, May 2010.
- [58] H. Miura and I. Shimoyama, “Dynamic walk of a biped,” *The International Journal of Robotics Research*, vol. 3, pp. 60–74, June 1984.

- [59] J. K. Hodgins and M. H. Raibert, "Adjusting step length for rough terrain locomotion," *IEEE Transactions on Robotics and Automation*, vol. 7, pp. 289–298, June 1991.
- [60] C. Cocaud and A. Jnifene, "Stability control of a 6 DOF biped in the dual-support phase using fuzzy control," in *Proceedings of the IEEE-RAS International Conference on Humanoid Robots*, (Santa Monica, California, USA), pp. 842–854, IEEE, 2004.
- [61] Y. Fujimoto and A. Kawamura, "Simulation of an autonomous biped walking robot including environmental force interaction," *IEEE Robotics and Automation Magazine*, vol. 5, no. 2, pp. 33–42, 1998.
- [62] Napoleon, S. Nakaura, and M. Sampei, "Balance control analysis of humanoid robot based on ZMP feedback control," in *Proceedings of the IEEE/RSJ International Conference on Intelligent Robots and Systems*, (Lausanne, Switzerland), pp. 2437–2442, IEEE, 2002.
- [63] E. R. Westervelt and J. W. Grizzle, "Design of asymptotically stable walking for a 5-link planar biped walker via optimization," in *Proceedings of the IEEE International Conference on Robotics and Automation*, vol. 3, (Washington, D.C., USA), pp. 3117–3122, IEEE, 2002.
- [64] A. Sano and J. Furusho, "Realization of natural dynamic walking using the angular momentum information," in *Proceedings of the IEEE International Conference on Robotics and Automation*, (Cincinnati, OH, USA), pp. 1476–1481, IEEE, May 1990.
- [65] J. Pratt and G. Pratt, "Intuitive control of a planar bipedal walking robot," in *Proceedings of the IEEE International Conference on Robotics and Automation*, vol. 3, (Leuven, Belgium), pp. 2014–2021, IEEE, May 1998.
- [66] Y. Choi, D. Kim, Y. Oh, and B.-J. You, "Posture/walking control for humanoid robot based on kinematic resolution of CoM Jacobian with embedded motion," *IEEE Transactions on Robotics*, vol. 23, pp. 1285–1293, Dec. 2007.
- [67] D. Wollherr and M. Buss, "Posture modification for biped humanoid robots based on Jacobian method," in *Proceedings of the IEEE/RSJ International Conference on Intelligent Robots and Systems*, (Sendai, Japan), pp. 124–129, IEEE, 2004.

- [68] T. Sugihara and Y. Nakamura, “Whole-body cooperative balancing of humanoid robot using COG Jacobian,” in *Proceedings of the IEEE/RSJ International Conference on Intelligent Robots and Systems*, (Lausanne, Switzerland), pp. 2575–2580, IEEE, 2002.
- [69] T. Sugihara, *Mobility enhancement control of humanoid robot based on reaction force manipulation via whole body motion*. PhD thesis, University of Tokyo, 2004.
- [70] K. Ogata, K. Terada, and Y. Kuniyoshi, “Falling motion control for humanoid robots while walking,” in *Proceedings of the IEEE-RAS International Conference on Humanoid Robots*, (Pittsburgh, Pennsylvania, USA), pp. 306–311, IEEE, Nov. 2007.
- [71] C. Fu and K. Chen, “Gait synthesis and sensory control of stair climbing for a humanoid robot,” *IEEE Transactions on Industrial Electronics*, vol. 55, pp. 2111–2120, May 2008.
- [72] T. Fukuda, Y. Komata, and T. Arakawa, “Stabilization control of biped locomotion robot based learning with GAs having self-adaptive mutation and recurrent neural networks,” in *Proceedings of the IEEE International Conference on Robotics and Automation*, (Albuquerque, New Mexico, USA), pp. 217–222, IEEE, 1997.
- [73] F. Miyazaki and S. Arimoto, “A control theoretic study on dynamical biped locomotion,” *Journal of Dynamic Systems, Measurement, and Control*, vol. 102, pp. 233–239, Dec. 1980.
- [74] J. Furusho and M. Masubuchi, “Control of a dynamical biped locomotion system for steady walking,” *Journal of Dynamic Systems, Measurement, and Control*, vol. 108, pp. 111–118, June 1986.
- [75] K. Hirai, M. Hirose, Y. Haikawa, and T. Takenaka, “The development of Honda humanoid robot,” in *Proceedings of the IEEE International Conference on Robotics and Automation*, (Leuven, Belgium), pp. 1321–1326, IEEE, 1998.
- [76] Q. Huang, K. Kaneko, K. Yokoi, S. Kajita, T. Kotoku, N. Koyachi, H. Arai, N. Imamura, K. Komoriya, and K. Tanie, “Balance control of a biped robot combining off-line pattern with real-time modification,” in *Proceedings of the IEEE International Conference on Robotics and Automation*, (San Francisco, California, USA), pp. 3346–3352, IEEE, 2000.

- [77] L. Sentis and O. Khatib, "A whole-body control framework for humanoids operating in human environments," in *Proceedings of the IEEE International Conference on Robotics and Automation*, (Orlando, Florida, USA), pp. 2641–2648, IEEE, 2006.
- [78] S. Kajita, F. Kanehiro, K. Kando, K. Yokoi, H. Hirukawa, and K. Kaneko, "The 3D linear inverted pendulum mode: a simple modeling for a biped walking pattern generation," in *Proceedings of the IEEE/RSJ International Conference on Intelligent Robots and Systems*, (Maui, Hawaii, USA), pp. 239–246, IEEE, 2001.
- [79] S. Kajita, F. Kanehiro, K. Kaneko, K. Fujiwara, K. Harada, K. Yokoi, and H. Hirukawa, "Resolved momentum control: Humanoid motion planning based on the linear and angular momentum," in *Proceedings of the IEEE/RSJ International Conference on Intelligent Robots and Systems*, (Las Vegas, Nevada, USA), pp. 1644–1650, IEEE, 2003.
- [80] J. Pratt, J. Carff, S. Drakunov, and A. Goswami, "Capture point: A step toward humanoid push recovery," in *Proceedings of the IEEE-RAS International Conference on Humanoid Robots*, (Genova, Italy), pp. 200–207, IEEE, Dec. 2006.
- [81] A. Goswami and V. Kallem, "Rate of change of angular momentum and balance maintenance of biped robots," in *Proceedings of the IEEE International Conference on Robotics and Automation*, (New Orleans, Louisiana, USA), pp. 3785–3790 Vol.4, Ieee, 2004.
- [82] T. Komura, A. Nagano, H. Leung, and Y. Shinagawa, "Simulating pathological gait using the enhanced linear inverted pendulum model," *IEEE Transactions on Biomedical Engineering*, vol. 52, pp. 1502–13, Sept. 2005.
- [83] J. Pratt and R. Tedrake, "Velocity-based stability margins for fast bipedal walking," in *Fast Motions in Biomechanics and Robotics* (M. Diehl and K. Mombaur, eds.), vol. 340 of *Lecture Notes in Control and Information Sciences*, pp. 299–324, Springer Berlin / Heidelberg, 2006.
- [84] B. Stephens, "Humanoid push recovery," in *Proceedings of the IEEE-RAS International Conference on Humanoid Robots*, (Pittsburgh, Pennsylvania, USA), pp. 589–595, IEEE, Nov. 2007.
- [85] S.-h. Hyon and G. Cheng, "Gravity compensation and full-body balancing for humanoid robots," in *Proceedings of the IEEE-RAS International Conference on Humanoid Robots*, (Genova, Italy), pp. 214–221, IEEE, Dec. 2006.

- [86] S.-H. Hyon, J. G. Hale, and G. Cheng, "Full-body compliant human-humanoid interaction: Balancing in the presence of unknown external forces," *IEEE Transactions on Robotics*, vol. 23, pp. 884–898, Oct. 2007.
- [87] T. Takubo, K. Inoue, K. Sakata, Y. Mae, and T. Arai, "Mobile manipulation of humanoid robots - control method for CoM position with external force," in *Proceedings of the IEEE/RSJ International Conference on Intelligent Robots and Systems*, (Sendai, Japan), pp. 1180–1185, IEEE, 2004.
- [88] C. K. Chow and D. H. Jacobson, "Further studies of human locomotion: Postural stability and control," *Mathematical Biosciences*, vol. 15, no. 1-2, pp. 93–108, 1972.
- [89] Y. Hwang, A. Konno, and M. Uchiyama, "Whole body cooperative tasks and static stability evaluations for a humanoid robot," in *Proceedings of the IEEE/RSJ International Conference on Intelligent Robots and Systems*, (Las Vegas, Nevada, USA), pp. 1901–1906, IEEE, 2003.
- [90] Y. Nishihama, K. Inoue, T. Arai, and Y. Mae, "Mobile manipulation of humanoid robots - control method for accurate manipulation," in *Proceedings of the IEEE/RSJ International Conference on Intelligent Robots and Systems*, (Las Vegas, Nevada, USA), pp. 1914–1919, IEEE, 2003.
- [91] K. Harada, S. Kajita, K. Kaneko, and H. Hirukawa, "Pushing manipulation by humanoid considering two-kinds of ZMPs," in *Proceedings of the IEEE International Conference on Robotics and Automation*, (Taipei, Taiwan), pp. 1627–1632, IEEE, 2003.
- [92] K. Harada, H. Hirukawa, F. Kanehiro, K. Fujiwara, K. Kaneko, S. Kajita, and M. Nakamura, "Dynamical balance of a humanoid robot grasping an environment," in *Proceedings of the IEEE/RSJ International Conference on Intelligent Robots and Systems*, (Sendai, Japan), pp. 1167–1173, IEEE, 2004.
- [93] K. Harada, S. Kajita, H. Saito, M. Morisawa, F. Kanehiro, K. Fujiwara, K. Kaneko, and H. Hirukawa, "A humanoid robot carrying a heavy object," in *Proceedings of the IEEE International Conference on Robotics and Automation*, (Barcelona, Spain), pp. 1712–1717, IEEE, 2005.
- [94] K. Inoue, H. Yoshida, T. Arai, and Y. Mae, "Mobile manipulation of humanoids-real-time control based on manipulability and stability," in *Proceedings of the IEEE International Conference on Robotics and Automation*, (San Francisco, California, USA), pp. 2217–2222, IEEE, 2000.

- [95] J. A. Vince, *Mathematics for Computer Graphics*. London: Springer-Verlag, 3rd ed., 2010.
- [96] A. Hourtash, “The kinematic Hessian and higher derivatives,” in *Proceedings of the IEEE International Symposium on Computational Intelligence in Robotics and Automation*, (Espoo, Finland), pp. 169–174, IEEE, 2005.
- [97] L. Biagiotti and C. Melchiorri, *Trajectory planning for automatic machines and robots*. Berlin Heidelberg: Springer-Verlag, 2008.
- [98] S. Kajita, K. Yokoi, M. Saigo, and K. Tanie, “Balancing a humanoid robot using backdrive concerned torque control and direct angular momentum feedback,” in *Proceedings of the IEEE International Conference on Robotics and Automation*, vol. 4, (Seoul, South Korea), pp. 3376–3382, IEEE, 2001.
- [99] S. Kajita, F. Kanehiro, K. Kaneko, K. Fujiwara, K. Harada, K. Yokoi, and H. Hirukawa, “Biped walking pattern generation by using preview control of zero-moment point,” in *Proceedings of the IEEE International Conference on Robotics and Automation*, (Taipei, Taiwan), pp. 1620–1626, IEEE, 2003.
- [100] P. Pierro, O. Stasse, A. Kheddar, K. Yokoi, and C. Balaguer, “Humanoid feet trajectory generation for the reduction of the dynamical effects,” in *Proceedings of the IEEE-RAS International Conference on Humanoid Robots*, (Paris, France), pp. 454–458, IEEE, 2009.
- [101] T. Buschmann, S. Lohmeier, M. Bachmayer, H. Ulbrich, and F. Pfeiffer, “A collocation method for real-time walking pattern generation,” in *Proceedings of the IEEE-RAS International Conference on Humanoid Robots*, (Pittsburgh, Pennsylvania, USA), pp. 1–6, IEEE, Nov. 2007.
- [102] O. Stasse, B. Verrelst, B. Vanderborght, and K. Yokoi, “Strategies for humanoid robots to dynamically walk over large obstacles,” *IEEE Transactions on Robotics*, vol. 25, pp. 960–967, Aug. 2009.
- [103] J. Vaganay, M.-J. Aldon, and A. Fournier, “Mobile robot attitude estimation by fusion of inertial data,” in *Proceedings of the IEEE International Conference on Robotics and Automation*, (Atlanta, Georgia, USA), pp. 277–282, IEEE, May 1993.
- [104] J. M. Pflimlin, T. Hamel, and P. Souères, “Nonlinear attitude and gyroscope’s bias estimation for a VTOL UAV,” *International Journal of Systems Science*, vol. 38, no. 3, pp. 197–210, 2007.

- 
- [105] H. Rehbinder and X. Hu, “Drift-free attitude estimation for accelerated rigid bodies,” in *Proceedings of the IEEE International Conference on Robotics and Automation*, vol. 4, (Seoul, South Korea), pp. 4244 – 4249, IEEE, 2001.
- [106] S. P. N. Singh and K. J. Waldron, “Attitude estimation for dynamic legged locomotion using range and inertial sensors,” in *Proceedings of the IEEE International Conference on Robotics and Automation*, (Barcelona, Spain), pp. 1663–1668, IEEE, 2005.
- [107] B. Barshan and H. F. Durrant-Whyte, “Inertial navigation systems for mobile robots,” *IEEE Transactions on Robotics and Automation*, vol. 11, pp. 328–342, June 1995.
- [108] H. Rehbinder and X. Hu, “Nonlinear pitch and roll estimation for walking robots,” in *Proceedings of the IEEE International Conference on Robotics and Automation*, vol. 3, (San Francisco, California, USA), pp. 2617 –2622, IEEE, 2000.
- [109] P. Pierro, N. Mansard, P. Souères, C. A. Monje, and C. Balaguer, “Attitude estimation for humanoid robots using sensorial integration and Extended Kalman Filtering,” in *Proceedings of the Perception in Robotics Workshop - Intelligent Vehicles Symposium 2012*, (Madrid, Spain), 2012.
- [110] S. Kajita, O. Matsumoto, and M. Saigo, “Real-time 3D walking pattern generation for a biped robot with telescopic legs,” in *Proceedings of the IEEE International Conference on Robotics and Automation*, vol. 3, (Seoul, South Korea), pp. 2299–2306, IEEE, 2001.
- [111] M. A. Diftler, R. O. Ambrose, K. S. Tyree, M. Goza, and E. Huber, “A mobile autonomous humanoid assistant,” in *Proceedings of the IEEE-RAS International Conference on Humanoid Robots*, vol. 1, (Santa Monica, California, USA), pp. 133–148, IEEE, 2004.
- [112] T. B. Martin, R. O. Ambrose, M. A. Diftler, R. Platt, and M. J. Butzer, “Tactile gloves for autonomous grasping with the NASA/DARPA Robonaut,” in *Proceedings of the IEEE International Conference on Robotics and Automation*, (New Orleans, Louisiana, USA), pp. 1713–1718 Vol.2, IEEE, 2004.
- [113] N. E. Sian, T. Sakaguchi, K. Yokoi, Y. Kawai, and K. Maruyama, “Operating Humanoid Robots in Human Environments,” in *Proceedings of the Robotics, Science and Systems Workshop on Manipulation for Human Environments*, (Philadelphia, Pennsylvania, USA), 2006.

- [114] A. Edsinger and C. C. Kemp, "Human-robot interaction for cooperative manipulation: Handing objects to one another," in *Proceedings of the IEEE International Symposium on Robot and Human Interactive Communication*, (Jeju, South Korea), pp. 1167–1172, IEEE, 2007.
- [115] H. A. Yanco and J. Drury, "Classifying human-robot interaction: An updated taxonomy," in *Proceedings of IEEE International Conference on Systems, Man and Cybernetics*, vol. 3, (Hague, Netherlands), pp. 2841–2846, IEEE, 2004.
- [116] J. Scholtz, "Theory and evaluation of human robot interactions," in *Proceedings of the Annual Hawaii International Conference on System Sciences*, (Big Island, USA), pp. 125–134, IEEE, 2003.
- [117] C. A. Ellis, S. J. Gibbs, and G. Rein, "Groupware: Some issues and experiences," *Communications of the ACM*, vol. 34, pp. 39–58, Jan. 1991.
- [118] P. J. Hinds, T. L. Roberts, and H. Jones, "Whose job is it anyway? A study of human-robot interaction in a collaborative task," in *Human-Computer Interaction*, pp. 151–181, 2004.
- [119] O. Khatib, L. Sentis, J. Park, and J. Warren, "Whole-body dynamic behavior and control of human-like robots," *International Journal of Humanoid Robotics*, vol. 1, no. 1, pp. 29–43, 2004.
- [120] P. Pierro, C. A. Monje, and C. Balaguer, "The virtual COM joints approach for whole-body RH-1 motion," in *Proceedings of the IEEE International Symposium on Robot and Human Interactive Communication*, (Toyama, Japan), pp. 285–290, IEEE, 2009.
- [121] A. Weiss, J. Igelsböck, P. Pierro, R. Buchner, C. Balaguer, and M. Tscheligi, "User perception of usability aspects in indirect HRI - a chain of translations," in *Proceedings of the IEEE International Symposium on Robot and Human Interactive Communication*, (Viareggio, Italy), pp. 539–545, IEEE, 2010.
- [122] P. Pierro, D. Hernández, M. González-Fierro, L. Blasi, A. Milani, and C. Balaguer, "Humanoid teleoperation system for space environments," in *Proceedings of the International Conference on Advanced Robotics*, (Munich, Germany), pp. 1–6, IEEE, 2009.
- [123] M. Arbulú, D. Kaynov, L. Cabas, and C. Balaguer, "The RH-1 full-size humanoid robot: Design, walking pattern generation and control," *Applied Bionics and Biomechanics*, vol. 6, pp. 301–344, Dec. 2009.

- 
- [124] M. Arbulú, J. M. Pardos, L. Cabas, P. Staroverov, D. Kaynov, C. Pérez, M. Rodríguez, and C. Balaguer, “RH-0 humanoid full size robot’s control strategy based on the lie logic technique,” in *Proceedings of the IEEE-RAS International Conference on Humanoid Robots*, (Tsukuba, Japan), pp. 271–276, IEEE, 2005.
- [125] C. A. Monje, S. Martínez, A. Jardón, P. Pierro, C. Balaguer, and D. Muñoz, “Full-size humanoid robot TEO: Design attending mechanical robustness and energy consumption,” in *Proceedings of the IEEE-RAS International Conference on Humanoid Robots*, (Bled, Slovenia), IEEE, 2011.
- [126] T. Shigeo, K. Koichi, I. Hiyoshi, O. Keita, and T. Ryuichi, “Development of small humanoid robot HOAP-3,” *Nippon Robotto Gakkai Gakujutsu Koenkai Yokoshu*, vol. 3, pp. 1–35, 2005.
- [127] H. Hasunuma, K. Harada, and H. Hirukawa, “The tele-operation of the humanoid robot-whole body operation for humanoid robots in contact with environment,” in *Proceedings of the IEEE-RAS International Conference on Humanoid Robots*, (Genova, Italy), pp. 333–339, IEEE, Dec. 2006.
- [128] L. Blasi and O. Stasse, “Robot@CWE Deliverable D3.3: Design support software for ROBOT@CWE,” tech. rep., Robot@CWE, 2008.
- [129] M. Narita, M. Shimamura, and M. Oya, “Reliable protocol for robot communication on Web services,” in *Proceedings of the International Conference on Cyberworlds*, (Singapore), pp. 220–227, IEEE Comput. Soc, 2005.